NORTHWESTERN UNIVERSITY

Mechanisms of Acentrosomal Spindle Assembly and Maintenance in *C. elegans* Oocytes

A DISSERTATION

SUBMITTED TO THE GRADUATE SCHOOL

IN PARTIAL FULFILLMENT OF THE REQUIREMENTS

for the degree

DOCTOR OF PHILOSOPHY

Field of Interdisciplinary Biological Sciences

By

Ian D. Wolff

EVANSTON, ILLINOIS

September 2020

ABSTRACT

Mechanisms of Acentrosomal Spindle Assembly and Maintenance

in *C. elegans* Oocytes

Ian D. Wolff

Although centrosomes nucleate and organize microtubules in mitotically-dividing cells, spindles in female reproductive cells (oocytes) form in their absence. In some organisms acentrosomal spindle assembly is mediated by acentriolar microtubule organizing centers (MTOCs) that are thought to functionally replace centrosomes. However, spindle assembly in human oocytes does not require MTOCs; little is known about the molecular mechanisms underlying this MTOC-independent pathway. In this dissertation, I demonstrate that acentrosomal spindle assembly in *C. elegans* oocytes is also MTOC-independent, establishing it as powerful model system to investigate this process. High resolution imaging of acentrosomal spindle formation revealed that following nuclear envelope breakdown, microtubules of mixed polarity surround the chromosomes in a cage-like structure adjacent to the disassembling nuclear envelope. Microtubules are then sorted so that minus ends are forced to the periphery of the array where they coalesce into multiple nascent poles before achieving bipolarity. I characterized how two essential proteins, KLP-18/kinesin-12 and MESP-1 (**me**iotic **sp**indle **1**), act to promote acentrosomal spindle bipolarity. Following KLP-18 or MESP-1 depletion,

the microtubule cage forms but then minus-ends rapidly converge, bypassing the multipolar stage and instead forming a monopolar spindle. BMK-1/Kinesin-5, the essential bipolarity-generating motor in many organisms, is not essential for spindle assembly in this system. Therefore, KLP-18/kinesin-12 and MESP-1 are likely the primary force generators that sort microtubule minus ends away from the chromosomes.

However, the biochemical mechanism of how these proteins generate force was unknown. To gain insight into this important problem I employed a combination of *in vitro* and *in vivo* approaches. First, I purified recombinant truncations of the KLP-18 coiled-coil stalk domain along with full length MESP-1 to use in microtubule binding experiments *in vitro*. I identified a non-motor microtubule binding site at the C-terminus of the KLP-18 stalk and found that this microtubule binding site is activated through MESP-1 interaction with an adjacent region of the stalk. I then tested the importance of the KLP-18 C-terminal microtubule binding site *in vivo* using a temperature sensitive mutant strain containing two amino acid substitutions in the mapped domain. Prolonged incubation at the restrictive temperature caused spindle assembly defects that are identical to those observed following depletion of KLP-18 by RNAi; monopolar instead of bipolar spindles formed. In addition, I found that short incubation of this mutant at the restrictive temperature caused the collapse of already formed bipolar spindles into monopoles. In both cases, KLP-18 still localized to the aberrant spindles, indicating that the protein is present but non-functional. These results demonstrate that the C-terminal microtubule binding site we identified *in vitro* is required for both spindle assembly and for the maintenance of spindle bipolarity *in vivo*. Altogether, this work sets the basis for further investigation into how microtubule associated proteins govern spindle assembly and maintenance, specifically in a system lacking centrosomes.

Acknowledgements

These acknowledgements are long, but so is graduate school.

First and foremost, I want to thank my lab mates with whom I spent every day working alongside. I was fortunate enough to start in the lab as a Research Technician along with Michael Tran and Chrissy Muscat, two amazing scientists and people. I have yet to meet someone as focused and determined as Mike, and I am so thrilled that he has blossomed into an amazing scientist who is bound to do great things at Stanford and beyond. Chrissy was truly the bedrock of the lab when we first started out- it was just Mike, an undergrad, and me, just out of undergrad, and neither of us knew how to do anything. Whether she knew it or not, I learned a lot about being a professional and simply being an adult from being around Chrissy every day. The first couple of years in the lab was a formative experience scientifically and personally, and although it was challenging at times, I would not trade the experience for anything easier. The first student to join the group was Keila Torre-Santiago, who brought a fresh perspective scientifically and culturally, and it was a pleasure to get to know her. Next came Amanda Davis-Roca, Tim Mullen, and Carissa Heath: a truly unique and amazing group that I am incredibly thankful to have worked with. Amanda was one of the most intelligent and hardest working people I have met and I was always impressed by what she consistently accomplished. She was the first of this group to graduate and set the bar high for all of us. Tim and I had projects that were very similar and so he was

the person I worked most closely with- our scientific conversations were always illuminating and I learned a great deal bouncing both good and more often bad ideas off of him. I am convinced I would not be the scientist I am without his influence, and I will always cherish those days. Were our non-science conversations always as constructive? Probably not, but they sure made me excited to come into lab every day. It's important that Tim always remembers that nothing actually matters. Carissa took on (in retrospect) an insane task- to pioneer mouse work in our lab, even though none of us had ever touched (or maybe even seen?) a lab mouse. But she did it and did it well, a testament to how intelligent, creative, and persistent she is. Due to my long tenure in the lab (first as a Tech then later as a Graduate Student), I've had the pleasure of seeing the first group of students come and go, and then to welcome the next group in. Nikita, Gabe, Hannah, and Emily are all incredible and unique people and are all truly fantastic scientists. It has been amazing to see them grow as scientists over the last few years and I know they will all go onto great things in the future. It is comforting to know that the Wignall Lab is in such good hands. Jeremy, who came to the lab as our lab manager sometime in between (time really gets delineated over a PhD), is one of the most interesting people- he is somehow able to juggle working full time in a lab with working on theater productions at night. And even more impressively he does them both really well! If Chrissy was the bedrock of the lab in the first few years, Jeremy has been our bedrock since. Graduate school is hard- it's hard academically, but it's also hard socially. Everyone faces their own challenges in their 20s as they grow and become the person they aim to be. To be able to spend my formative years with all of these amazing people has been unforgettable and I will always look back at my time in the lab with great fondness and happiness.

Next, I must thank Sadie. I bet every soon-to-be graduate says this about their advisor, but I truly mean it: I would not be here without her. After I graduated from college, I did not have a job lined up but decided to move to Chicago anyway, simply because I wanted to live here. I was sleeping on my friend's couch and had no idea what I was going to do. Thankfully, Sadie took a chance on me, a chemistry major who had never worked with worms and had not even taken a cell biology class, to help start her cell biology lab. And here I am writing a thesis for a PhD in cell biology. She is a brilliant scientist who has taught me literally everything I know about cell biology, genetics, microscopy, *C. elegans*, mitosis, meiosis, grant writing, paper writing, thesis writing, abstract writing, talk giving, poster giving- and I'm sure I'm leaving some things out. She has been an incredible mentor to not only me but to everyone in the lab, and I can not thank her enough for creating a truly positive and nurturing environment in which to learn and to make mistakes. Academia is full of toxic labs and toxic advisors, and I am so thankful to have been lucky enough to have Sadie as a mentor. I hope to someday live up to the example she has set.

Thank you to my thesis committee: John Marko, Volodya Gelfand, and Laura Lackner. Their insights have been invaluable to the development of my project and my development as a scientist. I must also especially thank Sarah Rice, who taught me fundamental biochemical techniques that I used in this dissertation. I have used many things she taught me throughout my work and without her early guidance I do not think I would have been able to do much of the biochemistry in the following pages. Thanks to Tim Mullen and Justin Finkle who helped me adapt the LaTeX code I used to prepare this dissertation.

I also must thank my sources of funding: National Institutes of Health/National Institute of General Medical Sciences Molecular Biophysics Training Grant and the American Heart Association Predoctoral Fellowship. I thank the various training and seminar groups from

which I have learned a great deal: Cancer Cell Biology Super Group, Chicago Cytoskeleton Meeting, Northwestern Center for Reproductive Science, Molecular Biophysics Training Program, and the various seminars organized by the IBiS graduate program and the IBiS student organization.

I also want to take this opportunity to acknowledge those artists, musicians, authors, and activists who have inspired me and whose work has broadened my experience, especially Annie Clark, James Murphy, David Bowie, Gord Downie, David Lynch, David Byrne, Carrie Brownstein, Alexandria Ocasio-Cortez, Anthony Bourdain, and Bernard Sanders. Thank you to the mainstay institutions that defined my graduate school experience and made me feel at home in Chicago: Guthrie's Tavern, The Music Box Theatre, GMan Tavern, Lincoln Hall, The Hideout, The Empty Bottle, Nisei Lounge, Thalia Hall, The Metro, Sleeping Village, and Delilah's.

To all of my family and friends for their support and their inspiration.

Chicago is a truly amazing city and I can not even begin to describe all of the amazing things that I love about it. The lake, the diversity, the music culture, the seasons, the energy, the Malort. But most of all, I am thankful to Chicago for giving me my wife, Monica. She has been the bright light in the sometimes darkness of graduate school, and I would not be where I am without her. I will miss Chicago with all my heart, but I could not be more excited to build a community wherever life takes us.

To my family; my dad Kirk, my mom Patty, and my brother Kevin. They always supported me even when they had no idea what I was doing or why I was doing it. They supported me when I moved to Chicago with no job lined up, when I decided to stay in Chicago for graduate school, and when they had no idea when I would graduate. I am lucky to have such a supportive and loving family.

Abbreviations

AID: auxin inducible degradation

CPC: chromosome passenger complex

CRISPR: clustered regularly interspaced short palindromic repeats

DIC: differential interference contrast

DNA: deoxyribonucleic acid

EICs: Eg5 independent cells

GFP: green fluorescent protein

GST: glutathione-S-transferase

GVBD: germinal vesicle breakdown

IF: immunofluorescence

IVF: in vitro fertilization

KLP: kinesin like protein

kMT: kinetochore microtubule

MESP: meiotic spindle

MAP: microtubule associated protein

MTOCs: microtubule organizing centers

NEBD: nuclear envelope breakdown

NGM: nematode growth medium

PCM: pericentriolar material

RNAi: RNA interference

SEC-MALS: size exclusion chromatography coupled multi-angle light scattering

SUMO: small ubiquitin-like modifier

TEM: transmission electron microscopy

TIRF: total internal reflection fluorescence

Dedication

To my grandmother, Kay.

Come and show me another city with lifted head singing so proud to be alive and coarse and strong and cunning.

Carl Sandberg, "Chicago"

This is a damn fine cup of coffee.

Special Agent Dale Cooper, "Twin Peaks"

Table of Contents

ABSTRACT 3

Acknowledgements 5

Abbreviations 9

Dedication 11

List of Tables 17

List of Figures 18

Chapter 1. Introduction 21

1.1. Why study female meiosis? 22

1.2. Microtubule nucleation 24

1.3. Microtubule organization and sorting 31

1.4. Building spindle poles and stabilizing bipolarity 34

1.5. Biochemical basis of force generation 39

1.6. *C. elegans* as a model to study cell division 47

Chapter 2. Assembly of *Caenorhabditis elegans* acentrosomal spindles occurs without evident microtubule-organizing centers and requires microtubule sorting by KLP-18/kinesin-12 and MESP-1 52

2.1. Introduction 53

2.2. Acentrosomal spindle assembly proceeds by microtubule nucleation followed by formation and coalescence of multiple poles 55

2.3. Microtubules of mixed polarity are nucleated and then sorted during acentrosomal spindle assembly 59

2.4. KLP-18/kinesin-12 and MESP-1 are required to sort microtubule minus ends away from the chromosomes 63

2.5. KLP-18/kinesin-12 and MESP-1 are interdependent for localization and can interact 64

2.6. MESP-1 is a rapidly evolving protein that may be performing the kinesin-12 targeting role of TPX2 68

2.7. Discussion 71

Chapter 3. Acentrosomal spindle assembly and stability in *C. elegans* requires a kinesin-12 non-motor microtubule interaction domain 74

3.1. Summary 75

3.2. The KLP-18 coiled-coil stalk domain contains a regulated microtubule binding site 76

3.3. KLP-18 is targeted to microtubules through a direct interaction with microtubule associated protein MESP-1 83

3.4. The KLP-18 stalk microtubule interaction domain is essential for spindle assembly 87

3.5. KLP-18 sorting activity is essential to maintain spindle bipolarity 91

3.6. Discussion 94

Chapter 4. Summary of findings and future directions 98

4.1. Summary of findings 99

4.2. Future directions 102

4.3. Final remarks 116

Chapter 5. Materials and Methods 118

5.1. Worm strains 119

5.2. Image Acquisition Statement 120

5.3. Immunofluorescence 120

5.4. Live cell time-lapse imaging 121

5.5. Quantification of Spindle Morphology 122

5.6. RNA Interference (RNAi) 123

5.7. Large-scale worm growth and protein extraction 123

5.8. Protein domain analysis 124

5.9. Protein expression and purification 125

5.10. GST pull-down assay 127

5.11. Microtubule co-sedimentation assay 127

5.12. Microtubule bundling assay 129

5.13. MBP pulldown 130

5.14. Hydrodynamic analysis 130

5.15. Western Blots 131

5.16. Chapter 3 Figure Quantification 132

References 137

Appendix A. Methods paper: *Methods for studying cell division mechanisms in C.elegans* 158

A.1. Abstract 159

A.2. Introduction 159

A.3. Materials 164

A.4. Methods 167

Appendix B. MESP-1 can nucleate microtubule assembly *in vitro* 180

Appendix C. KLP-18 and MESP-1 can form droplets that concentrate tubulin and associate with microtubules *in vitro* 182

Appendix D. Kinesin-5 BMK-1 localization and effect on late anaphase 194

Appendix E. ZYG-9 is required for *C. elegans* oocyte spindle assembly 200

Appendix F. KLP-18 motility 202

List of Tables

5.1 Worm strains 119

List of Figures

1.1 Simplified diagrams of acentrosomal oocyte spindle microtubule nucleation, sorting, and bipolar stability 27

1.2 Biochemical models for kinesin-5 and kinesin-12/Kif15 force generation 41

1.3 Comparison of common imaging techniques used with *C. elegans* oocytes and embryos 48

1.4 Schematic of the *C. elegans* germ line 50

2.1 Acentrosomal spindle assembly in meiosis I proceeds through a cage and multipolar stage 56

2.2 Quantification of spindle structures at different positions in the *C. elegans* germ line 57

2.3 KLP-18 and MESP-1 sort microtubules during spindle assembly 61

2.4 GFP-ASPM-1 localization indicates microtubule sorting during spindle assembly 62

2.5 KLP-18 and MESP-1 colocalize and are interdependent for localization 66

2.6 MESP-1 is a rapidly evolving protein that may perform the kinesin-12–targeting role of TPX2 70

2.7 Model for MTOC-independent acentrosomal spindle assembly 73

3.1	The kinesin-12/KLP-18 coiled-coil stalk domain contains a regulated microtubule binding site	79
3.2	Protein expression and purification details	81
3.3	Domain diagram of KLP-18 stalk and a putative hinge region	82
3.4	MESP-1 is an unstructured and disordered microtubule binding protein	84
3.5	KLP-18 is targeted to microtubules through a direct interaction with microtubule associated protein MESP-1	86
3.6	KLP-18 stalk microtubule interaction domain is essential for spindle assembly	89
3.7	KLP-18 sorting activity is essential to maintain spindle bipolarity	93
3.8	Model. KLP-18 C-terminal microtubule binding site is activated by MESP-1 and is essential for spindle assembly and maintenance of bipolarity	95
4.1	Alignment of KLP-18 motor domain with *Caenorhabditis* homologs	107
4.2	Alignment of KLP-18 stalk domain with *Caenorhabditis* homologs	109
4.3	Alignment of MESP-1 with *Caenorhabditis* homologs	110
4.4	Two proposed models of spindle pole construction	113
A.1	Comparison of common imaging techniques used with *C. elegans* oocytes and embryos	177
A.2	Schematics of the *C. elegans* germ line and of spindle assembly in oocytes	178
A.3	Examples of each imaging technique	179

B.1 MBP-MESP-1 can nucleate microtubule assembly *in vitro* 181

C.1 KLP-18 stalk and MESP-1 form droplets in the presence of 9% PEG *in vitro* 188

C.2 MESP-1 is required for KLP-18 stalk droplets to incorporate tubulin 190

C.3 KLP-18 stalk / MESP-1 droplets are associated to microtubules *in vitro* 191

C.4 Tubulin and pole proteins persist after nocodazole treatment 193

D.1 BMK-1 colocalizes with KLP-18 during spindle assembly and localization is affected by MESP-1 depletion 196

D.2 BMK-1 redistributes to spindle microtubules during anaphase and depletion results in unfocused late anaphase microtubule bundles 198

E.1 ZYG-9 is required for *C. elegans* oocyte spindle bipolarity 201

F.1 Microtubule gliding assay shows KLP-18 is a relatively fast kinesin-12 motor 203

CHAPTER 1

Introduction

Parts of this chapter have been adapted from a manuscript submitted to Methods in Molecular Biology entitled "Methods for studying cell division mechanisms in C. elegans", in particular the final section of the introduction "C. elegans as a model to study cell division". Complete text of this article can be found in Appendix A.

1.1. Why study female meiosis?

Many animals reproduce sexually through fertilization of female (oocyte) by male (sperm) haploid gametes. To facilitate this process, diploid animals must reduce the amount of genetic information by half so that when haploid sperm fertilizes a haploid oocyte the resulting embryo is diploid. If either gamete contains an incorrect number of chromosomes the resulting embryo will be aneuploid, which can result in genetic disorders or early death. Chromosome number in diploid precursor cells is halved through the reductional meiotic divisions. Both sperm and oocytes are generated through meiotic divisions, however, female meiosis is much more perilous. In humans, it is estimated that 10-25% of fertilized eggs are aneuploid, and, strikingly, that most aneuploidies are derived from errors in female meiosis specifically[1]. In addition, the incidence of errors in female meiosis increases with maternal age; at the end of a woman's reproductive fertility the error rate can be as high as 50%. Although the societal implications of this phenomenon are clear, there has been a relative scarcity of basic science investigation into the cellular and genetic causes of errors in female meiosis, and many fundamental questions remain. Through this dissertation I aim to shed light on this important biological phenomenon by investigating the molecular machines driving the oocyte meiotic divisions in the model organism *C. elegans*.

Meiosis has two defining events: pairing of homologous chromosomes during prophase and separation of homologous chromosomes then sister chromatids during the meiotic divisions. After one round of DNA replication, homologous chromosomes (one paternal and one maternal) are physically paired during meiotic prophase, aligned on a microtubule based spindle during prometaphase and metaphase, then divided in anaphase. Homologous chromosomes are separated in Meiosis I and sister chromatids are separated in Meiosis II. In oocytes, after each round of division half of the genetic information is extruded in polar

bodies, eventually resulting in a haploid gamete. There is a wealth of literature describing meiotic prophase in mammals[2,3], *C. elegans*[4], yeast[5], and across organisms[2]. In addition, there has been much research done on chromosome segregation in anaphase in mammals[6], *Drosophila*[7], and *C. elegans*[8]. Here, I will focus on the less thoroughly studied prometaphase and metaphase stages of the meiotic divisions, and specifically the mechanisms by which an oocyte builds and maintains a microtubule based spindle.

In mitotically dividing cells and during the meiotic divisions in sperm, chromosomes are aligned and separated on a microtubule based spindle that is nucleated and organized by centriole containing centrosomes[9]. Microtubules are long filaments of α/β tubulin heterodimers that grow and shrink dynamically in the cell[10]. The microtubule filament has a dynamic plus-end and a more stable minus-end. Centrosomes polymerize and stabilize spindle microtubules by anchoring stable minus-ends and recruiting polymerizing factors to growing plus-ends[11–13]. However, in oocytes, microtubules in the meiotic spindle are nucleated and stabilized in the absence of centrosomes; hereafter referred to as 'acentrosomal'[14]. There are many fundamental differences between centrosome-based and acentrosomal spindles[15], and therefore the molecular mechanisms driving acentrosomal spindle nucleation and stability must be considered in their own right. As we continue to learn, it is not adequate to rely only on assumptions based on the well characterized properties of centrosome-based mitotic spindles.

A fundamental challenge in studying acentrosomal oocyte meiosis is that it is very difficult to obtain and to perform mechanistic studies on human samples. Some important studies have been performed but they rely on unused oocytes during IVF treatment; it is unclear if these oocytes truly represent "healthy" or "wild type" human oocytes, or what the definitions of these terms really are. Therefore, it is crucial to supplement these findings

with deeply mechanistic work from model organisms. In this introduction I will describe the current state of knowledge in the five major model organisms used to study the oocyte meiotic divisions: human, mouse, fruit fly (*Drosophila melanogaster*), frog (*Xenopus laevis*), and nematode worm (*Caenorhabditis elegans*). I will focus on the stages of meiosis that most directly inform my work: nucleation of spindle microtubules, microtubule bundling and sorting, molecular architecture of acentrosomal spindle poles, and the biochemical basis of force generation by kinesin motors. Throughout this introduction I hope to summarize conserved mechanisms across organisms and identify important outstanding questions.

1.2. Microtubule nucleation

The first step in forming a meiotic spindle is to nucleate microtubules, the tubulin filaments that physically attach to chromosomes and pull them apart. Meiotic spindles are small relative to the size of the oocyte and form a characteristic barrel shape of dense microtubules[8]. The basis of oocyte microtubule nucleation is particularly interesting because they lack canonical microtubule nucleating centrosomes and therefore different and unique mechanisms must predominate (Figure 1.1A).

1.2.1. Nucleation from the inside-out

Xenopus is a particularly powerful system to study the molecular mechanisms of meiotic spindle assembly because of the ability to construct a spindle *in vitro* within egg extract. The frog's eggs are arrested in Meiosis I and when crushed then cleared by centrifugation the lysate retains biochemical activity[16]. A seminal study found that proteins within this lysate are able to construct a functional spindle around DNA coated beads in the absence of centrosomes, showing that DNA itself is sufficient to initiate nucleation of microtubules[17]. Further investigation using this system identified RanGTP as a key factor that initiates

microtubule assembly through interaction with the protein importin. Importin binds to and inactivates spindle assembly factors that, when free of this regulation, act to nucleate microtubules. The chromatin component RCC1 is a guanine nucleotide-exchange factor that helps to convert inactive RanGDP to active RanGTP[18], which then binds importin and disrupts the importin-TPX2 interaction, liberating the spindle assembly factor TPX2 to nucleate microtubules[19,20]. Once microtubules are nucleated in proximity to chromatin, the chromosome passenger complex (CPC) aids to stabilize microtubule bundles through interaction with Dasra[21,22], a chromatin associated protein. In addition to stabilizing microtubules nucleated by the Ran pathway, the CPC can also mediate a distinct nucleation pathway. Extracts depleted of the CPC component Incenp do not nucleate microtubules[21], and artificial recruitment of Incenp to beads can trigger nucleation in the absence of Ran[23]. An additional CPC component, the Aurora B kinase, also aids in microtubule stability[24] through interaction with Incenp[25]. There is additional evidence that the Ran pathway also plays a role in mouse oocyte spindle nucleation, however, it is not the primary generator of microtubules (further explained in the next section).

Microtubule nucleation in *Drosophila* oocytes is similarly initiated around chromatin[26,27], however, this process does not require the Ran gradient[28]. Mutations in the CPC component Incenp delay microtubule nucleation but a spindle of normal length eventually forms[29,30]. However, other studies have shown that the CPC is essential for microtubule nucleation[31]. This raises the possibility that there could be redundant microtubule nucleation mechanisms in *Drosophila* oocytes. An appealing hypothesis is that the large protein complex augmin mediates microtubule-stimulated branching nucleation of longer microtubules from small seeds formed around chromatin. Augmin is a large multi-subunit complex discovered in mitotic *Drosophila* S2 cell lines and shown to be important for microtubule nucleation away from

the centrosomes[32,33]. In oocytes, the augmin subunit Wac is not essential for microtubule nucleation but is essential for proper spindle assembly and spindle pole construction[34,35]. Augmin is thought to nucleate microtubules through interaction with γ-tubulin[36], a tubulin isoform that can form a nucleation template at the minus-end of a microtubule[37,38] as part of a large protein complex called γ-TURC (γ-tubulin ring complex)[39,40]. γ-tubulin localizes to both the poles and the center of the oocyte bipolar spindle[41,42], although it is not essential for initial microtubule nucleation[43,44]. Interestingly, augmin/γ-tubulin/γ-TURC have also been shown to mediate acentrosomal microtubule nucleation in *Xenopus* meiotic extract. γ-tubulin localizes across the spindle[17] and immunodepletion of augmin results in reduced microtubule nucleation and pole defects[45]. Beautiful *in vitro* biochemical work has shown that augmin, γ-tubulin, Ran, and TPX2 all contribute to "branching microtubule nucleation"; a mechanism by which microtubules are nucleated far from chromatin by using existing microtubules as a template[46]. Recently, it has been shown that the local concentration of spindle assembly factors drive branching microtubule nucleation and that this spatial concentration gradient acts to limit spindle size in *Xenopus* extract[47]. Taken together, microtubule nucleation in *Xenopus* and *Drosophila* oocytes appear to be mediated by initial nucleation of microtubules near chromatin through activation of TPX2 by RanGTP, then subsequent amplification of microtubule number through branching microtubule nucleation mediated by γ-tubulin and augmin.

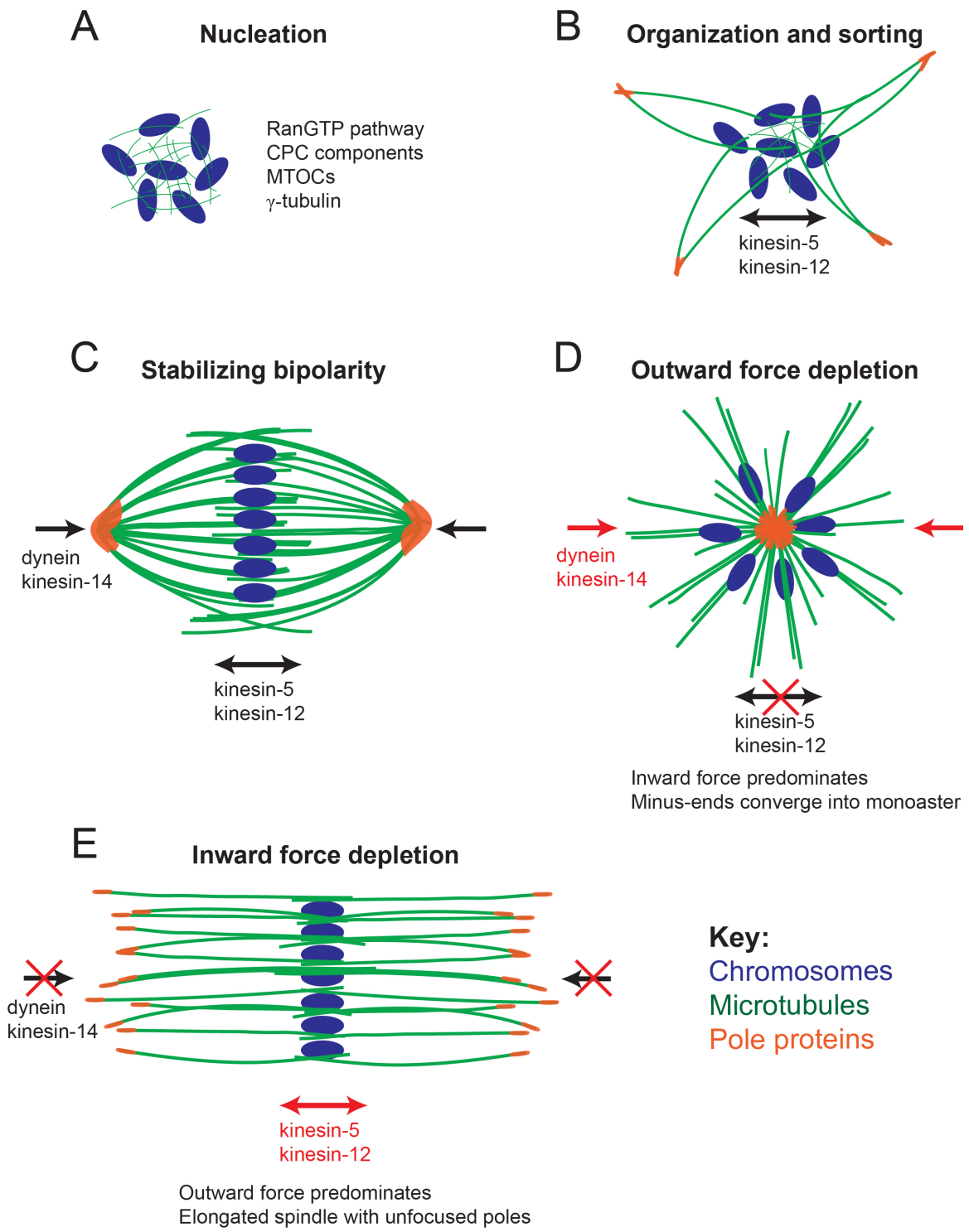
A
Nucleation
RanGTP pathway
CPC components
MTOCs
γ-tubulin
B
Organization and sorting
kinesin-5
kinesin-12
C
Stabilizing bipolarity
dynein
kinesin-14
kinesin-5
kinesin-12
D
Outward force depletion
dynein
kinesin-14
kinesin-5
kinesin-12
Inward force predominates
Minus-ends converge into monoaster
E
Inward force depletion
dynein
kinesin-14
kinesin-5
kinesin-12
Outward force predominates
Elongated spindle with unfocused poles
Key:
Chromosomes
Microtubules
Pole proteins

Figure 1.1

Figure 1.1. **Simplified diagrams of acentrosomal oocyte spindle microtubule nucleation, sorting, and bipolar stability.** Basic diagrams outlining the major molecular players during each stage of acentrosomal spindle assembly. Chromosomes are in blue, microtubules in green, and pole proteins in orange. (A) Upon initiation of spindle assembly, microtubules are nucleated through different pathways (indicated on right) near the chromosomes. (B) Plus-end directed kinesin motors then sort microtubules away from the chromosomes where minus-ends begin to coalesce into spindle poles (orange). In most organisms kinesin-5 provides this outward sorting force (black double-sided arrow), but in *C. elegans* kinesin-12 performs this role. (C) As microtubules continue to be sorted outwards away from chromosomes, minus-end motors (primarily dynein and kinesin-14) accumulate at spindle poles and provide an inward force (black arrows) that acts to both focus the poles and stabilize the bipolar structure. (D) If the primary outward force generating motor kinesin-5 or kinesin-12 is inhibited or depleted, outward sorting force is lost (red X) and inward force predominates (red arrows). This results in a collapse of the spindle structure and focusing of microtubule minus ends at the center of a monoaster. (E) If a primary inward force generating motor is inhibited or depleted, inward sorting force is lost (red Xs) and outward force predominates (red double-sided arrow). Without opposing inward force at spindle poles, the poles become splayed and the entire spindle structure elongates.

1.2.2. Nucleation from the outside-in

Microtubule nucleation in *C. elegans* oocytes is a particularly fascinating and open question. As I will describe in this work, oocyte spindle microtubules are organized adjacent to the disassembling nuclear envelope immediately after breakdown[48], forming a "cage-like" structure around the chromosomes. The canonical nucleation pathways found to be important in *Drosophila* and *Xenopus* appear to have little effect in *C. elegans* oocytes: there is no known augmin homolog[49], γ-tubulin does not localize to spindle microtubules[50–52], depletion of either γ-tubulin (TBG-1 in *C. elegans*) or Ran (RAN-1) do not have an effect on initial microtubule nucleation[52–55], microtubules in the initial "cage-like" structure do not appear to be nucleated in close proximity to chromatin[48], and the CPC is not required for microtubule nucleation or stabilization[56–58]. It should be cautioned that these results are not definitive and there are clues that perhaps these factors do play unappreciated roles. For

example, TBG-1 does not localize directly to spindle microtubules, but collects as a diffusive cloud around chromosomes, putting it in position where it could influence microtubule nucleation[52] by interacting with a reported "tubulin cloud" that forms immediately after nuclear envelope breakdown[59]. In addition, short-term RNAi depletion of RAN-1 shows a subtle phenotype, microtubules are nucleated but with a lower intensity[53], that may become more severe with complete depletion or inactivation using different methods. It is also possible that the inherent biophysical properties of *C. elegans* tubulin might render canonical microtubule polymerizing factors dispensable; *C. elegans* tubulin forms a 11-protofilament microtubule (as opposed to the canonical 13-protofilament) and has the fastest *in vitro* microtubule polymerization rate yet recorded, dwarfing that of bovine tubulin typically used in *in vitro* biochemical assays[60].

Similarly, initial microtubule nucleation in mouse oocytes is through an outside-in mechanism. Mouse oocytes contain discrete acentriolar microtubule organizing centers (MTOCs) that provide the first burst of microtubule nucleation during spindle assembly. Although they lack centrioles, MTOCs contain many proteins that are found in the pericentriolar material (PCM) that makes up a centrosome, and therefore MTOC activity is reminiscent of canonical centrosomes. For example, they contain the PCM components pericentrin[61–63], γ-tubulin[64–67], mouse γ-TURC (NEDD1)[68], Cep192[69], and TACC3[70]. A truly remarkable recent study in which localization of spindle proteins were systematically tested with immunofluorescence revealed 20 proteins localizing to MTOCs[71]. Before germinal vesicle breakdown (GVBD), MTOCs form *de novo* around the germinal vesicle and in the cytoplasm and initiate microtubule nucleation at the center of a microtubule aster[72]. MTOCs are surprisingly dynamic structures; they gradually decondense while increasing microtubule

nucleation ability[69,73] and are stretched and fragmented by dynein tethered to the nuclear envelope[69].

Upon GVBD, MTOCs are further fragmented[69] and congress towards chromosomes. MTOC decondensation, fragmentation, and microtubule nucleation ability are regulated by the kinases PLK1[69], Aurora A[74–76], and PLK4[77]. Strikingly, the story of microtubule nucleation doesn't end there. Once MTOCs fully congress towards chromosomes there is a surge of Ran-mediated microtubule nucleation to create what's termed the "microtubule ball"[72]. There has been some question if this nucleation event is truly Ran-mediated[78], however, a recent careful study using chemical inhibitors and a Ran double mutant showed that it is indeed dependent on Ran[79]. In agreement, most oocytes depleted of pericentrin and with dominant negative Ran are not able to nucleate any microtubules[63]. Ran mediated nucleation may proceed through the canonical TPX2 pathway, as depletion of TPX2 results in microtubule nucleation defects[70]. Recently, a phase separated structure termed liquid-like meiotic spindle domain (LISD) was identified[71]. Depletion of a core component of LISD, TACC3, resulted in smaller spindles and fewer microtubules, indicating the LISD plays a role in microtubule nucleation. How this structure cooperates in microtubule nucleation with MTOCs and the Ran pathway is unclear, but its presence underscores the recently emerging importance of phase-separated structures to both centrosomal and acentrosomal cell division[80–84].

Microtubule nucleation in human oocytes has only recently been investigated. Human oocytes form barrel-shaped spindles that are morphologically very similar to the other model organisms described[67,85–89]. However, quite surprisingly, human oocytes do not contain pericentrin based MTOCs and therefore have a different nucleation mechanism than mouse

oocytes. Instead, microtubules are nucleated primarily through the Ran pathway[87], although oocytes exogenously expressing dominant negative Ran showed delayed microtubule nucleation, suggesting redundant nucleation mechanisms may exist. Perhaps this secondary mechanism relies on γ-tubulin localized to spindle microtubules[67,89].

1.3. Microtubule organization and sorting

After microtubule nucleation a variety of forces cooperate to sort disorganized microtubules into an organized oocyte spindle. A bipolar spindle is typically thought to be organized with microtubule minus-ends clustered at poles and plus-ends extending from poles towards the chromosomes in the middle of the spindle (Figure 1.1B). The cell must physically organize microtubules to achieve and maintain this shape and the mechanisms underlying this force generation have been extensively studied in some organisms. The main force generating proteins performing this organizing function are the kinesin family of microtubule motors. Kinesins are ATPases that bind to microtubules with a globular motor domain and then hydrolyze ATP to induce a conformational shift that walks the protein along the microtubule[90]. There are many families of kinesins, which all perform different roles in the cell. The biochemical mechanisms underlying this movement are described later in this introduction, but first I will describe important *in vivo* cellular roles within the oocyte.

1.3.1. Kinesin based microtubule sorting

In most centrosomal systems, the kinesin-5 family of motors push apart the two centrosomes that form the poles of a bipolar spindle[91,92]. This important role for kinesin-5 to establish spindle poles holds true in *Xenopus* extract meiotic spindles, mouse oocyte spindles, and even in human oocyte spindles. This was first discovered in *Xenopus* extract spindles: newly

nucleated microtubules are translocated towards the spindle poles[17], and this sorting is dependent on kinesin-5 Eg5[93,94]. Immunodepletion[93] or chemical inhibition (with monastrol)[95] of Eg5 results in a monoaster; minus-ends of microtubules are no longer sorted outwards and form a single pole in the center of an aster (Figure 1.1D). Treatment of mouse oocytes with monastrol has a similar effect[96]. Kinesin-5 Kif11 in mouse oocytes fragments MTOCs immediately after GVBD[69] and then sorts MTOCs from the "microtubule ball" around chromosomes outwards to the spindle poles[72]. In human oocytes, treatment with monastrol causes spindle collapse into a "ball-like" structure[89,97], showing that essential kinesin-5 force generation is conserved between mouse and human oocytes.

C. elegans and *Drosophila* similarly rely on kinesin motors to sort microtubules during oocyte spindle assembly, however, the specific dependence on kinesin-5 force generation is not conserved. Force generation in *C. elegans* is most notably diverged. *C. elegans* kinesin-5, BMK-1, is completely dispensable for proper oocyte and mitotic spindle assembly[98]. The only phenotype thus far characterized in BMK-1 mutants or in BMK-1 depletion is a faster rate of chromosome segregation during anaphase in mitosis[99] and oocyte meiosis[100]. Instead, the kinesin-12 family is the dominant outward force generating motor during *C. elegans* meiosis. Depletion or mutants of *C. elegans* kinesin-12 KLP-18 results in monopolar spindles similar to the kinesin-5 depletion phenotype found in *Xenopus*, mouse, and human oocytes[56,101–104]. My work in this dissertation characterizes the molecular mechanism of KLP-18 force generation *in vivo* and *in vitro*. In *Drosophila* oocytes, the kinesin-5 KLP61F aids in generating proper spindle symmetry, but spindles remain bipolar through activity of kinesin-12 KLP54D and microtubule associated protein (MAP) ASP[105]. The main molecular determinant in this system is a different type of kinesin altogether: the kinesin-6 Subito[106]. Subito localizes to a ring around the karyosome and is essential to establish the central spindle

through its ability to bundle microtubules[107], which is in turn essential for spindle bipolarity[106,108]. There is significant crosstalk and interdependence between Subito and the CPC, and the CPC is essential for Subito localization to the karyosome and subsequent central spindle formation[29–31,108]. In mouse oocytes, the microtubule associated protein HURP[109,110] helps to assemble a central microtubule array on which kinesin-5 Kif11 can act to generate outward force[111], reminiscent of Subito's activity.

1.3.2. Microtubule architecture of acentrosomal spindles

Centrosomes help to nucleate long microtubules that often stretch from the centrosomal spindle pole to the chromosomes in the center of the cell[9,112,113]. This leads to a biased spindle organization that favors stable microtubule minus-ends at poles and dynamic plus-ends extending towards chromosomes. In oocytes lacking centrosomes, spindle organization, and the underlying microtubule architecture that defines it, is less clear. In the previous section I described the forces that act to push microtubules away from the chromatin-based area of nucleation, but the question remains: what is the resulting microtubule polarity of the bipolar acentrosomal spindle? Much of what we know about acentrosomal spindle architecture has been learned by studying spindles in meiotic *Xenopus* extract using a variety of innovative imaging techniques. For example, fluorescence speckle microscopy revealed that microtubule minus-ends are distributed throughout the meiotic spindle and that short microtubules were continuously nucleated and transported to poles, generating the original "slide and cluster" model for spindle assembly[114,115]. As opposed to mitosis where long microtubules extend through the spindle, short microtubules are tiled together to form longer microtubule bundles[116]. More recently, a different mechanism of assembly was proposed, where microtubules are nucleated non-uniformly along the spindle and that microtubule transport does not move short microtubules very long distances[117]. In either case, it is clear

that meiotic spindles have a fundamentally different microtubule architecture than mitotic spindles.

Spindles in *C. elegans* and *Drosophila* are also composed of a tiled array of short microtubules. Microtubules in a *Drosophila* oocyte spindle are of a mixed polarity throughout the spindle[118] and electron tomography of *C. elegans* oocyte spindles showed that short microtubules are tiled in a mixed orientation to generate spindle-scale microtubule bundles[119]. Long microtubules are severed by the homolog of the microtubule severing ATPase katanin, MEI-1[120–126]. MEI-1 mutants and depletions have also shown defects in microtubule bundling and pole assembly[102,127]. Through a beautiful combination of mutant analysis using *in vitro* microtubule severing assays and spindle length measurements *in vivo*, it was shown that MEI-1 microtubule severing activity is directly proportional to spindle length; lower biochemical severing activity led to unusually long spindles[128]. Once short microtubules are generated by MEI-1, they are likely bundled by kinesin-14 KLP-15/16 into tiled arrays. Depletion of KLP-15/16 results in completely disorganized and unbundled microtubule "balls" during spindle assembly[129]. Spindle architecture in mouse oocytes has not been closely investigated, and it will be interesting to learn if the centrosome-like MTOCs produce a spindle with long mitosis-like microtubules or if these spindles instead contain a tiled array.

1.4. Building spindle poles and stabilizing bipolarity

As microtubules are sorted away from the area of nucleation, they must be bundled and stabilized to ensure the structural integrity of the spindle and to maintain stable microtubule attachments to the chromosomes (Figure 1.1C). There is complicated interplay between microtubule associated proteins and microtubules that generate the highly ordered spindle. Computer simulations have predicted a model in which microtubules are continually

polymerized near chromosomes[115] or within the spindle[117] then are sorted by plus-end directed motors to the spindle poles where they are clustered by minus-end directed motors of opposing force[130]. To maintain a relatively consistent number of microtubules within the spindle, microtubules are also depolymerized at poles[115,131]. Three key prediction of this model are: 1. there is a constant force pushing microtubules outwards, even when spindle length remains constant; 2. proteins bundle and focus microtubules into discrete poles; and 3. there is significant microtubule depolymerizing activity at the poles. Experimental data has broadly supported this model and I will describe the key molecular players that fulfill these predictions.

1.4.1. A balance of forces maintain spindle bipolarity

Microtubule poleward flux in *Xenopus* extract was first characterized when pre-formed polarity marked microtubules were added to spindle reactions and the minus-ends moved to the pole[132]. Much like initial microtubule sorting during spindle assembly described in the previous section, the sorting forces that maintain spindle bipolarity are generated by kinesin motors. Much of the work done investigating these forces was performed on spindles nucleated around sperm DNA added to *Xenopus* egg extract arrested in meiosis II[133]. Sperm DNA contains centrioles that recruit PCM from the extract and therefore the spindle contains centrosomes. Although not strictly an acentrosomal system, discoveries using this method have informed our understanding of spindle architecture and dynamics. Acute inhibition of kinesin-5 Eg5 in this extract results in spindle collapse[95], showing that Eg5 is not only essential for spindle formation but also for persistent spindle bipolarity. The two main spindle pole focusing proteins in *Xenopus* are NuMA and dynein. In sperm DNA spindles from meiotic extract, dynein and NuMA translocate to the spindle pole where they both act to focus microtubule minus-ends[132,134,135]. When dynein is depleted, spindle poles fray and

become unfocused[17,93,132,136]. In addition, the minus-end directed kinesin-14 XCTK2 works with dynein to focus poles[93]. Augmin depletion results in pole defects, indicating microtubule polymerization at the poles may be important for spindle stability[45]. These factors all cooperate to generate an inward force to oppose the Eg5-generated outward force and this balance of forces is essential to maintain correct spindle morphology. When outward force is removed, microtubule minus-ends collapse inward; when inward force is removed, spindles lengthen and poles become unfocused and splayed (Figure 1.1D,E). Interestingly, when both Eg5 and dynein are depleted before initiation of spindle assembly, bipolar spindles can still form[136], indicating that back up mechanisms exist that can generate sufficient forces.

Proteins that help to build and stabilize spindle poles in *Xenopus* function similarly in other organisms. In *C. elegans*, there is significant cooperation between dynein, microtubule minus-end binding protein ASPM-1[137], and katanin (MEI-1). MEI-1 appears to be the defining pole protein: when MEI-1 is depleted, ASPM-1 does not localize to microtubule ends[102,127,128], but conversely, MEI-1 does not require ASPM-1 for spindle localization[128]. ASPM-1 depletion leads to unfocused poles[56] and is essential for dynein localization to the pole[138]. In kinesin-14 KLP-15/16 depletion, ASPM-1 is localized diffusely to a ball-like spindle that does not form discrete poles[129]. Spindles partially depleted of dynein show long, tapered poles[104] and other spindle morphology defects[139]. A recent study has shown that mammalian homologs of ASPM-1 directly interact with katanin to mediate microtubule disassembly at spindle poles[137], further confirming the interplay between these two proteins. ASPM-1 and dynein depletion resulting in long, tapered, and unfocused poles show the consequence of removing inward forces: the balance of forces is disrupted and the outward forces dominate, pushing microtubules past the poles without impediment. In this work, I will show that *C. elegans* kinesin-12 KLP-18, in addition to its essential role in initial

microtubule sorting during spindle assembly, also supplies essential outward force to maintain spindle bipolarity.

Drosophila bipolar spindles require kinesin-5 KLP61F to maintain spindle bipolarity[140]. What is providing the opposing inward force? The main player at *Drosophila* oocyte spindle poles is the minus-end kinesin-14 Ncd. In Ncd mutants, spindle poles splay and result in a multipolar spindle[37,141]. As a minus-end directed motor, Ncd is thought to be involved in the transport of other spindle pole focusing factors like D-TACC[142], minispindles[142], HURP[28], and augmin[35] to the poles. Asp, homolog of *C. elegans* ASPM-1, is also present at poles[143] along with γ-tubulin[43]. Generally, depletion of these pole proteins result in either unfocused and tapered poles or multipolar spindles.

Similar to *Xenopus*, *C.elegans*, and *Drosophila*, the major outward force generating motor that acts during spindle assembly is also essential to maintain bipolarity in mouse oocytes. Bipolar spindles show a clear poleward flux, and kinesin-5 Kif11 is essential to maintain this flux and as a result, spindle length[144]. When bipolar spindles are treated with the kinesin-5 inhibitor monastrol, spindles shrink until they form a monopolar spindle or a disorganized microtubule array. It is unclear what the predominant minus-end directed motor is; however, based on results in other species, one can reasonably hypothesize that dynein plays an important role although this has not yet been directly tested. Depletion of the minus-end directed kinesin-14 HSET leads to defects in bipolar spindle formation and MTOC clustering at the spindle poles[145], indicating a role for this minus-end motor. Most of the work investigating spindle poles in mouse oocytes has focused on the factors regulating MTOC activity. The Aurora kinase family has been shown to regulate MTOC clustering[75,146], architecture[147], and activity[148]. Additionally, the pole proteins ASPM (homolog to *C. elegans* ASPM-1) and NuMA also have important roles in pole focusing: knockdown of either ASPM

or NuMa results in elongated spindles[149,150], with ASPM functioning through an interaction with calmodulin[149] similar to the *C. elegans* ASPM-1 interaction with calmodulin[138].

Human oocytes share similar force generation mechanisms with mouse oocytes. NuMA is present at spindle poles[151], and when centrosomes are experimentally depleted in human somatic cells, NuMA and dynein localize to a monopolar-like spindle assembly intermediate then are sorted to spindle poles by kinesin-5[97]. In addition, metaphase II arrested human oocyte spindles collapse into a monopole upon treatment of kinesin-5 inhibitor monastrol[152], indicating that kinesin-5 is essential to maintain spindle bipolarity. This is somewhat surprising because kinesin-5 is not essential to maintain spindle bipolarity in many mitotic somatic cell types[153], even while it is essential for initial centrosome separation and spindle assembly[154]. Therefore, it seems as if acentrosomal spindles require unique force generation properties to maintain bipolarity, possibly due to the lack of stabilizing astral microtubule interaction with the cell cortex.

Finally, the microtubule destabilizer kinesin-13 MCAK is also present at spindle poles and inhibition results in larger spindles in *Xenopus* extract[136]. The role of the *C. elegans* MCAK homolog, KLP-7, on the meiotic spindle is fairly well characterized. KLP-7 mutants result in an overabundance of spindle microtubules and spindles with multiple poles[59,155], potentially through a mechanism involving the kinetochore[103] or phosphorylation by Aurora kinases[156]. Maintaining the correct spindle size is particularly important for oocyte spindles because they are small relative to the oocyte itself. In fact, kinesin-13 has been proposed to be a major molecular determinant of spindle size across *genus*[157], showing the importance of microtubule depolymerizing activity.

1.5. Biochemical basis of force generation

Building an acentrosomal spindle requires the action of many molecular players, each using its biochemical properties to sort, bundle, and depolymerize microtubules to generate cell-scale forces. Therefore, much research has aimed to understand how different molecular motors function in isolation *in vitro*. This biochemical work makes predictions about how motors function within the cell and allows us to piece together how each motor's specific biochemical traits work in concert to organize a functional spindle. As I have described previously, acentrosomal spindles are formed through a combination of outward and inward forces. Outward forces, typically mediated by kinesin-5 or kinesin-12, push microtubules away from the points of nucleation near the chromosomes. Inward forces, typically driven by dynein and kinesin-14 along with non-motor microtubule bundlers, focus these microtubules into poles and constrict spindle size. Because they are most relevant to my work, I will focus on outward force generating motors in this section and I will not discuss the biochemical properties of inward force generating motors. Many reviews are available that describe the biochemical activity of dynein[158–161] and kinesin-14s[162–165] in great detail.

Almost all mechanistic dissection of kinesin-5 and kinesin-12 function has been performed within centrosome based cell division in somatic cell culture, underscoring the need to investigate these motors in an acentrosomal context. These studies have shown that kinesin-5 is essential for mitotic spindle bipolarity in many systems[91,92,95]. Initially, kinesin-12 was thought to be a dispensable motor because inhibition or depletion did not yield a noticeable phenotype, however, recently it was discovered that kinesin-12 can substitute for kinesin-5 function when kinesin-5 is inhibited[166,167]. Kinesin-5 is a common target of chemotherapeutics and cancer cells have the surprising ability to adapt and bypass kinesin-5 inhibition[168]. Spindle assembly driven by kinesin-12 is thought to allow cancer cells to bypass cell death

and therefore drug treatment[169], so it is important to understand the mechanism underlying kinesin-12 mediated force generation. Because of this newly appreciated importance of kinesin-12 activity and my focus on characterizing the kinesin-12 in *C. elegans*, KLP-18, I will focus mainly on describing kinesin-12 biochemistry after a brief overview of kinesin-5.

A Kinesin-5

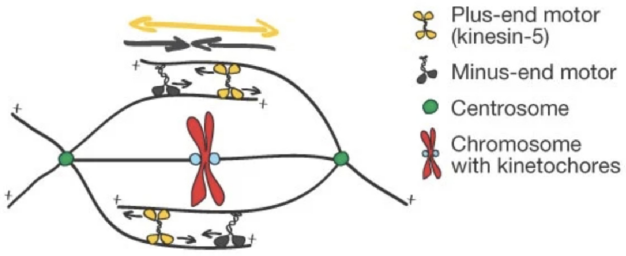

B Kinesin-12/Kif15: dimer model

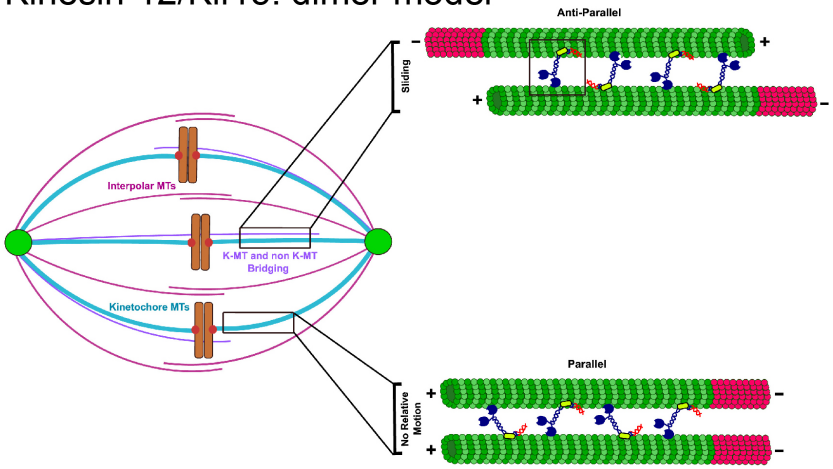

C Kinesin-12/Kif15: tetramer model

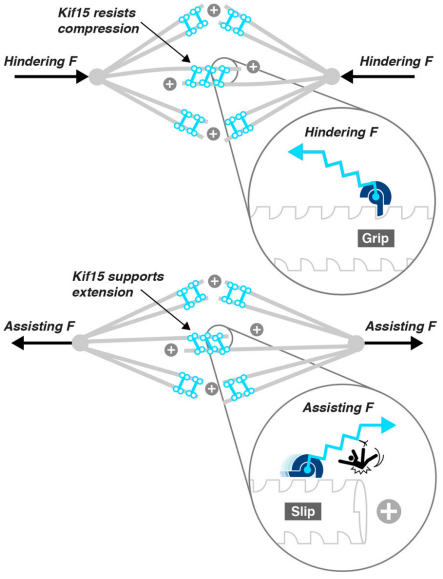

Figure 1.2

Figure 1.2. **Biochemical models for kinesin-5 and kinesin-12/Kif15 force generation.** (A) Kinesin-5 (yellow) forms a homotetramer and binds antiparallel microtubules with bipolar motor domains. By walking to the plus ends of each antiparallel microtubule, kinesin-5 pushes microtubule minus ends towards the poles and generates an outward force (yellow arrow). The contribution of minus-end motors (gray, gray arrows) is also shown. Figure adapted from Kapitein *et. al.*[170]. Mammalian kinesin-12, Kif15, has been proposed to act as a homodimer (B) and as a homotetramer (C). (B) In the dimer model, Kif15 binds to antiparallel microtubules through the motor domain and a non-motor stalk microtubule binding site (yellow oval on Kif15 cartoon). A Kif15 dimer generates force by walking to the plus end of one microtubule with its motor domain and statically 'pulling' the second microtubule to sort its minus end outwards. Kif15 dimer generates force when crosslinking antiparallel microtubules (right, top) but not when crosslinking parallel microtubules (right, bottom). Adapted from Reinemann *et. al.*[171]. (C) In the tetramer model, Kif15 associates to microtubules in a similar way as kinesin-5 described in (A). It is proposed to act as a 'mechanical ratchet': it resists inward spindle compression by gripping hindering force (top), and supports outward spindle extension by allowing assisting force (bottom). Adapted from McHugh *et. al.*[172].

1.5.1. Kinesin-5 biochemistry in brief

In human somatic cell culture, kinesin-5 localizes primarily to antiparallel non-kinetochore microtubules where it generates a sliding force to push microtubule minus-ends outwards[170,173–175]. To perform this function, kinesin-5 acts as a bipolar homotetramer (forming a dumbbell shape) that slides antiparallel microtubules by binding two microtubules and walking towards both plus-ends simultaneously[91,170,176] (Figure 1.2A). This sliding activity has been shown in kinesin-5s in *Drosophila*[177] and yeast[178,179], indicating that it is a well conserved phenomenon. Individual homodimers of kinesin-5 dimerize (to form a homotetramer) through interaction of a BASS domain composed of antiparallel coiled-coil helices in the stalk of the protein[180,181]. Importantly, kinesin-5 motor activity is sensitive to chemical inhibition; the drug monastrol was found to selectively inhibit kinesin-5 ATP hydrolysis and therefore motor activity[95] by binding in close proximity to the important loop 5 in the motor domain[182]. In addition, kinesin-5 contains a non-motor globular tail at its C-terminus that is required for microtubule crosslinking and sliding[183]. Very recently it was reported that this tail domain directly interacts with the adjacent motor domain and stabilizes the motor in an ATP-bound state, allowing the motor to generate greater force on spindle microtubules[184].

1.5.2. Kinesin-12 function *in vivo* and *in vitro*

Under pharmacological inhibition of kinesin-5, kinesin-12 Kif15 can generate sufficient force to mediate spindle assembly when ectopically overexpressed in mammalian somatic cell culture[166,167]. Stunningly, cells treated with gradually increasing amounts of kinesin-5 Eg5 inhibitor STLC (a derivative of monastrol[185]) can develop resistance to STLC and divide in complete absence of Eg5 activity[186]. Kif15 is activated in this cell type, termed EICs (Eg5 independent cells)[186–188], through phosphorylation by Aurora A[189]. Careful analysis

of motor localization showed that in normal Eg5 dependent cells, Kif15 localizes primarily to kinetochore microtubules (kMTs), the long stable bundle of parallel microtubules spanning from the centrosome to a chromosome's kinetochore, and kinesin-5 localizes primarily to non-kMTs, antiparallel bundles important for spindle stability[173,190]. Kif15 depletion in cells normally expressing Eg5 have slightly shorter spindles[166] but are otherwise morphologically normal. In EICs, Kif15 is overexpressed and re-localizes to non-kMTs, potentially to generate an Eg5-like force on anti-parallel microtubules similar to what is described in the previous section. It was later found that EICs can naturally acquire a mutation in the kinesin-5 motor domain that result in a rigor motor[168]: the motor is able to bind to microtubules but unable to hydrolyze ATP and therefore cannot generate force through its movement. In these cells, the kinesin-5 rigor motor bundles non-kinetochore microtubules thereby creating the proper microtubule substrate for Kif15 re-localization and force generation without the need for the cell to overexpress Kif15. These results suggests that the main mechanism of Kif15 replacement of kinesin-5 function during spindle assembly is through re-localization from parallel kMTs to highly bundled anti-parallel non-kMTs. After a bipolar spindle forms, kinesin-5 is often dispensable to maintain spindle bipolarity and cells rely on kinesin-12 action on kMTs to stabilize bipolarity[153,167,191].

Considering the *in vivo* activity just described, one might assume that Kif15 has a similar molecular architecture and biochemical properties as kinesin-5. Surprisingly, Kif15 seems to be a much more complicated molecule with unique aspects that differentiate it from kinesin-5. One prevailing model is that Kif15 acts as a homodimer and contains a C-terminal microtubule binding site in a coiled-coil domain[168,171,192] (Figure 1.2B). In this model, Kif15 binds a microtubule as cargo in a non-motor region in the middle of its stalk domain but only when an inhibitory C-terminal coiled-coil is unfolded. In this way, the stalk domain

of Kif15 can fold and self-inhibit stalk microtubule binding. In the cell, the motor exists in an inactive folded state and an active unfolded state, and is only active when it is able to crosslink microtubules with both its motor domain and its stalk binding domain. The active motor preferentially acts within highly bundled kMTs[173,192]. Careful biochemical analysis using an optical trap to measure force generation of the Kif15 dimer showed that the stalk microtubule binding site can bear significant load during motility and, surprisingly, that the motor generates force on anti-parallel microtubules but not parallel microtubules[171]. The authors present a model in which Kif15 dimers act to statically bundle parallel microtubules in kMT bundles and act to tether kMTs with non-kMTs. It is on this anti-parallel microtubule orientation that the motor walks and generates forces on the spindle. This hypothesis is in line with *in vivo* data showing Kif15 primarily acts on kMTs in unperturbed cells.

A second and somewhat contradictory model is that Kif15 acts a homotetramer, a similar molecular construction as kinesin-5[172,193–195] (Figure 1.2C). TIRF (total internal reflection fluorescence) microscopy of single GFP-tagged Kif15 molecules showed the motor can crosslink short microtubules and transport them as cargo, switch microtubule tracks when microtubules are intersected, and even move in the minus-end direction[193,195]. Kif15 tetramer is more active on a parallel microtubule substrate and is able to sort microtubules into parallel bundles[194]. In addition, Kif15 tetramer can track polymerizing plus ends and suppress microtubule catastrophe, further explaining its function on parallel kMTs in cells. It has been proposed that Kif15 as a tetramer acts a "mechanical ratchet" by providing resistance to opposing inward force but not resisting assisting outward force[172] (Figure 1.2C). This model predicts that during spindle assembly, as microtubules are being sorted outwards by kinesin-5, Kif15 neither contributes to this force nor opposes it. However, once the spindle is assembled and bipolarity must be maintained, Kif15 locks into kMTs and opposes inward

forces to prevent spindle collapse. Interestingly, specific to the tetramer model, the adaptor protein TPX2 plays a large role. *In vivo*, TPX2 is essential for kinesin-12 localization to the spindle in both human cells[166,167] and in *Xenopus* extract[196]. The very C-terminus of TPX2 is essential for interaction with Kif15 and to target the motor to the spindle[195]. *In vitro*, TPX2 slows Kif15 motility[172,193] by binding to microtubules and creating a "roadblock" that requires the C-terminus of TPX2[195]. Conversely, it has been proposed that Kif15 acting as a dimer does not require TPX2 to function[192]. This discrepancy is likely due to the dimer and tetramer forms using fundamentally different biochemical mechanisms to generate force. Kinesin-5, a tetramer, is regulated *in vitro* by TPX2 in a similar way: TPX2 binds to microtubules and dampens kinesin-5 motility through an interaction in its C-terminus[197–199]. Interestingly, when visualizing GFP tagged endogenous kinesin-5 and TPX2, the proteins localize to different areas of the spindle[200], showing that there is much to learn about the spatial regulation of both of these proteins. Kif15 is also regulated by binding of a different accessory protein, KBP, which leads to mislocalization of Kif15 when overexpressed and slowing of motor velocity *in vitro*[201] through interaction with the Kif15 motor domain[202].

It is clear that the vast majority of work exploring kinesin-12 biochemistry and function has been done in mitotically dividing human somatic cells. Only a few papers describing the function of kinesin-12 in other systems exist, and therefore it is unclear how divergent or similar properties of kinesin-12s are across organisms. In addition, kinesin-12 has not been studied in any acentrosomal meiotic system. This is significant because kinesin-12 activity seems to be highly dependent on underlying microtubule architecture (kMT vs non-kMT, for example) and as I have described previously, meiotic spindles have a fundamentally different microtubule architecture than mitotic spindles. In this work, my main goal has been to characterize kinesin-12 activity in not only a unique organism, but also in a unique cell

type. I have utilized the nematode *C. elegans* for reasons described in the next section.

1.6. *C. elegans* as a model to study cell division

The self-fertilizing hermaphroditic worm *Caenorhabditis elegans* is a particularly powerful model organism to study the acentrosomal oocyte divisions. Each worm lays 250 eggs over its relatively brief 3-4 days of gravid adulthood, allowing for rapid characterization of a large population of oocytes. Moreover, once oocytes are fertilized, the resulting embryos serve as a powerful system for studies of the mitotic divisions[203]. Many proteins involved in both mitosis and meiosis are conserved between *C. elegans* and higher organisms, and the rapid reproductive rate allows for detailed characterization of cell division processes. In this section, I will introduce *C. elegans* as a model system and highlight several experimental advantages to using this worm to study acentrosomal spindle assembly and maintenance.

A major advantage of *C. elegans* is the variety of available genetic tools (reviewed in[204]). The worm is amenable to forward and reverse genetic approaches that can be used to dissect the molecular mechanisms of important cellular processes. The discovery of RNAi in *C. elegans* (reviewed in[205]) has been particularly impactful for the study of cell division, since this technique makes it straightforward to study genes essential for development by depleting proteins from adult worms and then looking for defects in their oocytes and embryos. Therefore, genome-wide and targeted RNAi screens have been performed to discover proteins involved in the mitotic[206–208] and meiotic divisions[56].

A second advantage of *C. elegans* is the ability to tag proteins of interest with fluorescent proteins, and then investigate their dynamics in the live cell (reviewed in[210]). Fluorescent proteins can be integrated into the genome for germline expression in a variety of ways, including inserting transgenes through MosSCI transposon-mediated transgenesis[211,212], and

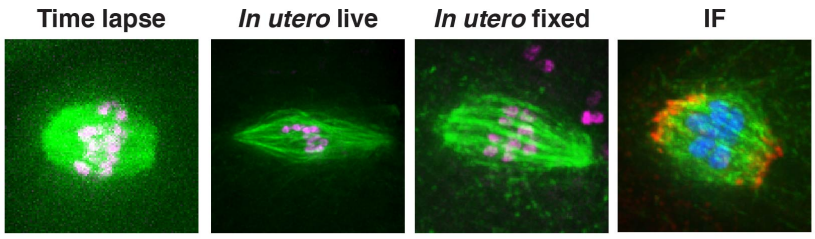

	Time lapse	*In utero* live	*In utero* fixed	IF
Time resolution	+	-	-	-
Germline position	+	+	+	-
Protein localization (3+ channels)	-	-	-	+
Requires fluorescent protein expression	+	+	+	-
High-resolution structural information	-	+	+	++
Large scale experiments	-	+	+	+

Figure 1.3. **Comparison of common imaging techniques used with *C. elegans* oocytes and embryos.** The advantages and limitations of various imaging techniques are presented in the chart. A representative image of a bipolar oocyte meiotic spindle is also displayed for each technique; a strain expressing GFP::tubulin and mCherry::histone was used. Methods for *in utero* live, *in utero* fixed, and immunofluorescence are presented in Chapter 5 and more extensively in Appendix A. Extensive methods for timelapse imaging were recently described and can be found in[209].

by using CRISPR-based genome editing to tag a protein of interest at its endogenous locus[213–215]; a thorough review of these and other *C. elegans* transgenic tools has been recently published[204]. Because worms are transparent, fluorescent proteins can be imaged in a live oocyte or embryo either *in utero* or *ex utero*; these methods have been widely applied to investigate protein dynamics with high temporal resolution (method recently described in[209]). However, one drawback to live imaging is that it can be time consuming and labor intensive. Moreover, since subjecting worms to high amounts of light often causes cells to arrest, the exposure times and the number of z-stacks acquired must be minimized, limiting the resolution of the resulting movies.

Given these challenges, it is often advantageous to pair time lapse imaging with other methods that enable higher resolution imaging and/or higher throughput analysis for quantification of phenotypes (Figure 1.3). One alternative is to image fluorescent proteins in intact worms at high resolution by increasing exposure times and acquiring more z-stacks. For this procedure, worms can either be fixed in ethanol, which preserves the fluorescence of tagged proteins, or live worms can be anesthetized. In the latter case, since the imaging conditions halt cell cycle progression, this type of "live" imaging is analogous to fixed, in that it provides high resolution snapshots of particular stages rather than dynamic information. Regardless, an advantage of these approaches is that a large number of images can be easily acquired, making these techniques higher throughput than time lapse imaging.

Another advantage of imaging oocytes and embryos in intact worms is that the organization of the *C. elegans* gonad makes it possible to correlate chromosome and spindle morphology with different stages of meiotic progression, based on the cell's position within the germ line (Figure 1.4). The *C. elegans* gonad contains two arms, each independently generating gametes. At the distal tip of each arm, there is a population of mitotically-dividing germline stem cells; as cells move away from this niche, they transition into meiosis and then proceed through the events of meiotic prophase I (e.g., homolog pairing and recombination) as they travel towards the proximal end of the germ line. In hermaphrodites, sperm are produced first and are packaged into the spermatheca, where they are stored; worms then switch to producing oocytes. Oocytes thus progress in a "production line" fashion towards the spermatheca, where they encounter sperm. Fertilization triggers nuclear envelope breakdown (at the "-1" position of the germline), and spindle assembly proceeds as the cell moves through and then exits the spermatheca (moving into the "+1" position). As the meiotic divisions end and the mitotic divisions begin, embryos have typically moved further down

this production line (into the +2 and +3 positions). Thus, imaging intact worms has the advantage of maintaining the oocyte or embryo position in the germ line, which is useful when assessing and quantifying mutant/depletion phenotypes. For example, since spindles are usually bipolar by the time the oocyte is in the +1 position, if a large percentage of oocytes in this position have disorganized spindles in a particular mutant, it would suggest that spindle assembly is either slowed or prevented (for examples of this type of quantification, see[129] and later chapters).

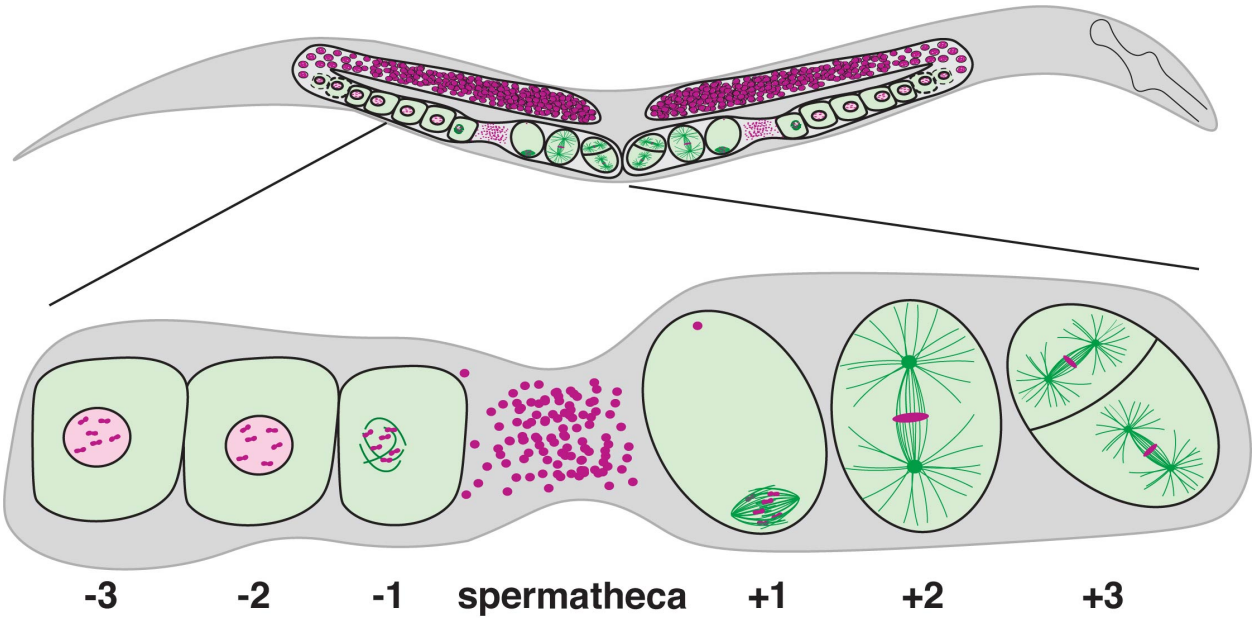

Figure 1.4. **Schematic of the *C. elegans* germ line.** Body of the worm is shown in grey, germ line is outlined, tubulin shown in green, and DNA shown in magenta. *C. elegans* are self-fertilizing hermaphrodites that contain both oocytes and sperm. Germ cells differentiate in the distal end of the gonad and then proceed through the stages of meiotic prophase I as they move towards the spermatheca. Once oocytes are in proximity to the spermatheca (in the -1 position), they are fertilized. Upon fertilization, the oocyte moves through the spermatheca and into the +1 position and the meiotic divisions proceed. The first mitotic divisions of the embryo then occur within the worm before the egg is laid. Oocytes in the zoomed diagram are shown progressing from left to right; magenta dots in the spermatheca represent condensed sperm nuclei.

Another complementary method is fixed-cell immunofluorescence, which also allows for high resolution imaging to gain precise structural information about spindle architecture. Although this technique eliminates positional information because it requires dissecting cells out of the worm to ensure efficient antibody staining, it still has a number of advantages. Notably, immunofluorescence eliminates the need for genetically-tagging proteins, and also enables the simultaneous visualization of three or more proteins in a single cell, facilitating studies of protein localization. This technique has therefore been especially useful in assessing the dependencies of particular proteins for proper localization and our lab has used it extensively to characterize spindle and chromosome architecture in oocytes (for examples see[48,56,104,129,216,217]). In the following chapters, I will use these imaging techniques along with *in vitro* biochemical assays to investigate the molecular mechanisms underlying oocyte spindle assembly and maintenance in *C. elegans*. Specifically, I aimed to characterize the stages of oocyte spindle assembly, the molecular mechanisms underlying the activity of essential proteins KLP-18 and MESP-1, and the biochemical basis for KLP-18 force generation and activation by MESP-1.

CHAPTER 2

Assembly of *Caenorhabditis elegans* acentrosomal spindles occurs without evident microtubule-organizing centers and requires microtubule sorting by KLP-18/kinesin-12 and MESP-1

This chapter has been adapted from my publication in Molecular Biology of the Cell[48]*. All experiments were performed by me unless otherwise specified in the figure legends.*

2.1. Introduction

During mitosis and male meiosis, duplicated centrosomes nucleate microtubules and then separate to opposite sides of the cell, forming the poles of a spindle capable of aligning and segregating chromosomes[13]. However, in female reproductive cells (oocytes) of many species, centriole-containing centrosomes are degraded before the meiotic divisions[218]. We are interested in understanding the mechanisms by which microtubules are organized into a bipolar spindle in their absence.

In mouse oocytes, spindle assembly involves multiple acentriolar microtubule-organizing centers (MTOCs), which are believed to functionally replace centrosomes. These MTOCs are small asters of microtubules that contain pericentriolar material (PCM) components at their center, including pericentrin and γ-tubulin[61,64,66], and they have been proposed to serve as major sites of microtubule nucleation. Live imaging studies have shown that greater than 80 of these MTOCs form in the cytoplasm, coalesce to the outside of the nucleus, and then are incorporated into the meiotic spindle, leading to the model that self-organization of these structures drives acentrosomal spindle assembly in mammalian oocytes[69,72]. Similar asters have also been observed in *Drosophila* oocytes[27], raising the possibility that this feature of acentrosomal spindle assembly is conserved. However, several lines of evidence support the view that acentrosomal spindle assembly does not absolutely require participation from MTOCs. First, a number of studies in *Drosophila* have not reported the formation of MTOCs and instead demonstrate that microtubules are nucleated in the vicinity of chromosomes[26,29]. Moreover, MTOC asters have not been observed during acentrosomal spindle formation in either *Xenopus* egg extracts or human oocytes, strengthening the idea that alternative strategies exist. In *Xenopus* extracts, spindle assembly involves microtubule nucleation in the vicinity of chromatin followed by motor-driven reorganization of these microtubules

into a bipolar structure[17,93]. However, because this is an *in vitro* system, it is possible that additional mechanisms may also contribute *in vivo*. In humans, microtubules also appear to nucleate in the vicinity of chromosomes[87], but the molecular mechanisms driving spindle assembly in these cells are poorly understood due to difficulties in obtaining and experimentally manipulating human oocytes.

Caenorhabditis elegans represents an ideal *in vivo* model in which to study acentrosomal spindle assembly since it is an experimentally tractable system that is amenable to live imaging of the meiotic divisions. To understand more about the molecular mechanisms driving spindle assembly in *C. elegans* oocytes, we previously performed an RNA interference (RNAi) screen and identified KLP-18 (kinesin-12) and the novel protein meiotic spindle 1 (MESP-1) as essential for acentrosomal spindle bipolarity. When either of these proteins was depleted, monopolar instead of bipolar spindles formed[56]. However, when and how these proteins act to promote bipolarity during acentrosomal spindle assembly are not understood.

In this study, we gain insight into these questions by first defining how acentrosomal spindles form in *C. elegans* oocytes and then investigating the roles of KLP-18/kinesin-12 and MESP-1 in this process. We find that in contrast to a recently proposed model[14,103], *C. elegans* oocyte spindles do not assemble via the nucleation and coalescence of MTOC asters, bolstering the idea that acentrosomal spindle formation does not universally require these structures. Instead, our findings are consistent with a model in which KLP-18 and MESP-1 sort microtubules of mixed polarity into a configuration in which their minus ends can be gathered into two oppositely oriented poles. We find that MESP-1 and KLP-18 are interdependent for localization and can interact, suggesting that they work together to perform this function. This work therefore sheds light on mechanisms by which acentrosomal spindles achieve bipolarity in *C. elegans*. Moreover, our findings establish *C. elegans* as a

model for *in vivo* investigation of pathways of acentrosomal spindle assembly that do not involve MTOC asters, which may provide future insight into mechanisms used by human oocytes.

2.2. Acentrosomal spindle assembly proceeds by microtubule nucleation followed by formation and coalescence of multiple poles

We set out to investigate the stages of acentrosomal spindle assembly *in vivo* using a strain expressing green fluorescent protein (GFP)–tubulin and GFP-histone to visualize microtubules and chromosomes, respectively (Figure 2.1A). Although meiotic spindle assembly was visualized in live worms in many previous studies[52,54,102,103,124,139], those experiments used conditions optimized to allow long-term filming, which limited the number of images that could be obtained at each time point without affecting viability, thereby limiting the number of z-stacks and the resolution of spindle structures. Therefore we took the complementary approach of acquiring high-resolution *in vivo* images representing each of the different stages of spindle assembly. We then ordered images into a spindle assembly pathway using three temporal markers: 1) the position of the oocyte within the gonad (since this position correlates with progression through meiosis), 2) the position of the chromosomes within the oocyte (since the chromosomes start in the center of the cell and move to the cortex as the spindle forms), and 3) the shape of the cell (since the morphology changes upon ovulation and again as the eggshell forms). We also quantified the types of microtubule structures we observed at specific locations in the gonad (Figure 2.2) and compared our images to our (Figure 2.1B) and published[52,54,102,103,124,139] lower-resolution time-lapse movies for additional confirmation. Our imaging has more precisely documented how microtubules form and reorganize during the process of acentrosomal spindle assembly *in vivo*.

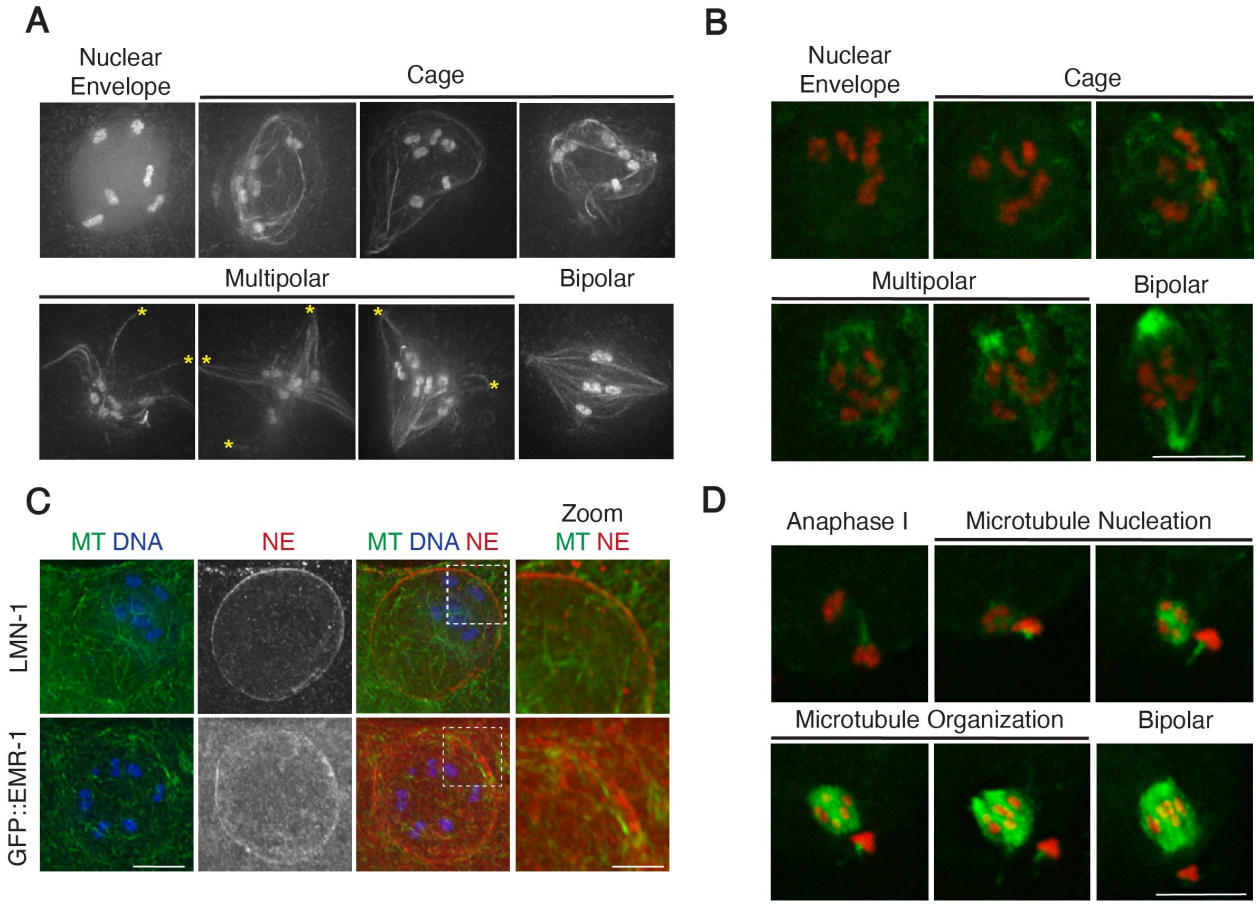

Figure 2.1. **Acentrosomal spindle assembly in meiosis I proceeds through a cage and multipolar stage.** (A) In vivo imaging of oocytes expressing GFP-tubulin and GFP-histone. After NEBD, a microtubule cage forms before microtubules are sorted into multiple nascent poles (asterisks) that coalesce until bipolarity is achieved. (B, D) Stills from movies capturing meiosis I (B) and meiosis II (D) spindle assembly in oocytes expressing GFP-tubulin and mCherry-histone. A microtubule cage does not form in meiosis II. (C) Fixed oocytes stained for tubulin (green), DNA (blue), and a nuclear envelope (NE) marker (red); top, LMN-1; bottom, GFP::EMR-1. Zooms show cage microtubule bundles adjacent to and within the nuclear envelope. Scale bars, 5 μm (full images), 1.25 μm (zoom). (A) performed by Sadie Wignall, (B) and (D) performed by Tim Mullen.

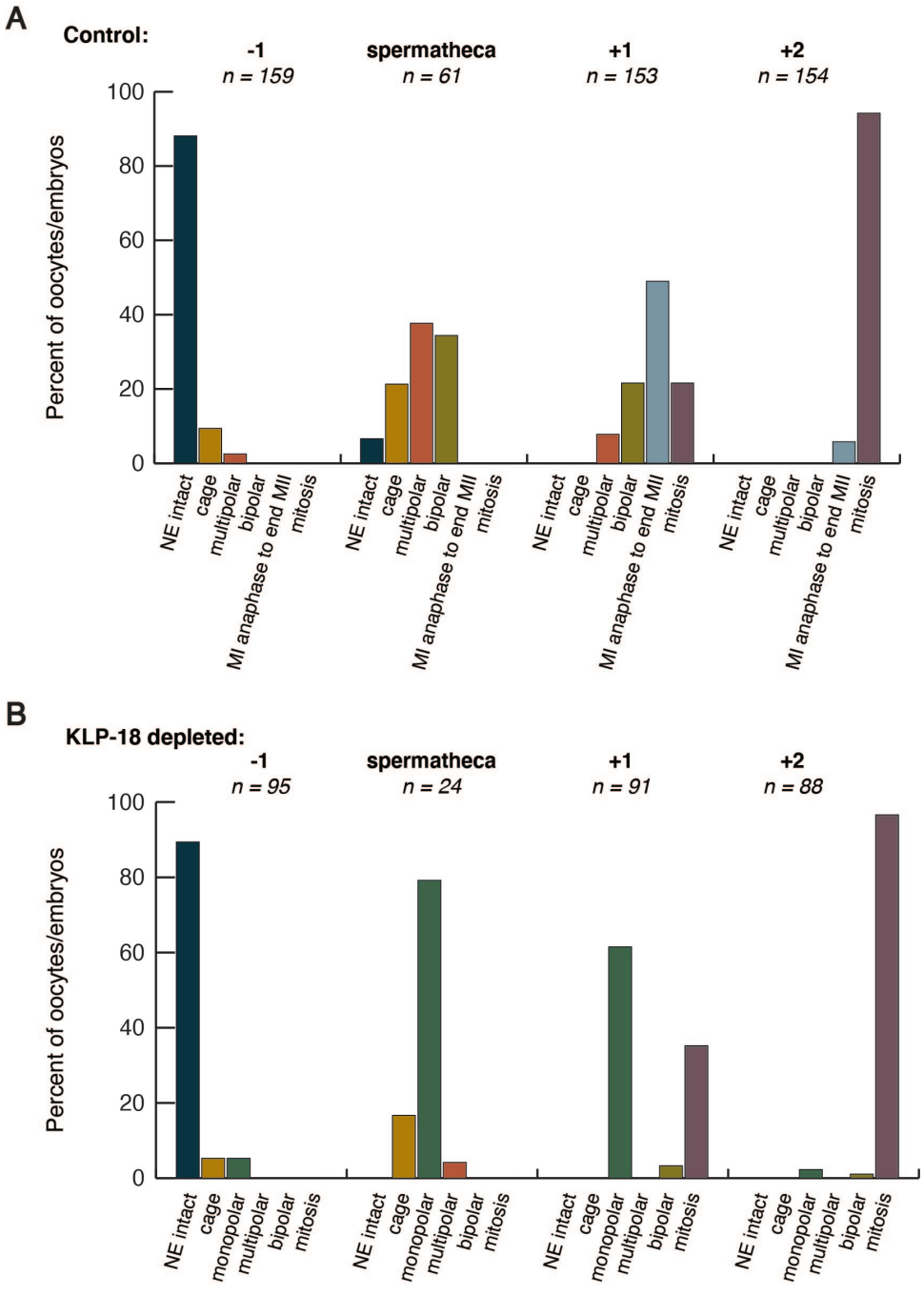
A
Control:
-1
n = 159
spermatheca
n = 61
+1
n = 153
+2
n = 154
Percent of oocytes/embryos
100
80
60
40
20
0
NE intact
cage
multipolar
bipolar
MI anaphase to end MII
mitosis
B
KLP-18 depleted:
-1
n = 95
spermatheca
n = 24
+1
n = 91
+2
n = 88
Percent of oocytes/embryos
NE intact
cage
monopolar
multipolar
bipolar
mitosis

Figure 2.2

Figure 2.2 **Quantification of spindle structures at different positions in the C. elegans germ line.** Percent of oocytes and embryos at each stage of spindle assembly at different positions in the germ line. (A) Quantification of control EU1067 (GFP::histone; GFP::tubulin) worms. In the -1 position, most oocytes have an intact nuclear envelope, with a small percentage of oocytes containing microtubule cages. In the spermatheca, multipolar and bipolar spindles can also be observed, with the percentage of multipolar spindles significantly decreasing in embryos by the time they have moved to the +1 position. These data support our proposed ordering of events, with cage formation being triggered upon nuclear envelope breakdown, followed sequentially by the multipolar and bipolar stages. (B) Quantification of SMW13 (*klp-18(tm2841)*; GFP::histone; GFP::tubulin) worms. Without KLP-18 function, the microtubule cage still forms. However, embryos found in the spermatheca and the +1 position predominantly contain monopolar spindles, suggesting that the multipolar stage is bypassed in this mutant.

First, we observed the early stages of spindle formation, beginning with nuclear envelope breakdown (NEBD). Oocytes progress through the *C. elegans* gonad in a production line manner, approaching the spermatheca, where sperm entry triggers NEBD and initiation of the meiotic divisions[219]. Oocytes with intact nuclear envelopes could be distinguished by hazy GFP-histone fluorescence confined within that area (Figure 2.1A). Whereas most oocytes adjacent to the spermatheca had intact nuclear envelopes (Figure 2.2), oocytes that had initiated NEBD were discernible due to dispersal of the hazy GFP signal and the presence of a microtubule array. This array was similar to the size and shape of the previously intact nuclear envelope, forming a "microtubule cage" comprising bundles of microtubules with the chromosomes contained inside (Figure 2.1A and B). Imaging of nuclear lamin (LMN-1) and the integral nuclear membrane protein emerin (EMR-1) revealed that a significant amount of nuclear envelope material was still present at this stage, suggesting that this structure may be analogous to the array that forms in mouse oocytes, where microtubules concentrate on the outside of the nuclear envelope before NEBD[72]. However, we instead found that the majority of the prominent microtubule bundles forming the cage were on the inside of the LMN-1/EMR-1 signal (Figure 2.1C), with microtubules both concentrated

near the nuclear envelope remnants and also projecting inward toward the chromosomes. These results suggest that after nucleation, microtubules are constrained into the cage-like array by the presence of the disassembling envelope, which likely accounts for the "spherical" appearance of microtubules during spindle assembly previously documented in these cells[54]. Consistent with this idea, we did not observe formation of a microtubule cage during meiosis II (which is not preceded by NEBD, as the NE does not reform between the meiotic divisions), and microtubules instead appeared to nucleate in a smaller array in the vicinity of the chromosomes (Figure 2.1D).

After cage formation in meiosis I oocytes, we found that microtubule ends began to appear focused at multiple sites on the periphery of a large array, forming nascent poles (Figure 2.1A, asterisks). Quantification of spindle morphologies observed at various locations in the gonad supports the view that this multipolar stage precedes the bipolar stage (Figure 2.2), suggesting that the nascent poles then coalesce until bipolarity is achieved. Lower-resolution time-lapse imaging also supported this ordering of events (Figure 2.1B;[52,54,102,103,124,139]). After microtubule nucleation around the chromosomes in meiosis II, we observed a similar progression of events (Figure 2.1D). Together our observations indicate that acentrosomal spindle assembly in *C. elegans* proceeds by microtubule nucleation followed by the formation and subsequent coalescence of multiple poles, as has been proposed previously[103].

2.3. Microtubules of mixed polarity are nucleated and then sorted during acentrosomal spindle assembly

As previously mentioned, spindle assembly in mouse oocytes involves the nucleation and coalescence of many small MTOC asters containing PCM components at their centers[27,69,72]. In *C. elegans* oocytes, live imaging of the spindle pole protein ASPM-1, which is presumed to

mark microtubule minus ends, revealed that this protein forms foci during spindle assembly, leading to a model in which acentrosomal spindle assembly in this system might also be driven by the nucleation and coalescence of MTOC-like structures[14,103]. However, previous work demonstrated that *C. elegans* oocyte spindles do not have the PCM components γ-tubulin, SPD-2, or SPD-5 at their poles[50,220]. Moreover, we did not detect MTOC-like asters in either our high-resolution live or fixed imaging (Figure 2.1). Thus we set out to examine what these previously observed ASPM-1 foci represent.

To address this question, we performed fixed imaging of ASPM-1 throughout the process of spindle assembly (Figure 2.3A, Figure 2.4), achieving a higher level of resolution than the published live imaging. Consistent with our other images (Figure 2.1), we did not find evidence for MTOC-like microtubule asters, indicating that such structures do not form or are very transient and/or unstable. Instead, in early spindle assembly, we observed small foci of ASPM-1 dispersed throughout the cage structure that often appeared to localize at the tips of individual microtubule bundles (Figure 2.3A, Figure 2.4, asterisks), suggesting that these foci mark minus ends. Many ASPM-1 foci were in the vicinity of the disassembling envelope, but some were also near the chromosomes, suggesting that these minus ends are distributed throughout the cage structure. Further, some foci appeared to colocalize with microtubule bundles but were not at the ends (Figure 2.3, Figure 2.4, arrows), suggesting that the bundles themselves likely are composed of multiple microtubules and that the ends are not all focused together at this stage.

At later stages, ASPM-1 foci continued to decorate the ends of microtubules. In the multipolar stage, these foci were enriched on the periphery of the microtubule array, away from the chromosomes (Figure 2.3A and Figure 2.4, arrowheads), and then began to form

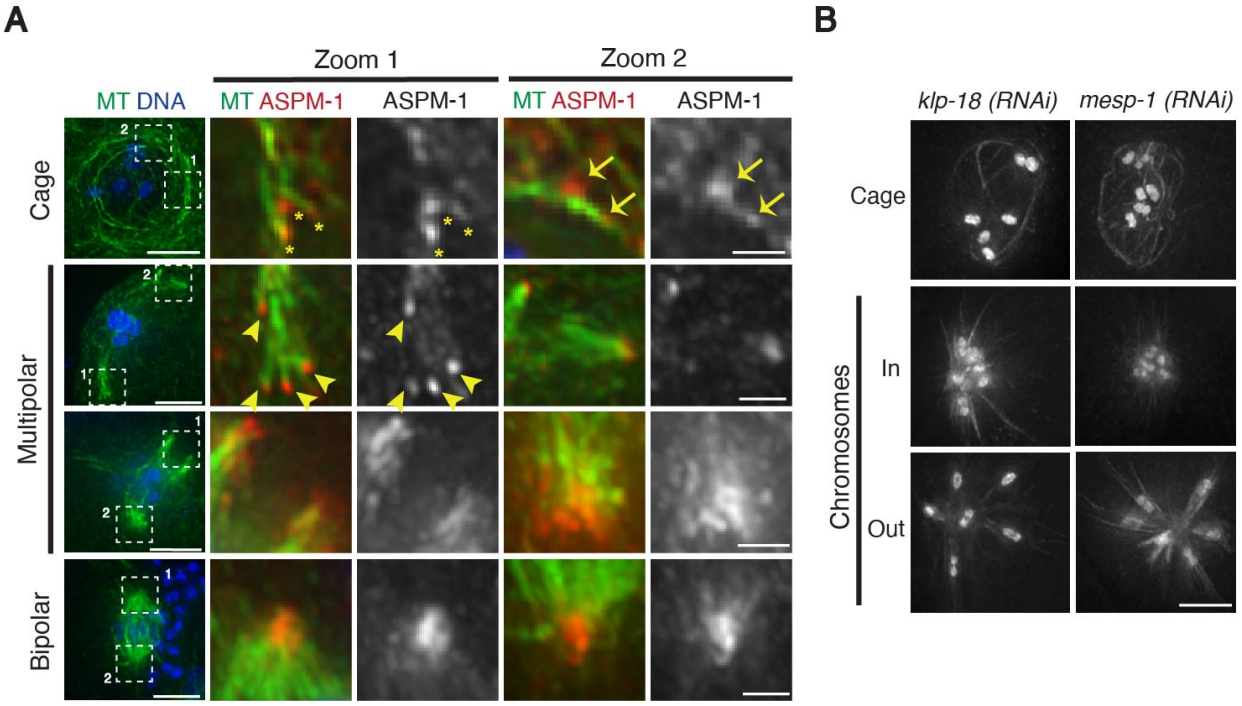

Figure 2.3. **KLP-18 and MESP-1 sort microtubules during spindle assembly.** (A) Fixed wild-type oocytes stained for tubulin (green), DNA (blue), and microtubule minus end marker ASPM-1 (red). All images are projections encompassing the entire spindle structure, except for the cage zoom images, which are a single z-plane to better show direct ASPM-1 and MT colocalization. ASPM-1 forms puncta at the ends of microtubule bundles at the cage and multipolar stages (asterisks and arrowheads, respectively) and sometimes within or along the side of a bundle (arrows), and then ASPM-1 marks larger stretches associated with spindle poles as spindle assembly proceeds. Minus ends are distributed throughout the microtubule cage and then are sorted away from the chromosomes as spindle assembly proceeds. (B) In vivo imaging of *klp-18(RNAi)* and *mesp-1(RNAi)* worms expressing GFP-tubulin and GFP-histone. Microtubules form a cage, but then minus ends collapse into a single aster. Scale bars, 5 μm (full images), 1.25 μm (zoom)

larger stretches connecting multiple microtubule bundles and forming the nascent poles (Figure 2.3A and Figure 2.4). Taken together, our data suggest that MTOC asters (which are undetectable in either of our imaging conditions) do not play a major role in acentrosomal spindle assembly in *C. elegans* oocytes. Instead, we propose that spindle assembly proceeds through 1) formation of a disordered array of microtubules within the remnants of the nuclear envelope, 2) sorting of microtubule minus ends away from the chromosomes to the

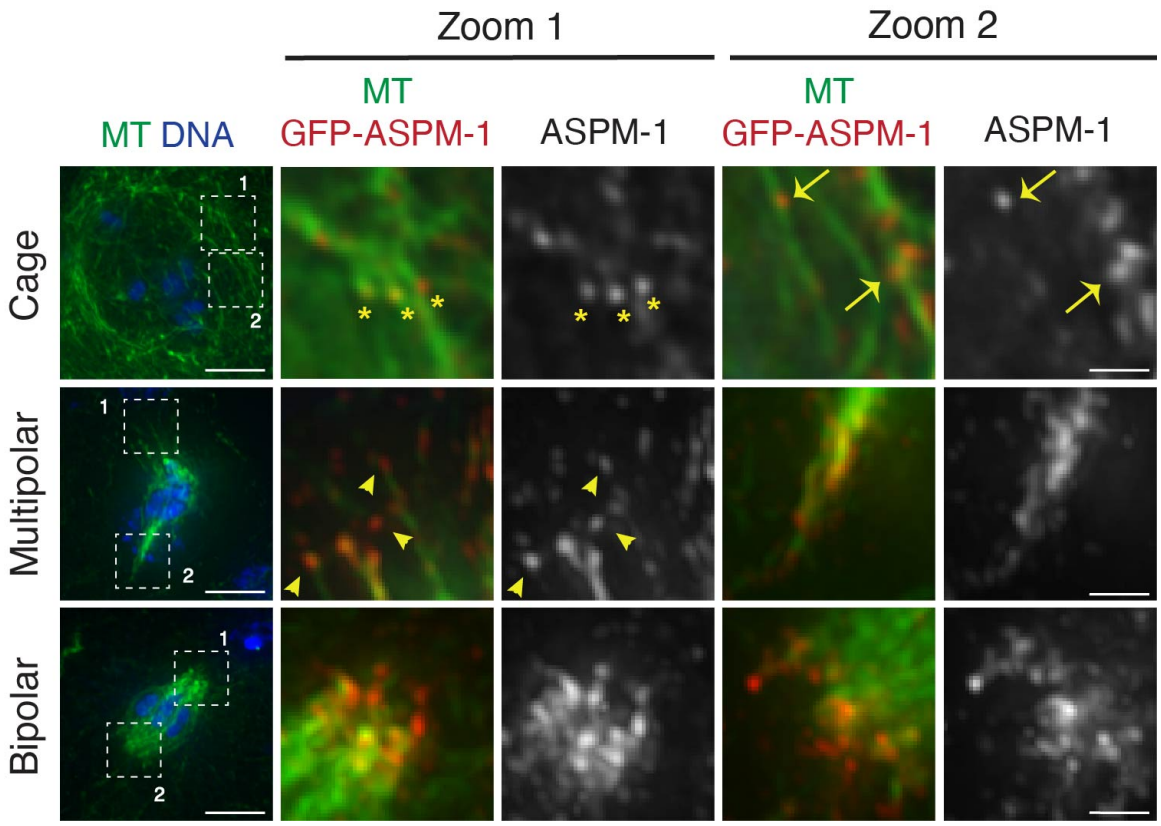

Figure 2.4. **GFP-ASPM-1 localization indicates microtubule sorting during spindle assembly.** Images of fixed oocytes expressing GFP-ASPM-1 stained for tubulin (green), DNA (blue), and GFP to visualize ASPM-1 (red). All images are projections encompassing the entire spindle structure, except for the cage zoom images, which are a single z-plane to better show ASPM-1 and MT colocalization. Similar to our analysis using an ASPM-1 antibody (Figure 2), GFP-ASPM-1 localizes to the ends of MT bundles in the cage and multipolar stages (asterisks and arrowheads, respectively), and also can be observed within and along the sides of MT bundles (arrows). In later stages of spindle assembly GFP-ASPM-1 marks stretches of MTs at the spindle poles.

periphery of the array, 3) organization of these ends into nascent poles, and 4) progressive coalescence of these poles until bipolarity is achieved.

2.4. KLP-18/kinesin-12 and MESP-1 are required to sort microtubule minus ends away from the chromosomes

Next we sought to investigate how bipolarity is established, given this pathway of spindle assembly. To address this question, we initiated analysis of KLP-18 (kinesin-12 family) and MESP-1, two proteins that we previously found to be required for spindle bipolarity in an RNAi screen[56]. Using high-resolution *in vivo* imaging, we found that the microtubule cage forms normally after depletion of either KLP-18 or MESP-1 (Figure 2.3B). However, after cage formation (at the stage at which multipolar spindles form in wild-type oocytes), microtubule ends converge into one central point, forming a microtubule aster with the chromosomes located close to the center; chromosomes then move outward, away from the pole (Figure 2.3B). ASPM-1 localizes to the center of these asters, confirming that they represent monopolar spindles[56,102,127]. Therefore KLP-18 and MESP-1 are not required for the earliest steps in the assembly pathway but are required to establish acentrosomal spindle bipolarity. Our observations are consistent with the idea that in the absence of these proteins, microtubule minus ends fail to be sorted away from the chromosomes after cage formation; consequently, factors that focus minus ends organize all of these ends into a single pole, bypassing the multipolar stage. These data therefore suggest that KLP-18 and MESP-1 are required to provide an outward force to sort microtubule minus ends away from the chromosomes, enabling bipolar spindle formation.

2.5. KLP-18/kinesin-12 and MESP-1 are interdependent for localization and can interact

Because both KLP-18 and MESP-1 are required for acentrosomal spindle bipolarity, we investigated the relationship between the two proteins. First, we assessed the localization of each during wild-type spindle assembly. KLP-18 was shown previously to localize to the poles of the bipolar spindle[101]. Using high-resolution microscopy, we confirmed this localization and also determined that KLP-18 and MESP-1 colocalize at all stages of acentrosomal spindle assembly (Figure 2.5A). Before NEBD and during early stages of spindle assembly, both proteins are broadly distributed in areas of high microtubule density (i.e., on microtubules adjacent to the nuclear envelope and also on the cage structure). As microtubules are further bundled and organized during spindle formation, KLP-18 and MESP-1 become enriched at the nascent poles of multipolar spindles and at the poles of the bipolar spindle, although they are also present at lower levels in the middle region of the spindle.

Given their colocalization, we next sought to investigate whether MESP-1 and KLP-18 are dependent on one another for spindle targeting. For this analysis, we took advantage of two *klp-18* mutants, *ok2519* and *tm2841*. *ok2519* is an in-frame deletion that results in the production of a truncated protein missing part of the motor domain (Figure 2.5B), and *tm2841* is a deletion that results in a predicted early stop. Because our antibody recognizes only the C-terminus of KLP-18 (amino acids 508–932[101]), we cannot determine whether a truncated form of KLP-18 is made or targeted to the spindle in this second mutant. As expected from the *klp-18(RNAi)* phenotype, both *klp-18(ok2519)* and *klp-18(tm2841)* homozygotes have monopolar oocyte spindles and 100% embryonic lethality. Moreover, in *ok2519*, we did not observe KLP-18 localization to microtubules (Figure 2.5C). Therefore

the deleted portion of the motor domain is required for proper spindle localization. Of importance, we found that MESP-1 did not target properly to spindle microtubules in either mutant (Figure 2.5C). This represents defective localization and not decreased protein abundance, since MESP-1 is present at similar levels in both *klp-18* mutants (Figure 2.5B). In the converse experiment, KLP-18 failed to target to microtubules after *mesp-1(RNAi)* (Figure 2.5D). Therefore KLP-18 and MESP-1 are interdependent for localization.

Given this finding, we predicted that KLP-18 and MESP-1 might associate *in vivo*. Therefore, we used pull-down experiments to determine whether they are present in the same protein complex. Specifically, we incubated recombinant glutathione S-transferase (GST)–MESP-1 with wild-type worm extract, retrieved GST–MESP-1 with glutathione Sepharose beads, and eluted associated proteins. Endogenous KLP-18 was detected in the eluate by Western blot (Figure 2.5E), indicating that MESP-1 and KLP-18 can form a complex and suggesting that they work together *in vivo*.

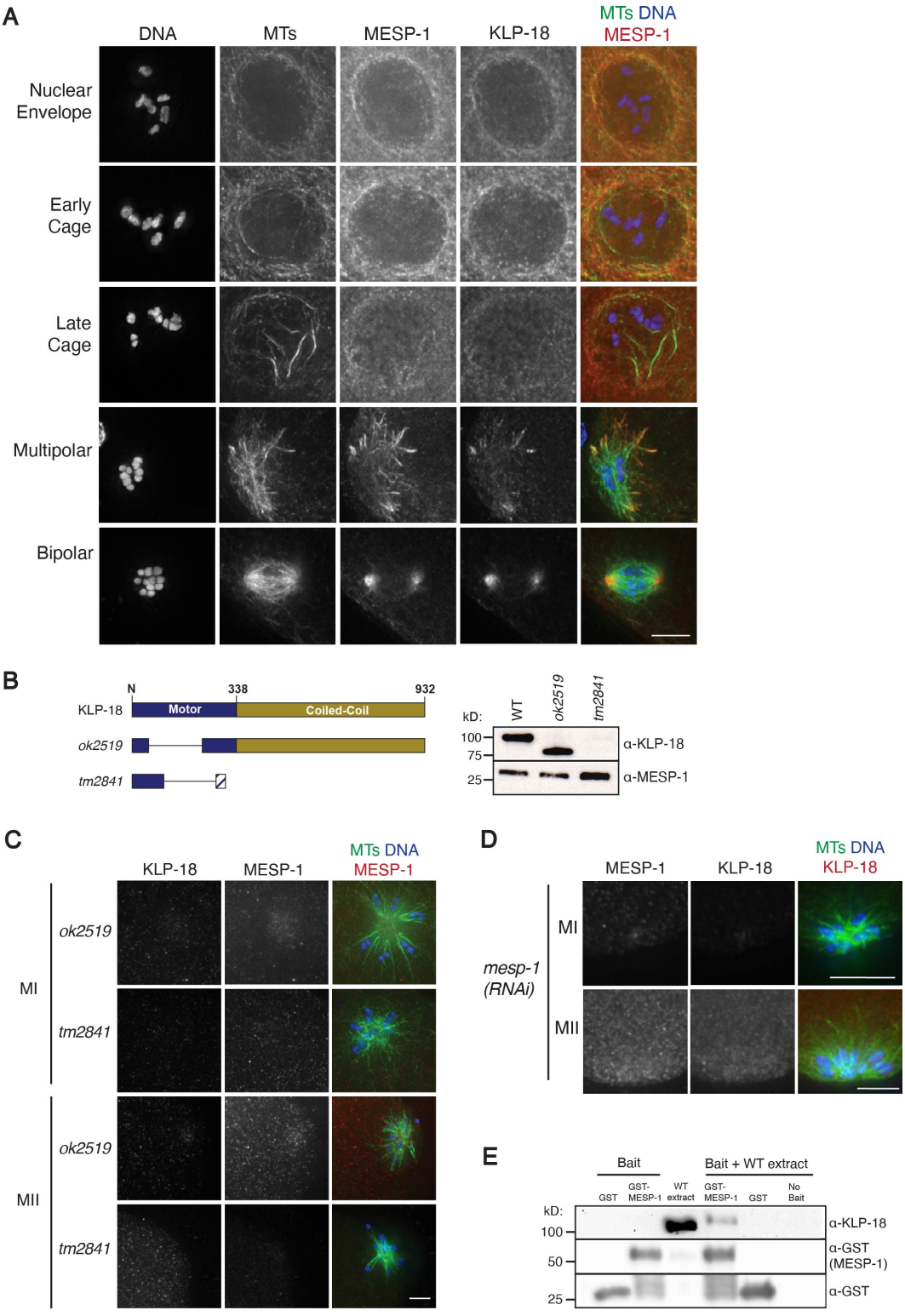
A
DNA
MTs
MESP-1
KLP-18
MTs DNA
MESP-1
Nuclear Envelope
Early Cage
Late Cage
Multipolar
Bipolar
B
N
338
932
KLP-18
Motor
Coiled-Coil
ok2519
tm2841
kD:
WT
ok2519
tm2841
100
75
25
α-KLP-18
α-MESP-1
C
KLP-18
MESP-1
MTs DNA
MESP-1
MI
MII
ok2519
tm2841
D
MESP-1
KLP-18
MTs DNA
KLP-18
mesp-1 (RNAi)
MI
MII
E
Bait
Bait + WT extract
GST
GST-MESP-1
WT extract
GST-MESP-1
GST
No Bait
kD:
100
50
25
α-KLP-18
α-GST (MESP-1)
α-GST

Figure 2.5

Figure 2.5. **KLP-18 and MESP-1 colocalize and are interdependent for localization.** (A) Images of fixed wild-type oocytes stained for DNA (blue), tubulin (green), MESP-1 (red in merge), and KLP-18 (not shown in merge). KLP-18 and MESP-1 colocalize along microtubules during the early cage and become enriched at poles during multipolar and bipolar stages. Pearson's correlation coefficient for MESP-1/KLP-18 colocalization at cage, multipolar, and bipolar stages was 0.74, 0.78, and 0.92 respectively. (B) Schematic of full-length KLP-18 (top) and analyzed mutants (bottom). *klp-18(ok2519)* contains an in-frame 510–base pair deletion that removes 170 residues from the motor domain, and *klp-18(tm2841)* contains a 162–base pair deletion that results in a predicted early stop. Western blotting with a KLP-18 antibody shows that *ok2519* results in a truncated protein with about 25 kDa removed, but KLP-18 is not detected in *tm2841*, indicating that either it is not expressed or lacks the C-terminal domain. (C) *ok2519* and *tm2841* oocytes in meiosis I (MI) and meiosis II (MII) stained for DNA (blue), tubulin (green), KLP-18 (not shown in merge), and MESP-1 (red in merge). MESP-1 does not localize to the spindle in either mutant. (D) *mesp-1(RNAi)* oocytes stained for DNA (blue), tubulin (green), MESP-1 (not shown in merge), and KLP-18 (red in merge). KLP-18 does not localize after MESP-1 depletion. (E) GST pull down demonstrating interaction between KLP-18 and MESP-1. GST-MESP-1 or GST-alone was incubated with wild-type (WT) worm extract and then retrieved. Bait proteins are shown before incubation on the left, and the eluate after incubation is shown on the right. A KLP-18 antibody was used to visualize KLP-18, and a GST antibody was used to visualize both GST and GST-MESP-1. KLP-18 is present in eluate from the GST–MESP-1 pull down but not from GST-alone. Scale bars, 5 μm. Western blot in (B) performed by Sadie Wignall.

2.6. MESP-1 is a rapidly evolving protein that may be performing the kinesin-12 targeting role of TPX2

Intriguingly, our findings regarding MESP-1 are reminiscent of a well-studied protein in vertebrates, TPX2, which performs many important functions during mitosis and meiosis[221,222]. Significant to this study, TPX2 is required for kinesin-12 targeting to the spindle[166,167,196,223,224]. A putative *C. elegans* TPX2 homologue, TPXL-1, was previously shown to perform some of the known functions of TPX2[225]. However, limited sequence homology and some functional differences between the two proteins has raised questions about whether TPXL-1 is a true TPX2 orthologue[226]. Of interest, we found that TPXL-1 depletion by RNAi did not cause defects in oocyte spindle morphology (as shown in[225]) and also did not affect KLP-18 targeting to the spindle (Figure 2.6A) under conditions in which we recapitulated the published mitotic phenotype (Figure 2.6B). Therefore *C. elegans* TPXL-1 does not appear to facilitate kinesin-12 targeting, and we propose that instead MESP-1 has taken on this role. Our findings support the idea that TPX2 has multiple functional counterparts in *C. elegans*, with TPXL-1 and MESP-1 providing different essential functions of this important protein.

Although the kinesin-12–targeting function of MESP-1 suggests that it may serve as a functional counterpart of TPX2, sequence analysis of MESP-1 did not identify homology with TPX2 or any previously studied proteins. However, TPX2 is not well conserved in invertebrates. For example, *Drosophila* Mei-38, identified as a putative TPX2 homologue based on only a few short conserved regions, lacks several key domains present in vertebrate TPX2, suggesting that TPX2 function may commonly be compartmentalized to multiple proteins and that these functional counterparts may not share strong sequence homology[227].

Independent of the question of homology to known proteins, our MESP-1 sequence analysis revealed two notable features. First, MESP-1 is a member of a rapidly evolving protein family. Homologues are detected only within the genus *Caenorhabditis*, and the number of paralogues varies among species (Figure 2.6C). Diversification of this family appears to be an ongoing process, as gene duplications occurring both before and after speciation events have been detected. Second, the MESP-1 protein sequence is enriched for prolines, with proline residues accounting for 12% of its 193 amino acid residues. Because conservation among all family members is concentrated predominantly in the C-terminal 70–80 amino acids, we used a ClustalW alignment of this portion of the homologues to deduce an ancestral protein motif (Figure 2.6D); 9 of the 31 amino acid residues in this motif are prolines, suggesting that this proline-rich character may be important for MESP-1 function.

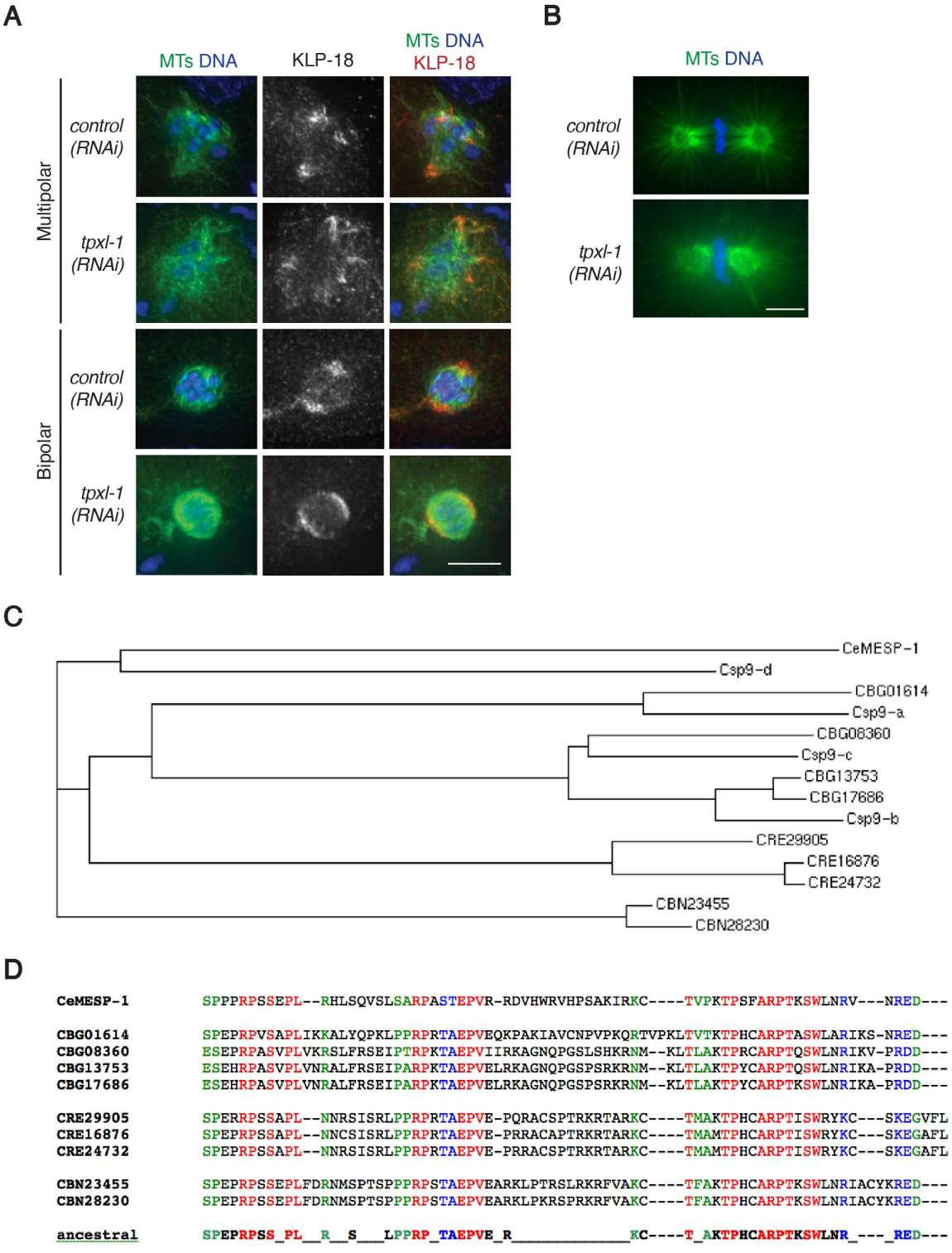
A
MTs DNA
KLP-18
MTs DNA
KLP-18
Multipolar
control
(RNAi)
tpxl-1
(RNAi)
Bipolar
control
(RNAi)
tpxl-1
(RNAi)
B
MTs DNA
control
(RNAi)
tpxl-1
(RNAi)
C
CeMESP-1
Csp9-d
CBG01614
Csp9-a
CBG08360
Csp9-c
CBG13753
CBG17686
Csp9-b
CRE29905
CRE16876
CRE24732
CBN23455
CBN28230
D
CeMESP-1 SPPPRPSSEPL--RHLSQVSLSARPASTEPVR-RDVHWRVHPSAKIRKC----TVPKTPSFARPTKSWLNRV---NRED---
CBG01614 SPEPRPVSAPLIKKALYQPKLPPRPRTAEPVEQKPAKIAVCNPVPKQRTVPKLTVTKTPHCARPTASWLARIKS-NRED---
CBG08360 ESEPRPASVPLVKRSLFRSEIPTRPKTAEPVIIRKAGNQPGSLSHKRNM--KLTLAKTPRCARPTQSWLNRIKV-PRDD---
CBG13753 ESEHRPASVPLVNRALFRSEIPARPKTAEPVELRKAGNQPGSPSRKRNM--KLTLAKTPYCARPTQSWLNRIKA-PRDD---
CBG17686 ESEHRPASVPLVNRALFRSEIPARPKTAEPVELRKAGNQPGSPSRKRNM--KLTLAKTPYCARPTKSWLNRIKA-PRDD---
CRE29905 SPERRPSSAPL--NNRSISRLPPRPRTAEPVE-PQRACSPTRKRTARKC----TMAKTPHCARPTISWRYKC---SKEGVFL
CRE16876 SPEPRPSSAPL--NNCSISRLPPRPRTAEPVE-PRRACAPTRKRTARKC----TMAMTPHCARPTISWRYKC---SKEGAFL
CRE24732 SPEPRPSSAPL--NNRSISRLPPRPRTAEPVE-PRRACSPTRKRTARKC----TMAMTPHCARPTISWRYKC---SKEGAFL
CBN23455 SPEPRPSSEPLFDRNMSPTSPPPRPSTAEPVEARKLPTRSLRKRFVAKC----TFAKTPHCARPTKSWLNRIACYKRED---
CBN28230 SPEPRPSSEPLFDRNMSPTSPPPRPSTAEPVEARKLPKRSPRKRFVAKC----TFAKTPHCARPTKSWLNRIACYKRED---
ancestral SPEPRPSS_PL__R__S___LPPRP_TAEPVE_R_____KC----T_AKTPHCARPTKSWLNR_---_RED---

Figure 2.6

Figure 2.6. **MESP-1 is a rapidly evolving protein that may perform the kinesin-12–targeting role of TPX2.** (A, B) Control and *tpxl-1(RNAi)* worms were fixed and stained for DNA (blue), tubulin (green), and KLP-18 (red). KLP-18 targeting is unaffected by *tpxl-1(RNAi)* (A), whereas the mitotic spindle in the one-cell-stage embryo is shorter than in wild type (B), confirming the previously described TPXL-1–depletion phenotype (Ozlu et al., 2005). Scale bars, 5 μm. (C) Divergence tree of MESP-1 paralogues from five *Caenorhabditis* species (*C. elegans*, *C. species 9*, *C. briggsae*, *C. remanei*, and *C. brenneri*) based on a ClustalW alignment (generated using the TimeLogic DeCypher server at Stanford University) of the regions corresponding to the C-terminal 65 amino acids from *C. elegans* MESP-1. The tree structure indicates that paralogues arose both via gene duplication events occurring specifically in the *C. briggsae*, *C. remanei*, and *C. brenneri* lineages and via earlier gene duplication events that occurred before divergence of *C. briggsae* and *C. species 9* (aka *C. nigoni*). (D) ClustalW alignment of the C-terminal domains of the MESP-1 paralogues from *C. elegans*, *C. briggsae*, *C. remanei*, and *C. brenneri*. Red indicates identity among all paralogues, blue indicates conservative substitutions, and green indicates semiconservative substitutions. (C) and (D) performed by Anne Villeneuve (Stanford University).

2.7. Discussion

In summary, we propose that in *C. elegans* oocytes, acentrosomal spindle assembly proceeds by the initial formation of a microtubule array of mixed polarity, followed by sorting of microtubule minus ends toward the periphery of this array and then gathering of minus ends into nascent poles. These poles then progressively coalesce until bipolarity is achieved (Figure 2.7). Although the coalescence of multiple spindle poles was previously observed[103], our work sheds light on the earliest events of spindle formation, as our studies do not favor the current idea that the nucleation and then coalescence of small MTOC asters drive the initial stages of spindle assembly[14,103], as occurs in mouse and possibly fly oocytes[27,69,72]. In contrast, our model aligns well with previous studies of acentrosomal spindle formation in *Xenopus* egg extracts, where microtubules are nucleated and then sorted by motors and organized into poles, as we proposed[17,93,132]. Of note, whereas microtubules seem to be nucleated primarily in the vicinity of the chromatin in the extract system[17] and in *C. elegans* oocytes during meiosis II (Figure 2.1D), we observe a high concentration of microtubule bundles

underlying the disassembling nuclear envelope in meiosis I, forming a cage-like structure (Figure 2.1A and B). Although this finding does not rule out the possibility that chromosomes also contribute to spindle assembly in these oocytes, it raises the intriguing possibility that there may be additional regions where microtubules can be nucleated and/or stabilized.

We also find that KLP-18/kinesin-12 and MESP-1 appear to collaborate to establish spindle bipolarity in this system. These proteins localize to microtubules early during spindle assembly, are interdependent for localization, and inhibition of either causes monopolar spindle formation. Our data are consistent with a model in which KLP-18 and MESP-1 are involved in the initial sorting of microtubules such that the minus ends are pushed to the outside of the microtubule array. Without this contribution, factors responsible for organizing minus ends dominate, and all of the minus ends collapse into a single pole (Figure 2.7).

Our model fits well with work in vertebrate cell lines that has implicated kinesin-12–family motors in spindle assembly. Although kinesin-5–family motors are the dominant motors promoting bipolarity in those cells, when kinesin-5 is inhibited/depleted, bipolar spindles form using a kinesin-12–mediated mechanism[166–168,173,186,228] that is believed to act by promoting the formation of parallel microtubule bundles[194]. Because it has been demonstrated that kinesin-5 is not an essential motor in *C. elegans*[98], KLP-18/kinesin-12 instead appears to be the dominant motor promoting spindle bipolarity in worm oocytes. In this context, MESP-1 may contribute to this process by taking on the kinesin-12–targeting role performed by TPX2 in other organisms, providing KLP-18 with the opportunity to sort microtubules. Future work determining the mechanisms by which KLP-18 and MESP-1 act to organize microtubules and generate bipolarity will shed light on this important but poorly understood specialized cell division, as well as on overall kinesin-12 function during cell division.

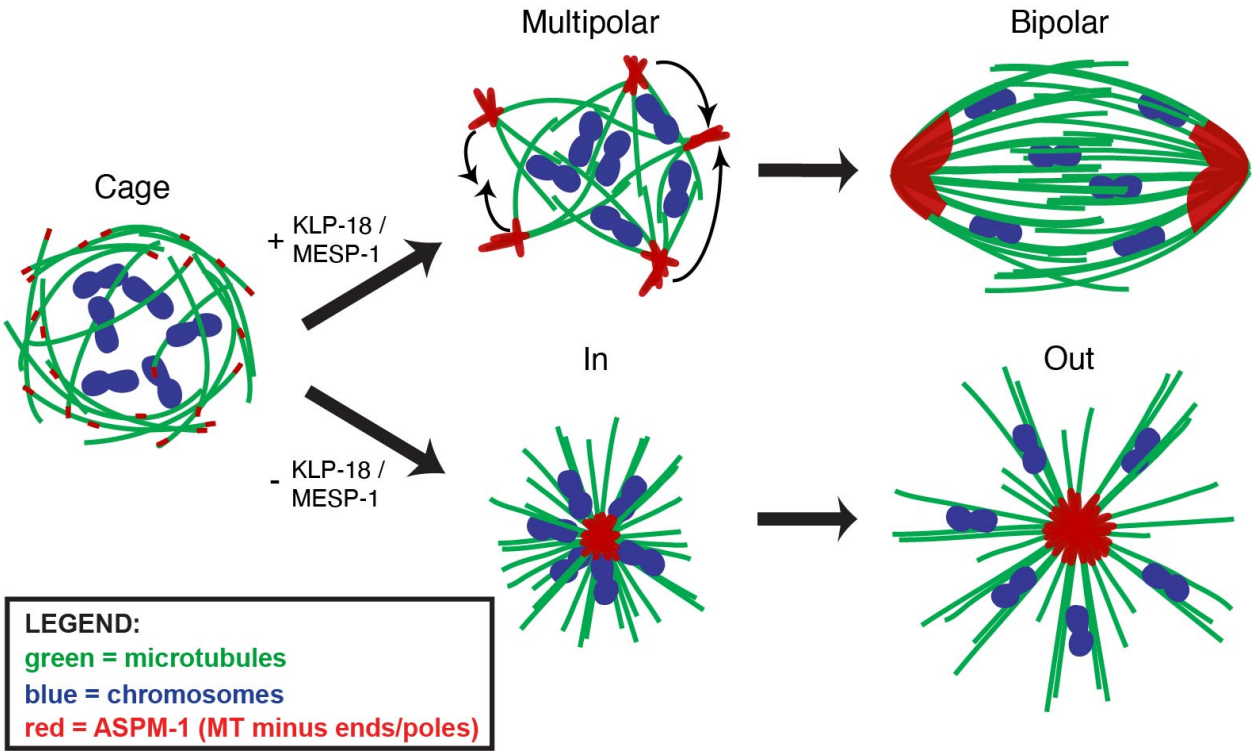

Figure 2.7. **Model for MTOC-independent acentrosomal spindle assembly.** Acentrosomal spindle assembly in *C. elegans* depicting microtubules (green), chromosomes (blue), and ASPM-1 (representing microtubule minus ends; red). After NEBD, microtubules of mixed polarity are organized adjacent to the disassembling nuclear envelope into a cage structure surrounding the chromosomes. The microtubule bundles are then sorted by KLP-18/MESP-1 such that the minus ends are oriented at the periphery of the array and bundled into nascent poles, forming a multipolar spindle (top). The nascent poles then coalesce to achieve bipolarity. In the absence of KLP-18/MESP-1, outward sorting of microtubule bundles is lost, and the minus ends collapse into a single aster and form a monopolar spindle (bottom).

CHAPTER 3

Acentrosomal spindle assembly and stability in *C. elegans* requires a kinesin-12 non-motor microtubule interaction domain

This chapter is adapted from a manuscript that is currently in revision as a Report. I performed all experiments in this chapter.

3.1. Summary

In oocytes lacking centrosomes, microtubules are sorted and organized by motor proteins to generate a bipolar spindle[8]. In most organisms, kinesin-5 family members crosslink and slide microtubules to generate outward force that promotes acentrosomal spindle bipolarity[72,89,93,94,96,105]. However, the mechanistic basis for how other kinesin families generate force in acentrosomal spindles has not been explored. We investigated this question in *C. elegans* oocytes, where kinesin-5 is not required to generate outward force[98]. Instead, the kinesin-12 family motor KLP-18 performs this function[48,56,101,102]. KLP-18 acts with adaptor protein MESP-1 (**me**iotic **sp**indle **1**) to sort microtubule minus ends to the periphery of a microtubule array, where they coalesce into spindle poles[48]. If either of these proteins is depleted, this outward sorting force is lost and minus ends converge to form a monoaster. Here we use a combination of *in vitro* biochemical assays and *in vivo* imaging to provide insight into the mechanism by which these proteins collaborate to generate force in the acentrosomal spindle. We identify a microtubule binding site on the C-terminal stalk of KLP-18 and demonstrate that a direct interaction between the KLP-18 stalk and MESP-1 activates non-motor microtubule binding. We also provide evidence that this C-terminal domain is required for KLP-18-mediated force generation during spindle assembly and show that KLP-18 is continuously required, indicating that KLP-18 is essential to maintain spindle bipolarity. This study thus provides new insight into the construction and maintenance of the acentrosomal spindle as well as into kinesin-12 mechanism and regulation.

3.2. The KLP-18 coiled-coil stalk domain contains a regulated microtubule binding site

Kinesin-12 family motors contain a globular N-terminal motor domain that can walk along microtubules in a plus end-directed fashion. However, in order to crosslink and slide microtubules to generate forces within the spindle, these motors must bind a second microtubule. Multiple microtubule cross-linking strategies have been proposed for mammalian kinesin-12 (Kif15): 1) Kif15 forms a homotetramer with antipolar motor domains[172,193–195], allowing both ends of the complex to bind to microtubules, and 2) a non-motor microtubule-binding site in the middle of the stalk domain mediates binding to a second microtubule[171,192]. Although KLP-18 is the major force-producing kinesin in the *C. elegans* oocyte spindle, it is unknown whether this motor can bind multiple microtubules.

Like other kinesin-12 motors, KLP-18 contains a C-terminal stalk domain[101], so we first examined if this domain could mediate crosslinking by directly binding to microtubules. Structural prediction of the KLP-18 stalk revealed that it contains discrete coiled-coil domains (Figure 3.1A), similar to Kif15[101,192]. To test if the stalk contains a non-motor microtubule binding site, we separately expressed and purified the N- and C-terminal halves of the KLP-18 stalk ("N-stalk" and "C-stalk") and performed a microtubule co-sedimentation assay[229] (Figures 3.1A, 3.1B, 3.2). After pelleting microtubules, N-stalk remained in the supernatant. In contrast, a sizable fraction of C-stalk pelleted, reflecting its ability to bind microtubules *in vitro* (Figure 3.1B, left). To investigate the nature of this interaction, we treated microtubules with subtilisin to cleave E-hooks, which are negatively-charged regions at the tubulin C-terminus that can bind to proteins through an electrostatic interaction[230,231]. We found that C-stalk bound to microtubules lacking E-hooks, but with decreased affinity (Figure 3.1B, right). These results are consistent with previous findings for

the non-motor microtubule binding sites in Kif15 and kinesin-1[171,232], and suggests that an electrostatic interaction increases the affinity of KLP-18 stalk to microtubules. To further assess the microtubule binding activity of C-stalk and N-stalk, we incubated these proteins with fluorescently-labeled microtubules *in vitro*. C-stalk addition dramatically increased microtubule bundling compared to buffer alone or N-stalk (Figure 3.1C), confirming that C-stalk is able to bind and bundle microtubules. Together, these data show that the stalk domain of KLP-18 contains a C-terminal microtubule binding site.

Next, we purified the full KLP-18 stalk (termed "stalk"; Figure 3.2) and paradoxically found that it showed very little bundling activity (Figure 3.1D), suggesting that full-length stalk alone is unable to bind microtubules. Since an autoinhibitory mechanism has been proposed for mammalian Kif15, where the motor folds its stalk domain to block the non-motor microtubule binding site[192], we tested whether KLP-18 could employ a similar regulatory mechanism. The coiled-coil prediction for the KLP-18 stalk contains a region of low probability in the center of the stalk domain (Figure 3.1A), and we hypothesized that this region may be a flexible hinge that could fold, thus preventing the C-terminal region from binding microtubules. To test this mechanism, we purified a version of the stalk with this putative hinge deleted (termed "Δhinge"), which is predicted to be completely coiled-coil (Figure 3.3B). Consistent with an auto-inhibitory mechanism, we found that deletion of the hinge region rescues microtubule bundling activity, and therefore the ability to bind microtubules (Figure 3.1D). In addition, we directly tested the coiled-coil flexibility of KLP-18 stalk by running a purified MBP-stalk construct (Figure 3.3A) through a size exclusion column in high salt (300mM) and low salt (20mM) buffers. In theory, if KLP-18 stalk was able to fold via an electrostatic interaction, high salt conditions would disrupt folding and lead to an extended conformation. This conformational change would be apparent in the molecule's

size exclusion chromatography elution volume. Indeed, in high salt, a population of MBP-stalk eluted at a lower elution volume, indicating that this sub-population contains extended molecules (Figure 3.3C). These results present the possibility that binding of the KLP-18 stalk to microtubules can be regulated by existing in either an inactive folded state or an active unfolded state.

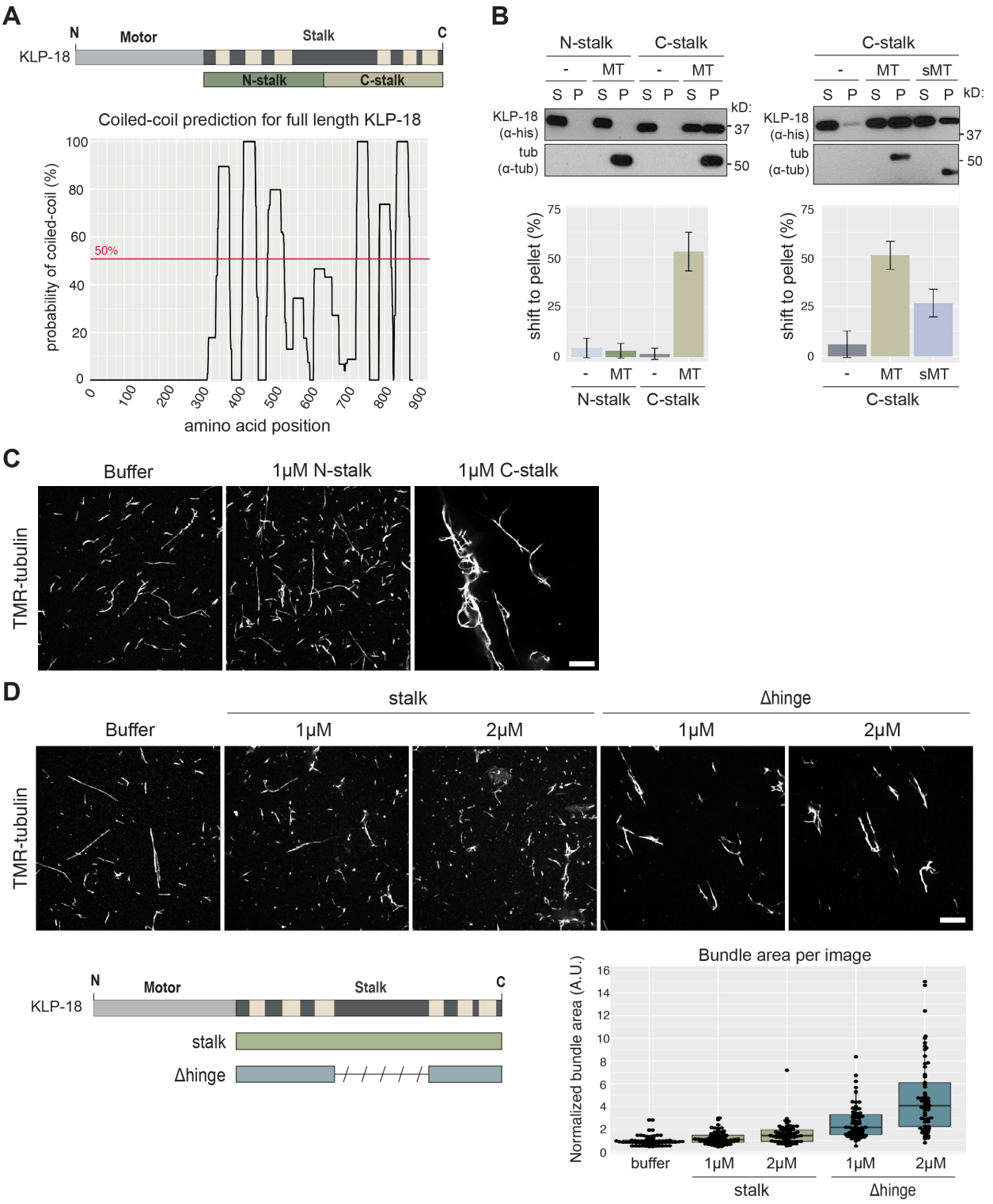
A
N
Motor
Stalk
C
KLP-18
N-stalk
C-stalk
Coiled-coil prediction for full length KLP-18
probability of coiled-coil (%)
50%
amino acid position
B
N-stalk
C-stalk
MT
S P
KLP-18 (α-his)
tub (α-tub)
kD:
37
50
shift to pellet (%)
sMT
C
Buffer
1μM N-stalk
1μM C-stalk
TMR-tubulin
D
stalk
Δhinge
1μM
2μM
Bundle area per image
Normalized bundle area (A.U.)
buffer

Figure 3.1

Figure 3.1. **The kinesin-12/KLP-18 coiled-coil stalk domain contains a regulated microtubule binding site.** a) Coiled-coil prediction software paircoil2 shows discrete coiled-coil domains in the KLP-18 stalk (bottom) marked on a KLP-18 domain diagram (top, coiled-coil domains denoted in white). N- and C-stalk constructs shown relative to full stalk. b) N-stalk and C-stalk microtubule binding activity tested by microtubule co-sedimentation assay with no microtubules added (-), undigested (MT), and subtilisin-digested (sMT) microtubules. Blots show supernatant (S) and pellet (P) samples, quantification is of average shift +/- sd. N = 3 experiments for each set. c, d) Microtubule binding activity assessed as microtubule bundling ability. Representative images of TMR-microtubules incubated with buffer alone, N-stalk, and C-stalk (c) or with buffer alone, full-length stalk, and Δhinge (d). Quantification of bundling below. Boxplot represents first quartile to third quartile and the median is indicated by a horizontal line. Quantified images were acquired over 2 independent experiments. See Chapter 5 for full description of quantification. Scale bar = 10μm.

A

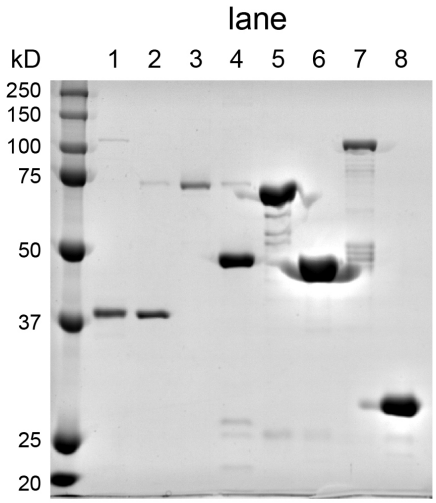

B

lane	protein	residues	tag	M.W.	plasmid	exp time / temp.
1	N-stalk	329-634	C-term 6xHis	35kD	pIW9	16°C, overnight
2	C-stalk	635-932	C-term 6xHis	35kD	pIW10	16°C, overnight
3	stalk	329-932	C-term 6xHis	70kD	pIW1	30°C, 4 hours
4	Δhinge	329-559, 770-932	C-term 6xHis	47kD	pIW8	16°C, overnight
5	MBP-MESP-1	full length	N-term 6xHis-MBP	64kD	pIW11	18°C, overnight
6	MBP	full length	N-term 6xHis	42kD	pET MBP	18°C, overnight
7	GFP-stalk	329-932	N-term 6xHis-GFP	98kD	pIW6	16°C, overnight
8	GFP	full length	-	28kD	addgene: #29663	16°C, overnight

Figure 3.2. **Protein expression and purification details.** a) SDS-PAGE gel stained with Coomassie showing purifications of all proteins used. For purification details, see Materials and Methods. Protein of interest is major band in each lane. Each purification was confirmed by Western Blot probed with an antibody against protein of interest (not shown). b) For each protein, the corresponding residues, affinity tag(s), molecular weight (M.W.), plasmid name, and expression time / temperature (after 0.1mM IPTG induction) is shown.

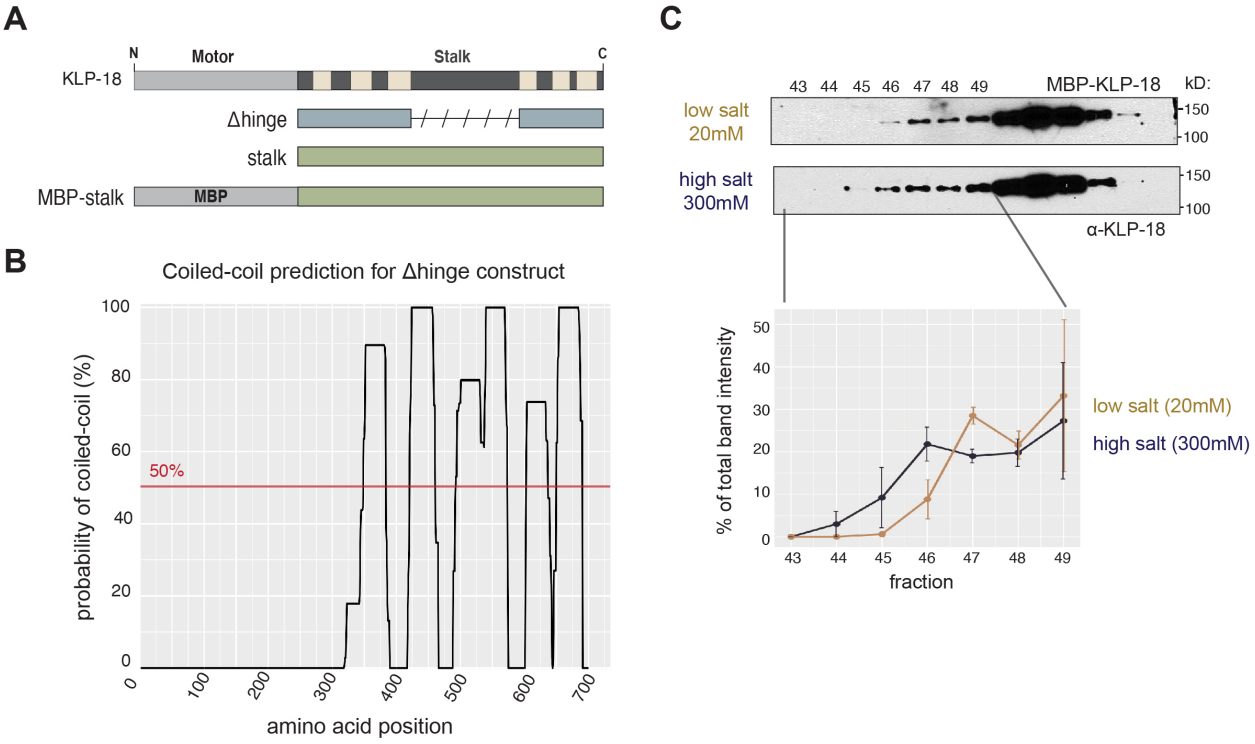

Figure 3.3. **KLP-18 stalk likely contains a flexible hinge region.** a) Schematics of Δhinge, full length stalk, and MBP-stalk constructs. Slanted dashed lines show area deleted in Δhinge. b) Paircoil2 prediction for Δhinge construct with putative hinge deleted. Δhinge is predicted to be completely coiled-coil and therefore presumably rigid (compare to full-length stalk in Figure 3.1). c) KLP-18 stalk flexibility tested in size exclusion chromatography experiment. MBP-stalk applied to a size exclusion column in high salt (300mM, blue) and low salt (20mM, gold) buffer. Indicated fractions probed for KLP-18 in a western blot then quantified. Mean +/- sd of percent of total band intensity is shown. High salt: n = 3 over 2 purifications, low salt: n = 2 over 1 purification.

3.3. KLP-18 is targeted to microtubules through a direct interaction with microtubule associated protein MESP-1

Given that KLP-18 contains a non-motor microtubule binding site that may be regulated via an auto-inhibitory mechanism, we next investigated how this inhibition could be relieved. In both *Xenopus* and mammals, the adaptor protein TPX2 is required for targeting kinesin-12s to the spindle[172,193,195,196,201,223], and our previous work suggests that MESP-1 performs this kinesin-12 targeting function in *C. elegans*. Specifically, we found that KLP-18 and MESP-1 colocalize on spindle microtubules, are found in a complex in worm extract, have identical depletion phenotypes, and are interdependent for localization[48] (and Chapter 2). We therefore hypothesized that MESP-1 may directly bind to KLP-18, relieve its auto-inhibition, and thereby target KLP-18 to microtubules.

We first set out to characterize MESP-1 biochemically by expressing GST-MESP-1, but this protein degraded significantly during purification (Figure 3.4A). This suggests that MESP-1 is unstable, consistent with the prediction that portions of MESP-1 are disordered (Figure 3.4B) similar to TPX2[83,229,233]. Therefore, we switched to an MBP tag[234–236], which increased MESP-1 stability (Figure 3.4A). MBP-MESP-1 pelleted with microtubules in a co-sedimentation assay (Figure 3.5A) and was able to bundle microtubules (Figure 3.4C), indicating that MESP-1 is a microtubule binding protein. In addition, we found that MESP-1's ability to bind microtubules was decreased when we used subtilisin-digested microtubules (Figure 3.5A, right). These results indicate that, similar to TPX2, MESP-1 is a microtubule associated protein. However, TPX2 binds along the microtubule lattice and does not require tubulin E-hooks[197,233], suggesting that MESP-1 employs a different microtubule binding mechanism.

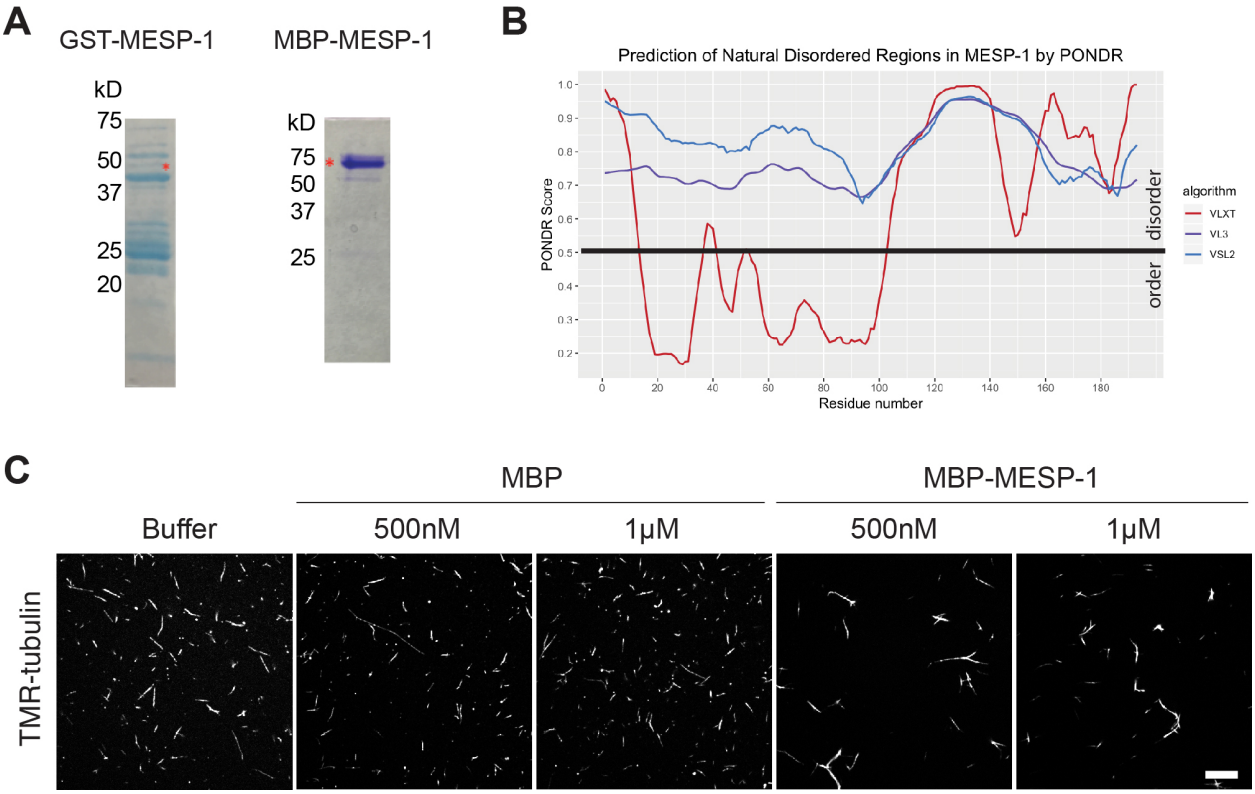

Figure 3.4. **MESP-1 is an unstructured and disordered microtubule binding protein.** a) Representative purifications shown for GST- and MBP-tagged MESP-1. GST-MESP-1 and MBP-MESP-1 band marked by red asterisk. GST-MESP-1 shows more degradation than MBP-MESP-1. b) Prediction of disordered regions within MESP-1 using PONDR. PONDR score for three algorithms (VXLT (red), VL3 (purple), and VSL2 (blue)) shown for each residue. Residues with PONDR scores above the black line (> 0.5) are predicted to be disordered. c) MBP-MESP-1 microtubule binding activity tested by microtubule bundling assay. Representative images of TMR-microtubules incubated with buffer alone, MBP, and MBP-MESP-1. Scale bar = 10μm.

Next, we tested whether MESP-1 could directly bind to KLP-18 *in vitro*. We incubated purified MBP-MESP-1 with the two KLP-18 stalk truncations individually and added amylose resin to retrieve MBP-MESP-1. We found that N-stalk was present in the eluted fraction but C-stalk was not, indicating that MESP-1 binds to the N-terminal half of the KLP-18 stalk (Figure 3.5B). However, this interaction appears to be weak, because only a small fraction of N-stalk was pulled out by MBP-MESP-1. This is similar to what has been reported for the interaction between mammalian TPX2 and Kif15[193], and suggests that the interaction between MESP-1 and KLP-18 may be transient or may require microtubules, as has been shown for *Xenopus* TPX2 and kinesin-12 (Xklp2)[196].

To investigate the significance of MESP-1's interaction with KLP-18, we purified a GFP-tagged version of the full length KLP-18 stalk (Figure 3.5C, termed "GFP-stalk") to visualize KLP-18 localization to microtubules in the presence and absence of MESP-1. Notably, GFP-stalk alone did not localize to microtubules (Figure 3.5D), consistent with our model of KLP-18 auto-inhibition. In contrast, we observed strong localization of GFP-stalk to microtubules in the presence of MBP-MESP-1, but not MBP alone (Figure 3.5D). Taken together, these results show that MESP-1 is a microtubule binding protein that directly interacts with KLP-18 and is sufficient to target KLP-18 to microtubules *in vitro*.

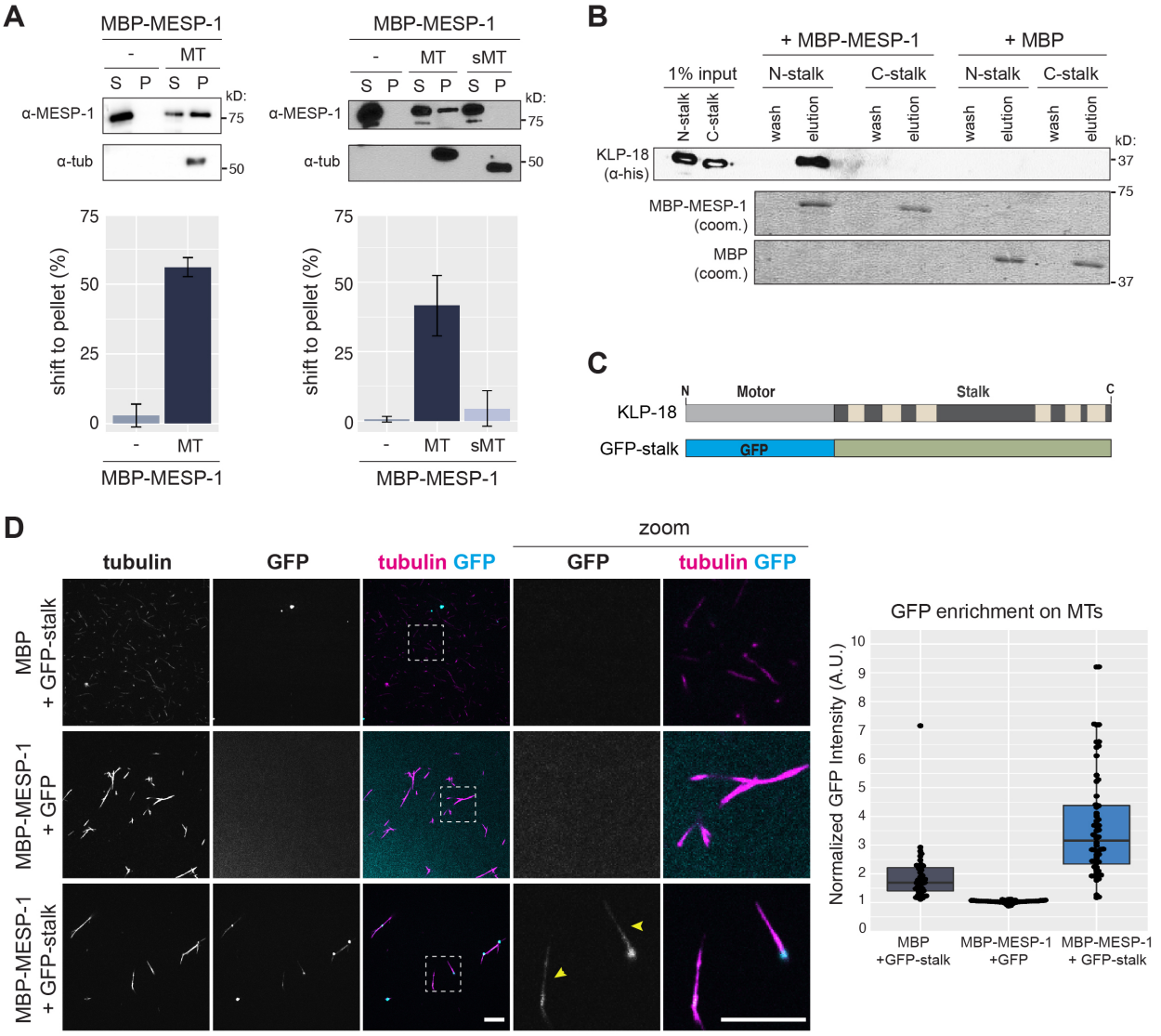
A
MBP-MESP-1
- MT
S P S P
α-MESP-1
α-tub
kD:
75
50
shift to pellet (%)
75
50
25
0
- MT
MBP-MESP-1
MBP-MESP-1
- MT sMT
S P S P S P
α-MESP-1
α-tub
kD:
75
50
shift to pellet (%)
75
50
25
0
- MT sMT
MBP-MESP-1
B
+ MBP-MESP-1
+ MBP
1% input
N-stalk
C-stalk
N-stalk
C-stalk
N-stalk
C-stalk
wash
elution
wash
elution
wash
elution
wash
elution
KLP-18
(α-his)
kD:
37
MBP-MESP-1
(coom.)
75
MBP
(coom.)
37
C
N
Motor
Stalk
C
KLP-18
GFP-stalk
GFP
D
zoom
tubulin
GFP
tubulin GFP
GFP
tubulin GFP
MBP
+ GFP-stalk
MBP-MESP-1
+ GFP
MBP-MESP-1
+ GFP-stalk
GFP enrichment on MTs
Normalized GFP Intensity (A.U.)
10
9
8
7
6
5
4
3
2
1
0
MBP
+GFP-stalk
MBP-MESP-1
+GFP
MBP-MESP-1
+ GFP-stalk

Figure 3.5

Figure 3.5. **KLP-18 is targeted to microtubules through a direct interaction with microtubule associated protein MESP-1.** a) Microtubule co-sedimentation assay for MBP-MESP-1 with no microtubules added (-), undigested (MT), and subtilisin digested (sMT) microtubules. Representative blots show supernatant (S) and pellet (P) samples, quantification is of average shift +/- sd. n = 2 experiments for non-subtilisin experiment, n = 3 experiments for subtilisin experiment. b) MBP-MESP-1 direct interaction to N-stalk or C-stalk was tested by MBP pulldown. Reactions using MBP-MESP-1 or MBP as bait are shown. KLP-18 truncations visualized on Western blot with anti-His antibody, MBP and MBP-MESP-1 visualized by Coomassie stain. c) Schematic of GFP-stalk. d) KLP-18 recruitment to microtubules was tested by visualization of GFP-stalk on TMR-microtubules. Representative images shown for each condition. Note that GFP-stalk localized along microtubules in the presence of MBP-MESP-1 (indicated by arrowheads), but was often enriched at microtubule ends. Quantification of normalized GFP intensity overlaid on microtubules is shown. Box represents first quartile to third quartile and the median is indicated by a horizontal line. Quantified images were acquired over 2 independent experiments. See Chapter 5 for full description of quantification. Scale bars = 10μm.

3.4. The KLP-18 stalk microtubule interaction domain is essential for spindle assembly

Next, we sought to investigate the relevance of the C-terminal microtubule binding site *in vivo*. We hypothesized that KLP-18 generates force by statically binding a microtubule with its stalk and dynamically walking on a second microtubule with its motor domain, thereby sliding microtubules relative to each other. To test this, we made use of a previously described *klp-18(or447)* temperature sensitive mutant, which contains two substitutions (V854M and G876S, Figure 3.6A)[102] in the C-terminal domain that we showed *in vitro* contains a microtubule binding site. At the restrictive temperature of 26°C, this mutant has high embryonic lethality, defects in polar body extrusion, and aberrant chromosome dynamics, thus recapitulating key features of the KLP-18 depletion phenotype[102]. However, the effect of this mutant form of KLP-18 on meiotic spindle architecture has not been investigated.

We quantified spindle assembly defects in *klp-18(or447ts)* by shifting worms to the restrictive temperature for 1 hour, thus inactivating KLP-18 before the initiation of spindle assembly (Figure 3.6A). During normal spindle assembly, microtubules form a cage-like structure and then minus ends are sorted outwards, enabling them to form multiple poles ("multipolar" category) that then coalesce to form a bipolar spindle ("bipolar" category)[48]. When KLP-18 is depleted, the cage forms but since the outward sorting force is lost, microtubules rearrange into a monopolar spindle with chromosomes arranged in a rosette ("monopolar")[48,56,101,102]; chromosomes then move inwards to the monopole during anaphase ("collapsed")[104]. In *klp-18(or447ts)* oocytes at the permissive temperature (15°C), we found that 22% of spindles were monopolar or collapsed. This indicates that KLP-18 function is partially compromised, consistent with previously-reported embryonic lethality at this temperature[102]. Upon shift to the restrictive temperature, the percentage of monopolar/collapsed spindles increased to over 60%. As expected, the poles of the monopolar spindles in *klp-18(or447ts)* oocytes were marked by the minus-end marker ASPM-1[56,137], phenocopying *klp-18(RNAi)* and confirming that microtubule sorting was aberrant (Figure 3.6C). However, ASPM-1 also localized to some microtubule ends on the outside of the aster in 24/30 monopolar spindles analyzed (Figure 3.6C, arrows), suggesting that this mutant may allow weak sorting activity during spindle assembly. Supporting this, 2% of oocytes contain bipolar spindles at 26°C (Figure 3.6A).

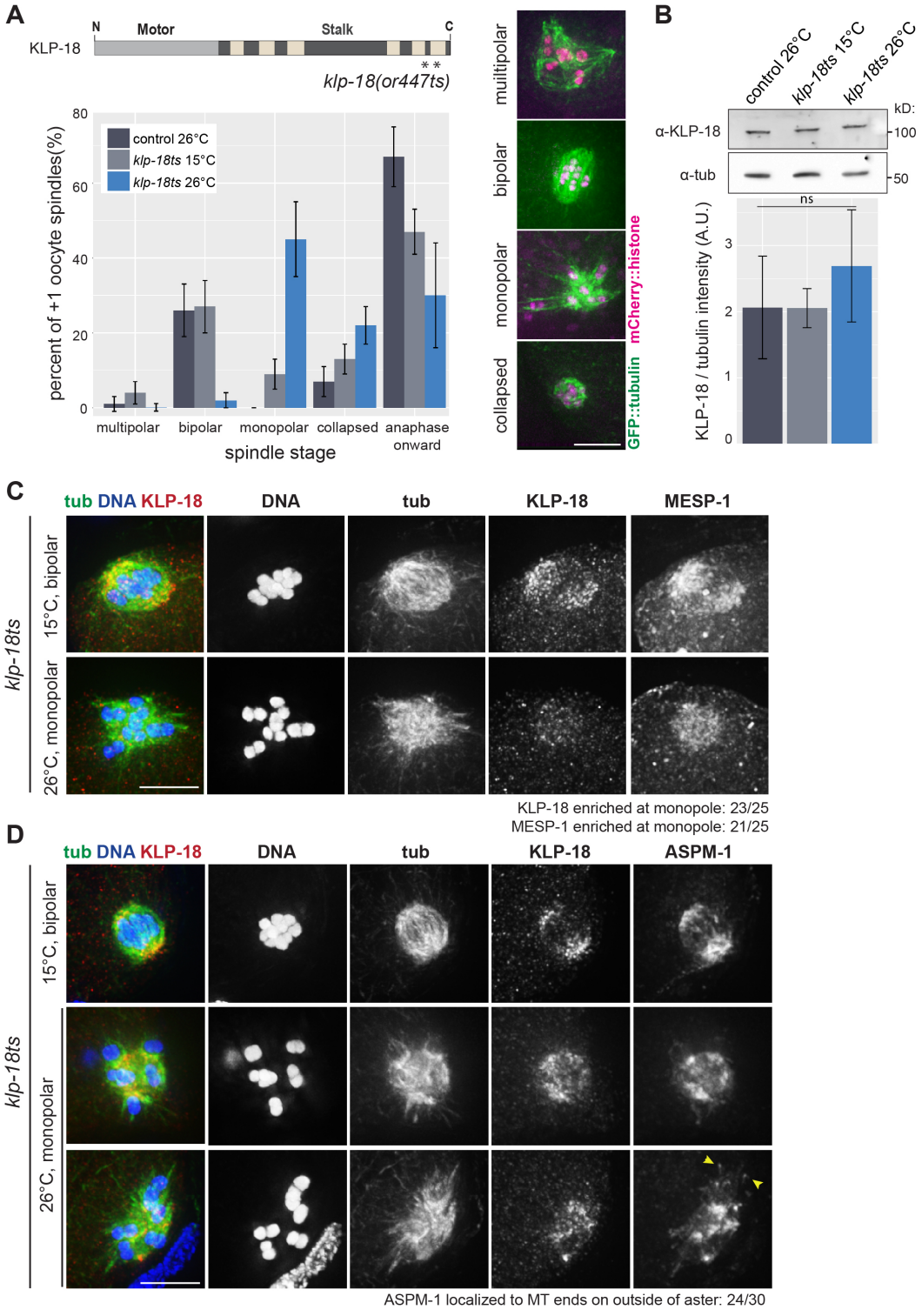
A
N
Motor
Stalk
C
KLP-18
* *
klp-18(or447ts)
percent of +1 oocyte spindles(%)
control 26°C
klp-18ts 15°C
klp-18ts 26°C
multipolar
bipolar
monopolar
collapsed
anaphase onward
spindle stage
multipolar
bipolar
monopolar
collapsed
GFP::tubulin
mCherry::histone
B
control 26°C
klp-18ts 15°C
klp-18ts 26°C
kD:
α-KLP-18
α-tub
100
50
ns
KLP-18 / tubulin intensity (A.U.)
C
tub DNA KLP-18
DNA
tub
KLP-18
MESP-1
klp-18ts
15°C, bipolar
26°C, monopolar
KLP-18 enriched at monopole: 23/25
MESP-1 enriched at monopole: 21/25
D
tub DNA KLP-18
DNA
tub
KLP-18
ASPM-1
klp-18ts
15°C, bipolar
26°C, monopolar
ASPM-1 localized to MT ends on outside of aster: 24/30

Figure 3.6

Figure 3.6. **KLP-18 stalk microtubule interaction domain is essential for spindle assembly.** a) Oocyte spindle morphology in the most recently fertilized (+1) embryo of *klp-18(or447ts)* worms expressing GFP::tubulin and mCherry::histone was quantified at permissive (15°C) and restrictive (26°C) temperatures. Location of the *klp-18(or447ts)* mutations within the microtubule binding region and representative images of the categories scored are shown. Bars represent mean percentage +/- sd. For all conditions n = 3 experiments. b) Western blot of control and *klp-18(or447ts)* worms at permissive (15°C) and restrictive (26°C) temperature. Representative blot (top) with quantification of normalized KLP-18 band intensity below (mean +/- sd). KLP-18/tubulin intensity was not significantly different between any of the 3 conditions over n = 3 experiments quantified ($p < 0.05$, paired one-tail Student's t-Test). c) DNA (blue), tubulin (green), KLP-18 (red), and ASPM-1 (not shown in merge) localization in *klp-18(or447ts)* worms at permissive (15°C) or restrictive (26°C) temperature. Two examples of monopolar spindles are shown: with ASPM-1 primarily enriched at monopole (top), and with ASPM-1 enriched both at monopole and on outer microtubule ends (bottom, end enrichment marked with arrows). d) DNA (blue), tubulin (green), KLP-18 (red), and MESP-1 (not shown in merge) localization in *klp-18(or447ts)* worms at permissive (15°C) or restrictive (26°C) temperature. See Chapter 5 for full description of quantification. Scale bar = 5μm.

Although our results suggest that the KLP-18 C-terminal domain is required for proper force generation, it is also possible that the *or447* mutations merely destabilize the KLP-18 protein. To test this, we shifted worms to the restrictive temperature and assessed protein levels by Western blot. We did not detect a decrease in KLP-18 abundance in *klp-18(or447ts)* worms at 15°C or 26°C compared to control worms (Figure 3.6B), suggesting that the observed phenotypes in the *klp-18(or447ts)* mutants are not due to loss of KLP-18 protein. Moreover, at the restrictive temperature, both KLP-18 and MESP-1 localized to the monopolar spindle pole (Figure 3.6D). These results suggest that KLP-18 remains spindle-associated in *klp-18(or447ts)* oocytes, either through its motor domain or through tethering by MESP-1. Despite remaining localized to microtubules, the mutant form of KLP-18 results in the formation of a monopolar spindle, suggesting that the mutations in the C-terminal microtubule interaction domain disrupt KLP-18 force generation in the meiotic spindle, preventing microtubule sorting.

3.5. KLP-18 sorting activity is essential to maintain spindle bipolarity

Given the importance of KLP-18 in spindle assembly, we next asked if KLP-18 is also necessary to maintain spindle bipolarity. In human acentrosomal oocytes, meiosis proceeds through an extended bipolar stage that can become unstable, and this instability is correlated with errors in chromosome segregation that result in aneuploidy[87]. Therefore, it is important to understand the molecular mechanisms that maintain meiotic acentrosomal spindle stability.

Kinesin-5 is essential for acentrosomal spindle maintenance in mouse and *Drosophila* oocytes[96,140,152], but whether kinesin-12 can similarly maintain spindle bipolarity has not been tested in oocytes of any system. The rapid *klp-18(or447)* temperature sensitive mutation allows us to address this question by inactivating KLP-18 function after spindles have already formed. To this end, we induced metaphase I arrest by depleting the anaphase promoting complex (APC) component EMB-30 using RNAi[237]. Since the *C. elegans* germline is organized in a production-line fashion, oocytes continue to be fertilized despite this depletion, and each forms a spindle that arrests at Metaphase I; this leads to a buildup of bipolar spindles in the germline (with the most-recently fertilized oocyte having the spindle that was most recently formed). In both *klp-18(or447ts) emb-30(RNAi)* worms at 15°C and the wild-type *emb-30(RNAi)* control at 26°C, at least 60% of the two most recently arrested oocyte spindles were bipolar (recently fertilized oocyte positions denoted +1 and +2; Figure 3.7A). In contrast, when *klp-18(or447ts) emb-30(RNAi)* worms were shifted to 26°C, the majority of oocyte spindles were monopolar (93% (+/- 6%) in +1 and 83% (+/- 12%) in +2). Moreover, we also observed monopolar spindles at positions beyond the +2 position in the germline (Figure 3.7D). Under the conditions of our temperature shift, spindles in the +1 position may have formed after KLP-18 was inactivated, but spindles in oocytes that had

been arrested longer should have established bipolarity before KLP-18 inactivation. These results suggest that KLP-18 is required to maintain spindle bipolarity.

Next, we used live imaging to confirm these results and to quantify the dynamics of spindle collapse. Upon dissecting and mounting *klp-18(or447ts) emb-30(RNAi)* embryos at room temperature (23-25°C), pre-formed oocyte spindles collapsed within 2 minutes (Figure 3.7B and C), confirming that KLP-18 activity is essential for spindle maintenance. Moreover, we again confirmed persistent KLP-18 and MESP-1 localization to the monopolar spindle in temperature-shifted worms (Figure 3.7E), indicating that KLP-18 remains spindle-associated but inactive. Taken together, these results show that KLP-18 activity is essential to maintain a bipolar spindle and that this force generation relies on the KLP-18 stalk microtubule binding domain.

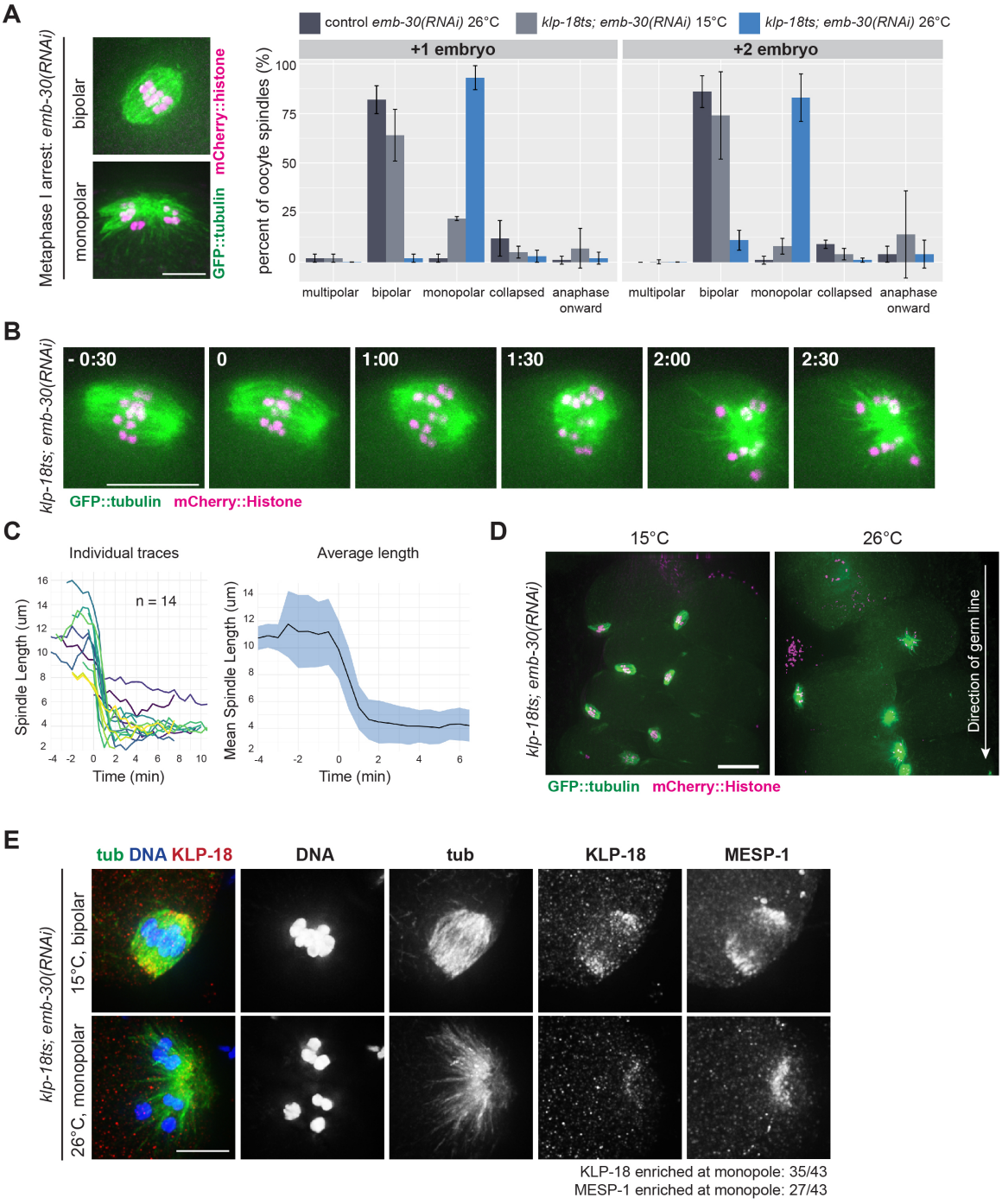
A
Metaphase I arrest: emb-30(RNAi)
bipolar
monopolar
mCherry::histone
GFP::tubulin
control emb-30(RNAi) 26°C
klp-18ts; emb-30(RNAi) 15°C
klp-18ts; emb-30(RNAi) 26°C
+1 embryo
+2 embryo
percent of oocyte spindles (%)
multipolar
bipolar
monopolar
collapsed
anaphase onward
B
klp-18ts; emb-30(RNAi)
- 0:30
0
1:00
1:30
2:00
2:30
GFP::tubulin mCherry::Histone
C
Individual traces
Average length
n = 14
Spindle Length (um)
Mean Spindle Length (um)
Time (min)
D
15°C
26°C
klp-18ts; emb-30(RNAi)
Direction of germ line
GFP::tubulin mCherry::Histone
E
tub DNA KLP-18
DNA
tub
KLP-18
MESP-1
klp-18ts; emb-30(RNAi)
15°C, bipolar
26°C, monopolar
KLP-18 enriched at monopole: 35/43
MESP-1 enriched at monopole: 27/43

Figure 3.7

Figure 3.7. **KLP-18 sorting activity is essential to maintain spindle bipolarity.** a) Spindle morphology in the +1 and +2 embryos of metaphase I-arrested *klp-18(or447ts) emb-30(RNAi)* worms expressing GFP::tubulin and mCherry::histone was quantified at permissive (15°C) or restrictive (26°C) temperature. Bars represent mean percentage +/- sd. For all conditions n = 3 experiments. Scale bar = 5μm. (b) and (c) Spindle collapse was filmed in metaphase I-arrested *klp-18(or447ts)* worms expressing GFP::tubulin and mCherry::histone. Spindle length measurements for individual spindles are shown on left and average +/- sd is shown on right (n = 14). Time = 0 min was set as first frame after shortening began. Representative stills of Movie S1 are shown in (b). Scale bar = 10μm. d) Representative images of *klp-18(or447ts) emb-30(RNAi)* germ lines at 15°C and 26°C. Arrow indicates direction of germ line; the most recently arrested spindle is at the top of each image. Scale bar = 15μm. e) DNA (blue), tubulin (green), KLP-18 (red), and MESP-1 (not in merge) localization in metaphase I arrest *klp-18(or447ts)* GFP::tubulin, mCherry::histone worms at 15°C and 26°C. See Chapter 5 for full description of quantification. Scale bar = 5μm.

3.6. Discussion

Our work is the first biochemical characterization of kinesin-12/KLP-18 and MESP-1, providing the first mechanistic dissection of force generation in a system in which kinesin-12 is naturally the dominant outward force generating motor. We propose a model in which KLP-18 exists in an autoinhibited state that is alleviated by binding to MESP-1. This enables a domain in the C-terminal half of the stalk to bind microtubules, which allows the complex to crosslink and slide spindle microtubules to generate force (Figure 3.8). If the C-terminal microtubule binding domain is disrupted, KLP-18 can no longer crosslink microtubules and generate force, even if the motor domain is still associated to microtubules. This suggests that a direct stalk-microtubule interaction facilitates force generation in the meiotic spindle.

In mammalian somatic cells, kinesin-5 generates outward force on microtubules to achieve spindle bipolarity[91,95,154], and when kinesin-5 function is altered, kinesin-12 can take over this role[166–168,173,186]. The molecular basis for this activity has been well characterized *in vitro* and in cell culture[171,172,192–195,238]. Our work confirms that certain properties of kinesin-12s are shared across species: presence of discrete coiled-coil domains in the C-terminal stalk,

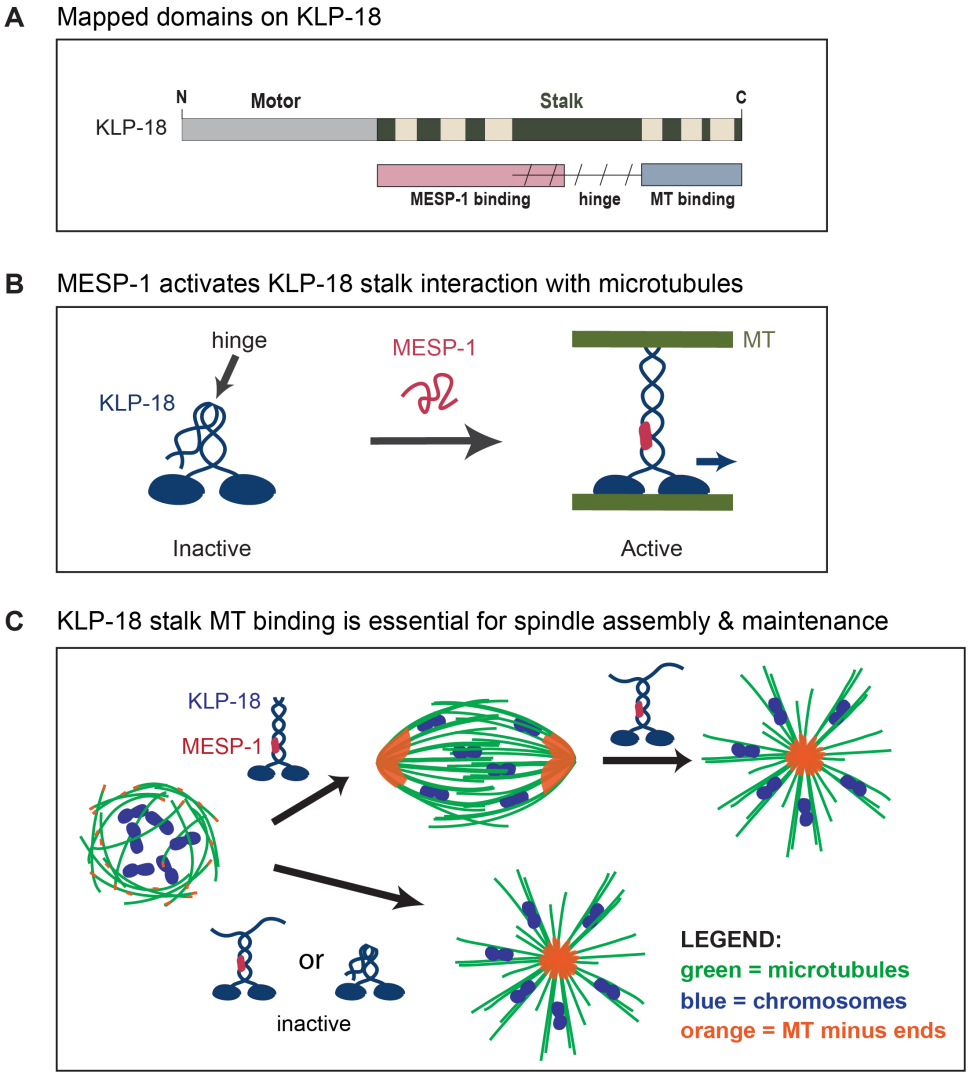

Figure 3.8. **Model. KLP-18 C-terminal microtubule binding site is activated by MESP-1 and is essential for spindle assembly and maintenance of bipolarity.** a) KLP-18 stalk contains a MESP-1 binding site in its N-terminal half (pink), a microtubule binding site in its C-terminal half (blue), and likely contains a flexible hinge region (slanted dashed lines) that functions to self-inhibit the motor. b) KLP-18 exists in an auto-inhibited inactive state that is activated through binding of MESP-1. MESP-1 binding targets KLP-18 to spindle microtubules and allows the motor to generate force on the spindle. c) Disruption of the C-terminal microtubule binding site impairs microtubule sorting during spindle assembly and leads to the collapse of pre-formed bipolar spindles. Both the C-terminal microtubule binding site and interaction with MESP-1 are essential for KLP-18 function. KLP-18 is shown as blue and MESP-1 is shown as red on cartoon. On spindle diagram, microtubules are green, chromosomes are blue, and microtubule minus ends are orange.

the requirement of a C-terminal non-motor microtubule binding site, self-inhibition of non-motor microtubule binding, and regulation by a TPX2-like adaptor protein. Mammalian kinesin-12 Kif15 has been described as both a homodimer and a homotetramer in recent studies[171,172,192–195], and it will be interesting to investigate the oligomerization state of KLP-18. In addition, Kif15 has a variety of interesting biophysical properties, including the ability to walk with minus-end directionality and to switch microtubule tracks[193], and it will be crucial to investigate similar properties in KLP-18 and to directly examine the effect these properties may have on acentrosomal spindles. Finally, *C. elegans* is the only known organism in which kinesin-12, and not kinesin-5, is the dominant force generating motor. Directly comparing force generating biochemical properties (e.g. motor velocity, stall force, processivity) between KLP-18 and kinesin-5 may help explain how a kinesin-12 is able to generate kinesin-5-like forces.

Our work provides insight into how meiotic spindle bipolarity is maintained in the absence of centrosomes and force-bearing kinetochore fibers (k-fibers). The importance of kinesin-5 in mitotic spindle maintenance is cell-line dependent and correlated to the stability of the cell's k-fibers[153]. In cells with stable k-fibers, kinesin-5 is dispensable for spindle maintenance but kinesin-12 Kif15 is required, presumably due to direct Kif15 stabilization of k-fibers. Therefore, k-fibers appear to be the stabilizing factor within formed mitotic spindles, and continuous kinesin-12 motor activity aids in their function. EM reconstructions have shown that *C. elegans* meiotic spindles are composed of short tiled microtubules as opposed to long k-fiber-like bundles[125] and previous work has suggested that microtubule associated proteins act to connect short microtubules into longer microtubule bundles comprising a functional spindle[129]. We speculate that kinesin-12 KLP-18 performs an analogous role in oocytes in the

absence of k-fibers, providing constant outward force on bundled microtubules to maintain spindle integrity.

Previously, we and others have proposed that KLP-18 acts to organize and sort microtubules during anaphase[100,129], but this hypothesis has not yet been directly tested. Understanding the role of KLP-18 may help to resolve different models of chromosome segregation proposed in *C. elegans* oocytes (reviewed in[8,14])[58,100,104,129,155,216,217,239]. Further characterization of KLP-18's role in spindle assembly, spindle maintenance, and chromosome segregation will be essential to fully understand *C. elegans* oocyte meiosis.

CHAPTER 4

Summary of findings and future directions

4.1. Summary of findings

My work described here has helped to establish *C. elegans* as a powerful system to study acentrosomal spindle assembly and the proteins essential in this process. Previous to publishing Chapter 2, the prevailing model in the field was that *C. elegans* oocyte spindles, like mouse spindles, contained canonical microtubule organizing centers (MTOCs) that helped to nucleate and organize spindle microtubules. This finding was based on live-cell time lapse imaging[14]. Although an extremely powerful technique to understand the dynamics and temporal organization of cellular processes, this type of imaging simply does not have adequate resolution to fully characterize cellular architecture (see Introduction for overview of imaging techniques discussed here). Therefore, when pole proteins were found in discrete foci with live-cell imaging, the authors reasonably concluded that these foci were canonical MTOCs[102].

To test this finding, we set out to fully characterize microtubule morphology during spindle assembly by visualizing oocyte spindles with both high-resolution live imaging and fixed immunofluorescence. Immunofluorescence had been used by our lab and others to characterize meiotic anaphase and the structure and regulation of the midbivalent ring complex[56,58,104], a complex of conserved proteins that forms a ring around the central region of the bivalent and is thought to be required for both proper chromosome congression and segregation[8]. However, high resolution immunofluorescence had not yet been used to carefully examine the stages of spindle assembly. By mounting and imaging live worms expressing GFP::tubulin and GFP::histone, we identified three distinct stages of spindle assembly: (1) After fertilization of the oocyte, the nuclear envelope breaks down and microtubules form a cage-like structure adjacent to the interior of the disassembling nuclear envelope; (2) Cage microtubules are sorted and organized such that microtubule minus ends are pushed to the

periphery of the array and bundled into the poles of a multipolar spindle; (3) Poles of the multipolar spindle coalesce into a bipolar spindle. These results were confirmed through our own live time-lapse imaging and with immunofluorescence. Importantly, we did not find any evidence of canonical MTOCs (small clusters of pericentriolar material proteins that nucleate microtubule asters), which challenged the current model in the field and proposed an unappreciated microtubule architecture during spindle assembly.

After characterizing spindle assembly at high resolution, the next logical question was: what proteins are providing the sorting force that reorganizes cage microtubules into multipolar spindle microtubules, then from multipolar spindles to bipolar ones? To answer this question, I followed up on two hits from a large-scale RNAi screen that had been performed previously[56]: *klp-18* and *mesp-1*. Neither protein had been carefully characterized; KLP-18 was known to be a kinesin-12 motor that was essential for spindle assembly[56,101,102] but the mechanism of this activity was unknown, and MESP-1 was a novel protein that had only been identified and named[56]. In the screen, *mesp-1(RNAi)* or *klp-18(RNAi)* depletion led to monopolar spindles and nonviable embryos, indicating that these proteins are essential to generate forces that lead to spindle bipolarity. To understand their activity *in vivo*, I used high-resolution immunofluorescence to investigate the localization and interdependency of KLP-18 and MESP-1. I found that the two proteins co-localized through all stages of spindle assembly: they first become enriched on the microtubule cage, then show extensive localization to both the poles and the spindle microtubules of multipolar spindles, then finally dramatically localize to the poles of the bipolar spindle and to a lesser extent to microtubules near chromosomes. I found that the two proteins are interdependent for localization and that they are present in a protein complex in worm extract. Interestingly, we found that the previously identified *C. elegans* homolog of TPX2, TPXL-1[225], was not essential

for KLP-18 localization to the spindle. We therefore proposed that MESP-1 is a functional ortholog of TPX2, due to its kinesin-12 targeting function, and that it is a rapidly evolving protein. This work represents the first cellular characterization of KLP-18 function, as well as the initial report of MESP-1 function.

Cellular characterization of KLP-18 and MESP-1 function allowed us to propose a model for MTOC-independent acentrosomal spindle assembly in *C. elegans*. However, this model was not mechanistically satisfying so I aimed to understand how KLP-18 and MESP-1 act biochemically to generate essential force on spindle microtubules. To do this, I initiated an *in vitro* biochemical approach with pure components of the complex: tubulin, KLP-18, and MESP-1. Nothing was known about the biochemistry of KLP-18 and MESP-1. I found that KLP-18 contains a non-motor microtubule binding site in its coiled-coil C-terminal stalk domain, and that this binding site is activated through direct interaction of MESP-1 to the stalk. Structural and biochemical characterization revealed that MESP-1 is an intrinsically disordered and unstable protein that interacts with microtubules. To test the *in vivo* relevance of the stalk microtubule binding site, I used a previously characterized temperature sensitive mutation in the mapped microtubule interacting domain[102], and found that this mutation disrupts KLP-18 force generation leading to monopolar spindles. In addition, I found that KLP-18 is not only essential for spindle assembly but also for spindle maintenance. This work revealed several novel aspects of KLP-18 and MESP-1 function: KLP-18 contains a microtubule binding site on its stalk, MESP-1 directly interacts with the KLP-18 stalk and activates stalk microtubule binding, the stalk binding site is essential for KLP-18 force generation *in vivo*, and KLP-18 force is continuously required through at least metaphase.

In summary, my work established the prevailing model for *C. elegans* oocyte spindle assembly, identified KLP-18 and MESP-1 as collaborators in building bipolar spindles, and began to elucidate the underlying biochemistry of KLP-18 and MESP-1 function. Our model for MTOC-independent spindle assembly, published in *Molecular Biology of the Cell*, is now the accepted model in this widely used and important model organism. Below, I will describe broad future avenues of research based on the results summarized here.

4.2. Future directions

This work sets the stage for new investigation into specific questions involving KLP-18 and MESP-1 biochemistry and its relation to cellular functions, conservation of kinesin-12 and adaptor protein function across organisms, genetic variation and rapid evolution of essential proteins within *Caenorhabditis*, and most broadly, fundamental questions about the physical nature of MTOC-free acentrosomal spindle poles. I will give brief background and proposed questions for each topic in hopes of inspiring future research endeavors.

4.2.1. What can the biochemical properties of KLP-18 and MESP-1 teach us about meiotic kinesin function?

Although some important aspects of KLP-18 and MESP-1 biochemistry have been identified in this work, a great number of questions remain. The surge in recent biochemical studies on mammalian kinesin-12, Kif15, has revealed a variety of surprising biochemical properties. Compelling evidence has shown that Kif15 is able to fold and self-inhibit[192], preferentially binds kinetochore-microtubule bundles[173], exists as a tetramer[193], can also exist as a dimer[192], walks to both the plus and minus ends of microtubules[193], generates significant force on spindle microtubules[171], switches microtubule tracks at intersections[193], carries microtubules as cargo[193], suppresses microtubule catastrophe[194], assembles microtubules into

bundles[194], and works as a mechanical ratchet[172]. The breadth of Kif15 biochemical ability is even more surprising considering it is a non-essential motor in most somatic cell types. The most obvious and straightforward extension to my work is to similarly characterize KLP-18 biophysically and test the importance of discovered biophysical properties *in vivo*.

It might be tempting to wonder what new insights could be gained from further investigation of a nematode kinesin while the mammalian homolog is so thoroughly characterized. A great advantage of using *C. elegans* as a model system for mechanistic studies is the relative ease in which genes can be edited to test a hypothesis generated from *in vitro* biophysical work directly within a live animal. I have shown in this dissertation that a feature discovered with purified proteins can be directly investigated *in vivo* using established genetics and imaging techniques. Therefore, it is easy to imagine that a thorough dissection of KLP-18 biophysical activity *in vitro* may yield interesting discoveries *in vivo*. It is important to point out that *C. elegans* is the only widely used model organism in which kinesin-5/Eg5 does not dominate and kinesin-12 is the main force generating motor during cell division. Studies investigating Kif15 function use somatic cells that have been artificially evolved to survive in an Eg5 independent manner. Investigating KLP-18 allows investigation of kinesin-12 in a live animal and in a cellular context in which it naturally functions as the main force generating motor.

The most illuminating future biophysical studies of KLP-18 will need to be done with purified full length motor, preferably tagged with a bright GFP. This in itself is quite an undertaking; the studies listed above were all done using motors purified from insect cell culture, and expressing KLP-18 in this system will need to be optimized. However, I have established protocols for purifying both the motor domain and the stalk domain, so purification of the full length motor should align reasonably well with these protocols. Once

expressed and purified, KLP-18 can be used in a wide variety of biophysical assays. A major outstanding question is if KLP-18 acts as a dimer or a tetramer. I have drawn my diagrams as if KLP-18 is a dimer, but this is an educated guess and not based on any experimental evidence. Oligomerization can be tested by SEC-MALS (size exclusion chromatography coupled multi-angle light scattering) or through negative stain electron microscopy. Elucidating KLP-18 oligomerization would further explain how KLP-18 can generate force on microtubules. It would also be possible to include MESP-1 in these experiments to test the oligomerization state of MESP-1 and to understand the molecular stoichiometry of the MESP-1/KLP-18 complex. A purified full length KLP-18 would allow more rigorous direct testing of the 'hinge' model proposed in Chapter 3. In addition, motor velocity, directionality, processivity, and microtubule sliding can be tested by single molecule TIRF, both with and without MESP-1 present.

Describing the biophysical properties of KLP-18 will more fully put it into context with other mitotic and meiotic kinesins. This would help answer a very intriguing outstanding question: Is KLP-18 biophysically more like a kinesin-12 or kinesin-5? Kinesins are typically grouped into families by the sequence identity of their motor domains and KLP-18's has the most homology to others in the kinesin-12 family. But is this grouping superficial? If one compares the most important biophysical properties that define the cellular function of KLP-18 with either Eg5 or Kif15, to which will it be more similar? The answers will reveal how kinesin-12s evolve to take on a more important cellular role; whether they optimize established kinesin-12 properties or if they evolve to mimic kinesin-5. Rather than exogenously altering a cell culture line to understand how kinesin-12 can adapt, we can potentially leverage an experiment nature has already performed for us.

As of this writing, my work is one of the few studies that examines the relationship between a kinesin motor's biochemical properties and its function specifically within an acentrosomal spindle. As I have described in the Introduction, acentrosomal oocyte spindles have a fundamentally different underlying microtubule architecture than centrosomal mitotic spindles. This is especially evident in *C. elegans*. Chromosomes in the meiotic divisions are holocentric, meaning that the kinetochore forms cup-like structures around the two lobes of the bivalent instead of forming a discrete point on each homolog. In *C. elegans* oocyte meiosis, microtubules do not make canonical end-on microtubule attachments to the chromosomes but rather associate with the chromosomes laterally. Lateral attachments in oocyte spindles are also present in mammalian oocytes (where they co-exist with kinetochore-microtubule attachments), however, the role and importance of these attachments are unclear. Nevertheless, because of the lack of kMT bundles in *C. elegans* oocyte spindles, KLP-18 lacks the main microtubule substrate on which Kif15 acts in mitotic spindles[173]. It is unknown what the preferred microtubule substrate for KLP-18 is, and this can be investigated through a combination of single molecule biophysics and *in vivo* mutational analysis. In addition, it is unclear what is regulating KLP-18 and MESP-1 localization to different parts of the spindle. Once the spindle reaches bipolarity, both proteins become enriched at the poles. The models in Chapter 2 and 3 propose that a KLP-18/MESP-1 complex is generating force in the middle of the spindle near the chromosomes. Although a population of the complex does exist there, this does not explain the role of these proteins at the poles. The motor's relative activity on parallel and anti-parallel microtubules *in vitro* might shed light on differing activities based on spindle localization. Considering the microtubule bundling activity described in Chapter 3, I hypothesize that KLP-18/MESP-1 statically bundle and stabilize

parallel microtubules at spindle poles, and dynamically slide anti-parallel microtubules in the middle of the spindle. This hypothesis could be tested using purified full-length KLP-18.

Finally, it is likely that all of the properties described in this section are regulated by some kind of post-translational modification. To test this, putative modified residues can easily be mutated by CRISPR and the resulting spindle phenotype can be visualized *in vivo*. I have included sequence alignments of KLP-18 motor domain (Figure 4.1), stalk domain (Figure 4.2), and MESP-1 (Figure 4.3) with homologs within *Caenorhabditis*. As explained in Chapter 2, MESP-1 is rapidly evolving within *Caenorhabditis* itself and therefore any conserved regions may potentially be significant for its function. Kinesin-12 motor domains are relatively well conserved, however, stalk domains are not (as evidenced by the alignment presented here), and any conserved regions across kinesin-12 stalks may be similarly significant. Using the GPS 5.0[240,241] kinase phosphorylation site prediction software I was able to identify both conserved and unconserved phosphorylation sites. Conserved predicted Aurora kinase sites at S837 and the striking cluster at S493, S494, T502, and S507 on the KLP-18 stalk and T182 on MESP-1 are worth further investigation, particularly considering the well established role for Aurora kinases during *C. elegans* meiotic divisions[54,217]. To date, there have been no large-scale studies that have identified post-translational modifications in these meiotic proteins, however, a high throughput interactome study identified the polo-like kinases PLK-1 and PLK-2 as interacting with MESP-1[242]. Recently, the post translational modification SUMO (small ubiquitin-like modifier) has been shown as an important regulator of meiotic events particularly during anaphase[216,243,244]. I identified three predicted SUMO interaction motifs (SIMs) on the KLP-18 stalk (Figure 4.2, orange) in close proximity to each other within the predicted hinge region described in Chapter 3. KLP-18 has been proposed to be important for microtubule sliding during anaphase[129], however, this has not

been directly tested. Upon initiation of chromosome segregation during anaphase, SUMO previously located on the midbivalent ring complex re-localizes to spindle microtubules. As I show in Appendix D, KLP-18 localizes to both the poles and the midzone spindle microtubules during anaphase. I therefore hypothesize that an interaction with spindle localized SUMO recruits KLP-18 from spindle poles to midzone microtubules, where it is activated and generates sliding force.

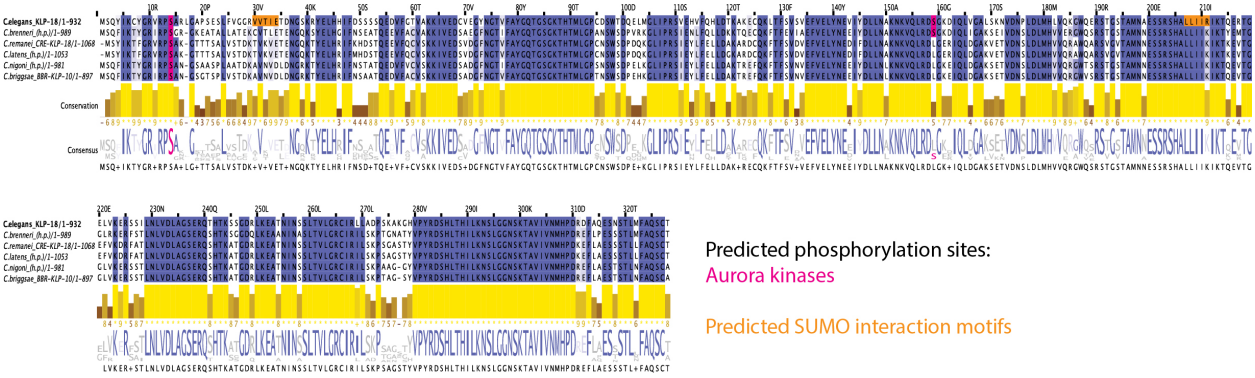

Figure 4.1. **Alignment of KLP-18 motor domain with *Caenorhabditis* homologs**. Alignment of KLP-18 motor domain with homologs found in other *Caenorhabditis* species. Blue indicates conserved amino acid residues, with darker blue showing more conserved. A consensus sequence is shown, along with a bar plot indicating the degree of conservation at a particular amino acid residue. KLP-18 was set as a reference for numbering. Alignment was performed with the MUSCLE algorithm and visualized using Jalview. Aurora kinase sites and SUMO interaction motifs were predicted using GPS 5.0[240] and GPS-SUMO[241].

4.2.2. Leverage inherent genetic variation within *Caenorhabditis* to understand structure-function of meiotic proteins

Genetic variation between nematodes in the *Caenorhabditis* genus presents a unique opportunity to directly test sequence and structural variation between homologous proteins. Particularly, the ability to adapt established experimental and husbandry techniques from *elegans* to a variety of *Caenorhabditis* species presents an interesting opportunity not possible with many other model organisms. As I have shown in the previous section, there is a surprising amount of genetic diversity between KLP-18 and MESP-1 homologs across *Caenorhabditis*. Do these species have similar oocyte spindle morphology? Do they proceed through the same spindle assembly steps? Are KLP-18 or MESP-1 homologs required? If differences are found, can underlying discrepancies in the biochemical activity or structure of homologs cause these differences? A similar concept has been applied to understand spindle size scaling differences within *Xenopus* species[245], a study that elegantly implicated katanin as a molecular determinant of spindle size across species. These types of studies are very difficult if not impossible in mammals, therefore any concepts gleaned from work in *Caenorhabditis* may help to explain how animals evolved differing strategies to accomplish faithful meiosis.

Not only is there significant genetic diversity across *Caenorhabditis*, it exists across natural isolates of *elegans* itself[246]. This diversity can be leveraged to build a molecular parts list of proteins that are important for oocyte meiosis. Up until now, proteins with important roles during cell division have been identified either through RNAi screens[56] or immunoprecipitation-mass spec (IP-MS) identification of interacting proteins[247]. These techniques have been highly rewarding and have led to important work, including this dissertation. However, these techniques have fundamental limitations. RNAi depletes protein

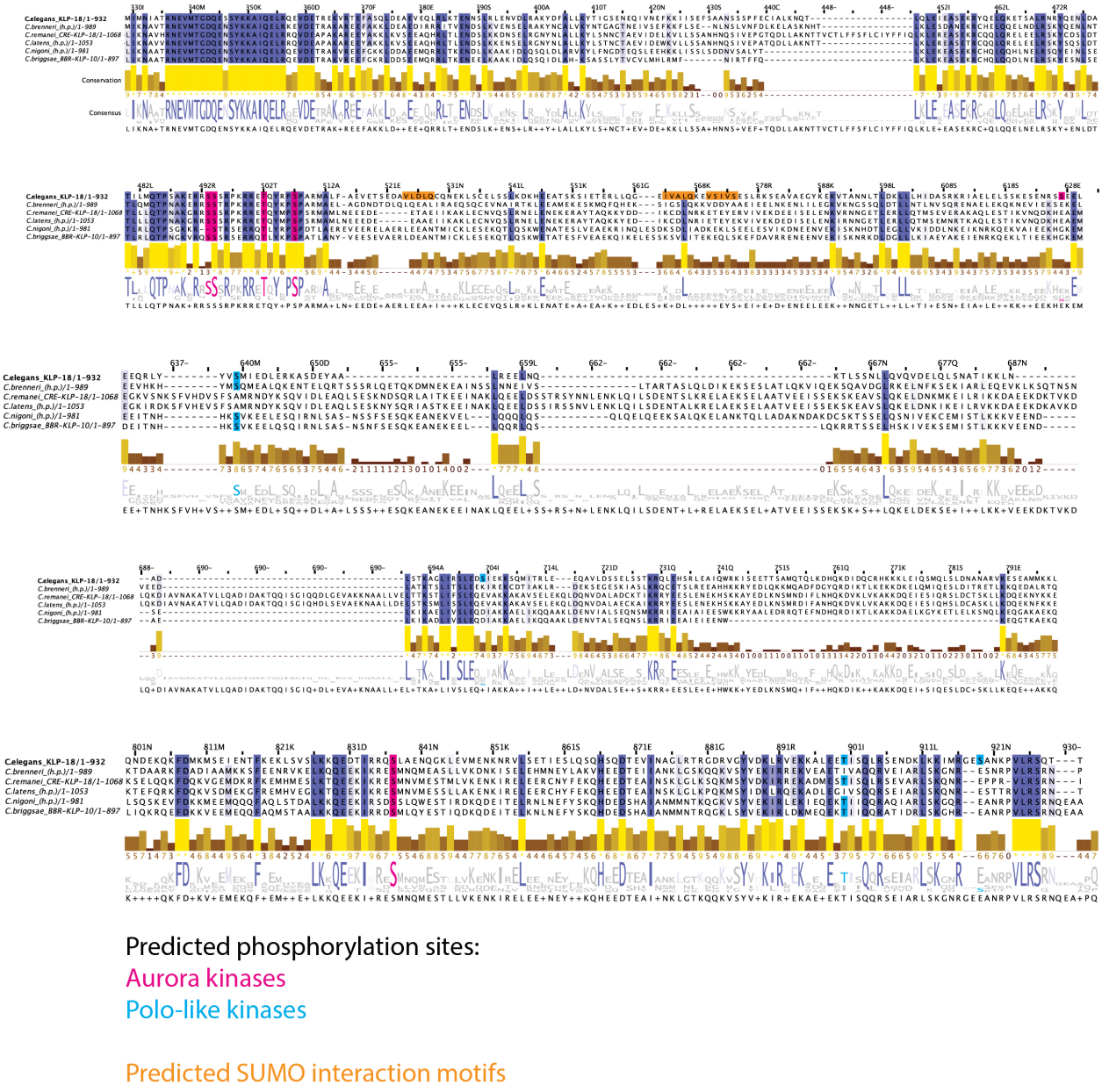

Figure 4.2. **Alignment of KLP-18 stalk domain with homologs found in other *Caenorhabditis* species.** Blue indicates conserved amino acid residues, with darker blue showing more conserved. A consensus sequence is shown, along with a bar plot indicating the degree of conservation at a particular amino acid residue. KLP-18 was set as a reference for numbering. Alignment was performed with the MUSCLE algorithm and visualized using Jalview. Aurora and polo-like kinase sites and SUMO interaction motifs were predicted using GPS 5.0[240] and GPS-SUMO[241]. KLP-18 residues 329-634 are the MESP-1 interacting region, 558-769 are the putative hinge region, and 635-932 are the microtubule interaction region (see Chapter 3).

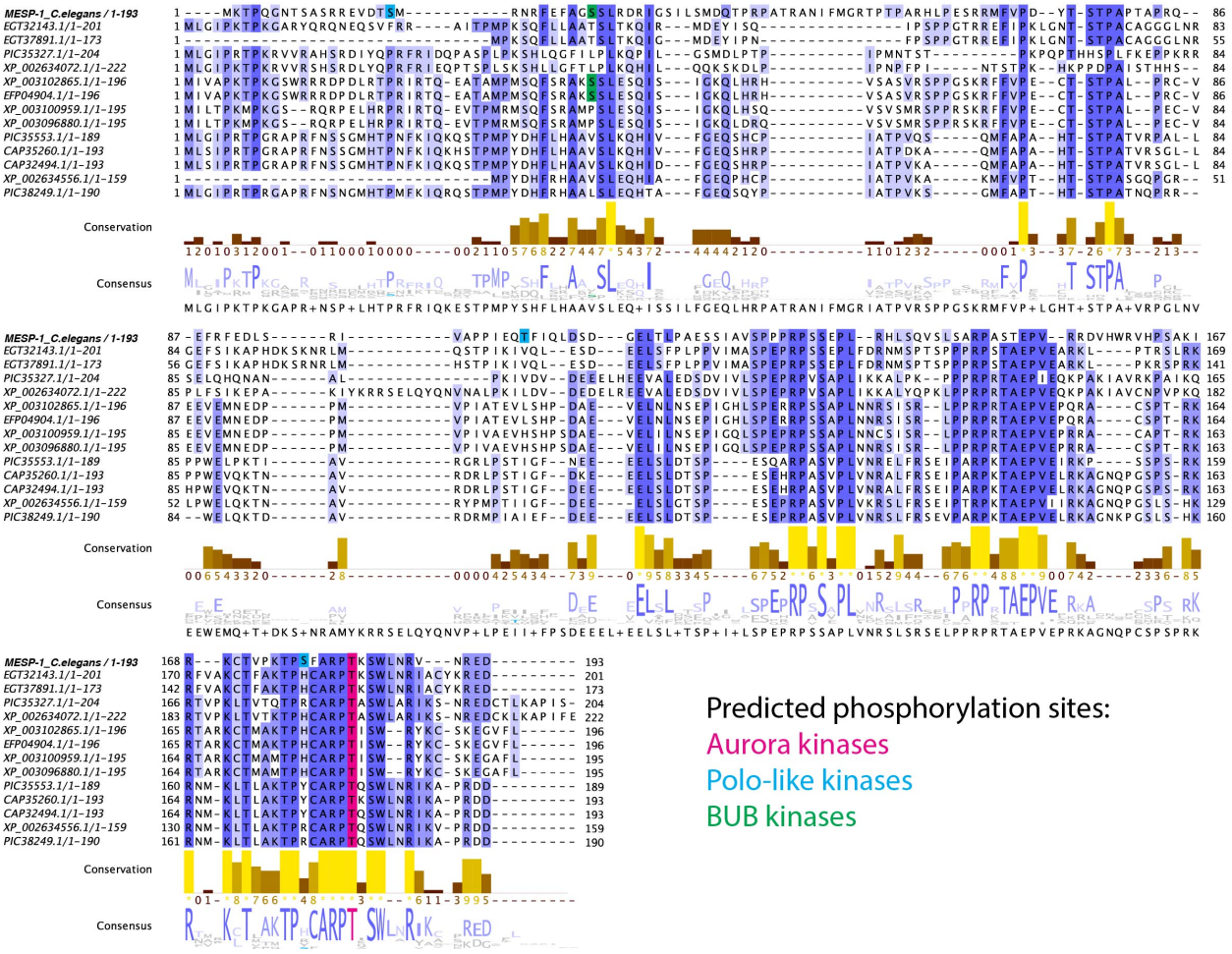

Figure 4.3. **Alignment of MESP-1 with homologs found in other *Caenorhabditis* species.** Blue indicates conserved amino acid residues, with darker blue showing more conserved. A consensus sequence is shown, along with a bar plot indicating the degree of conservation at a particular amino acid residue. KLP-18 was set as a reference for numbering. Alignment was performed with the MUSCLE algorithm and visualized using Jalview. Aurora, BUB, and polo-like kinase sites were predicted using GPS 5.0[240].

expression either in a worm's larval stage (long-term RNAi) or upon entry into adulthood (short-term RNAi). In both cases, only the very first phenotype can be characterized; KLP-18, for example, was known to be essential for spindle assembly, but this phenotype concealed KLP-18's subsequent role in spindle maintenance and continues to obscure any role in anaphase. Therefore, a RNAi screen shows first-order phenotypes but does not tell the whole story. Recently, the auxin inducible degradation (AID) approach has been adapted for use in *C. elegans*[248]. This allows for acute degradation of proteins of interest and allows for investigation of roles in later stages of meiosis, providing an exciting opportunity for future research. However, generating an AID strain is labor intensive and a protein of interest must first be identified and characterized. Similar to RNAi, an IP-MS fails to reveal a comprehensive list of molecular interactions. This technique relies on relatively strong interactions between the bait protein and any interacting proteins, and therefore any transient interactions will not be identified. For example, the interaction between MESP-1 and KLP-18 is so weak that it would likely not persist through the washes necessary in preparing a sample for mass spec. This essential interaction would be missed. As mentioned previously, there is an unappreciated complexity of post-translational modifications that regulate spindle associated proteins and these transient interactions would also likely be missed with an IP-MS approach.

Despite the success of these two techniques, a complementary third approach might be crucial: identifying important genes through quantitative imaging of the meiotic divisions. A pioneering study showed that this type of approach can yield important insights into cellular processes[249]. The authors developed a quantitative imaging technique to measure variations in mitotic spindle traits in *C. elegans* embryos across both *C. elegans* natural isolates and *Caenorhabditis* species. Using these measurements, variations in spindle traits

over a long evolutionary timescale could be quantitatively explained. In theory, a similar approach could be used to identify proteins essential for different aspects of the meiotic divisions. Microtubule cage diameter, bipolar spindle length, spindle assembly time scale, anaphase speed, and timing of meiotic events are a few examples of traits that could be quantified with some optimization. Quantitatively comparing these traits across many wild isolates or *Caenorhabditis* species could yield discrete quantitative trait loci (QTL)[250] and therefore reveal genes that are important in these processes. This approach has the potential to not only fill in the gaps of RNAi and IP-MS approaches by identifying regulatory proteins, but to also illuminate the evolution of meiotic events within a species and perhaps within a genus. Once identified, genes of interest could be verified through standard genetic and imaging techniques.

4.2.3. What is an acentrosomal spindle pole?

The primary morphological difference in spindle structure between somatic mitotic and oocyte meiotic divisions is the absence of centrosomes. As described in the Introduction, our understanding of the fundamental aspects underlying acentrosomal spindle microtubule nucleation, bundling, sorting, and stability lags far behind our understanding of the equivalent processes in centrosomal systems. All of these questions are interesting and important, however, I believe one of the most interesting avenues of future research will be to understand the underlying physical construction of an acentrosomal spindle pole. I propose two distinct models of acentrosomal pole construction: (1) the classic model of static crosslinking and (2) phase separated poles that act as a microtubule anchoring compartment (Figure 4.4). In the 'static crosslinking' model, microtubule associated proteins, like kinesins, dynein, and static microtubule associated proteins, act to form a complex crosslinked network in which individual microtubules are stitched together and heavily bundled at poles. In contrast, the

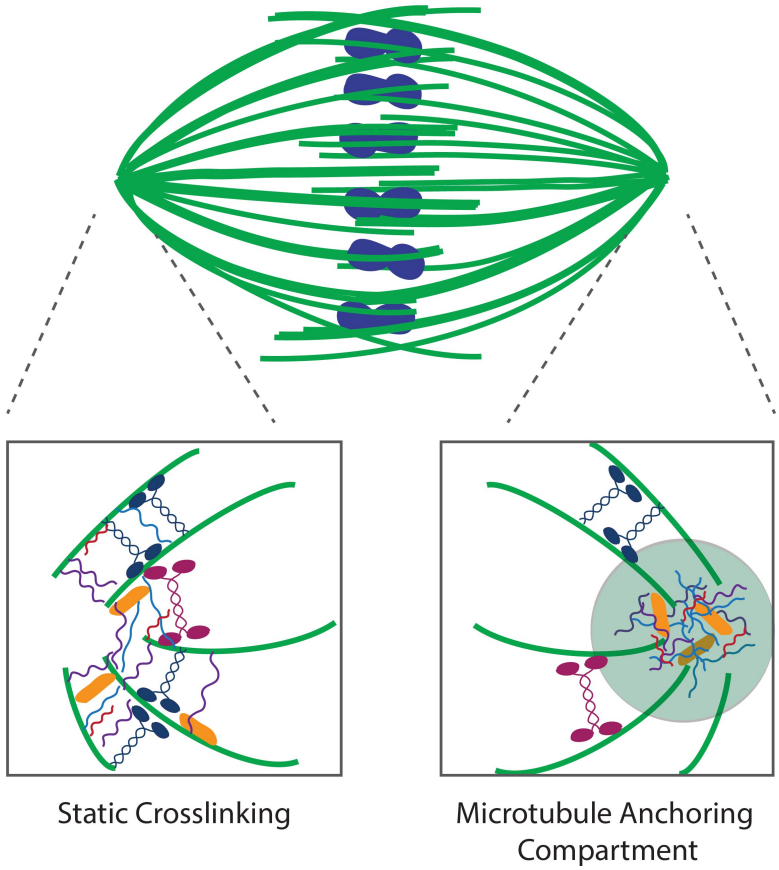

Figure 4.4. **Two proposed models of spindle pole construction**. Simplified cartoon showing my proposed models of pole construction: static crosslinking (left) and microtubule anchoring compartment (right). A random assortment of conceptual microtubule associated proteins are shown. These proteins are for illustration purposes and do not indicate specific proteins. See text for a description of models.

'microtubule anchoring compartment' model suggests that these same microtubule associated proteins form phase separated compartments that act to nucleate or anchor spindle microtubules into the pole. In this model, the pole is a distinct structure separate from spindle microtubules, in the 'static crosslinking' model, the pole is an extension of the spindle microtubule network itself.

There is an increasing body of evidence that points to the possibility of a microtubule anchoring compartment. Spindles in mouse oocytes contain a liquid-like spindle domain (LISD) that contributes to proper spindle assembly[71]. In *C. elegans* embryos, centrosomes

of the mitotic spindle are phase separated condensates[82]. These structures are built by core scaffold proteins, in this case PCM component SPD-5, that form the physical condensate and selectively recruit tubulin binding proteins such as ZYG-9 and TPXL-1. These proteins then recruit tubulin to initiate microtubule nucleation from the centrosome. Conceptually, the condensate exists to create a high local concentration of tubulin from which to nucleate microtubules. It is tempting to predict that the oocyte spindle, formed in the same cell as the eventual embryo, would adapt and employ similar mechanisms to ensure faithful spindle assembly. However, some major differences are obvious and must first be stated. First, PCM components SPD-5 and TPXL-1 that are essential for building the phase separated centrosomes are not essential for meiosis (however, ZYG-9 is, see Appendix E). Second, it is unclear if microtubules are nucleated from the poles or how important this nucleation site would be. And lastly, through live imaging it is easy to identify the phase separated centrosome: it is a bright circular spot that resembles phase separated droplets formed *in vitro*. Meiotic spindle poles do not have an obvious spherical, or droplet-like, shape. These differences may point to a slightly different role for meiotic condensates but do not formally rule out their existence. Conceptually, the idea of compartmentalized meiotic spindle poles is appealing when considering the mechanism of spindle assembly. Poles form early in the process during the multipolar stage then they coalesce to form a bipolar spindle. An important physical attribute of condensates are that they can fuse with one another; when two droplets collide *in vitro* or *in vivo* they fuse into a larger droplet. Could this be the underlying physical basis for pole coalescence? It is easy to imagine two condensates built at the end of the microtubule bundles fusing into a single larger pole. It is perhaps not as easy to imagine two static crosslinked networks colliding and reorganizing into a single crosslinked network. In addition, upon progression into anaphase, poles are dramatically

reorganized when the spindle rotates, shrinks, and broadens to create microtubule channels through which the chromosomes segregate. Again, conceptually, it is appealing to suggest that a phase separated compartment would be pliable and able to undertake such dramatic reorganization.

How can this new model of pole organization be directly tested? In Appendix C, I describe preliminary experiments indicating phase separation characteristics present in KLP-18 stalk and MESP-1 *in vitro*. Most compelling is the result that MESP-1 is essential for tubulin to be recruited into KLP-18 stalk droplets, and that these droplets are clearly able to anchor individual microtubules. These results beg the question: Why would KLP-18 and MESP-1, two force generating proteins that I have spent an entire dissertation proposing work at the middle of spindle, take such a form at spindle poles? I do not have an adequate answer to that question, however, future analysis of spindle pole hierarchy may explain how a pole is built and how it may recruit KLP-18 and MESP-1. Nevertheless, as mentioned previously, KLP-18 and MESP-1 are indeed present at spindle poles and these proteins can clearly phase separate and interact with microtubules *in vitro*. The very few *in vivo* experiments I performed to directly test for the existence of phase separated poles showed that the pole components KLP-18 and ASPM-1, along with tubulin, persisted after prolonged treatment with the microtubule depolymerizing drug nocodazole (Appendix C). This indicates that perhaps these proteins can exist in the absence of stable microtubules, and perhaps in discrete compartments. To test this model more rigorously, future experiments should test for phase separation properties in other known pole proteins (ASPM-1, ZYG-9, TAC-1) and the effect of adding these proteins to *in vitro* reactions along with KLP-18 and MESP-1. However informative *in vitro* work will be, it is most important to fully test for the existence of compartments *in vivo*. Treating live oocytes containing fluorescently tagged

tubulin with nocodazole and imaging simultaneously may reveal persistence of pole compartments after spindle microtubules are depolymerized. In addition, our lab is equipped to perform FRAP experiments on fluorescently tagged spindle proteins to measure cellular dynamics. Comparing the dynamics of spindle tubulin and pole tubulin, for example, may reveal differences in fluorescent recovery which may indicate different substructures. Dynamics could also be measured in different genetic knockdowns to understand which proteins are driving concentration of spindle components. Understanding the physical basis of acentrosomal poles will help to fully reveal how oocyte spindles function in the absence of centrosomes.

4.3. Final remarks

As of this writing on May 13, 2020, I am finishing Day 54 of Illinois' "Stay-At-Home" order in response to the COVID-19 global pandemic. The order requires all those with work deemed non-essential to stay home, and to only leave their home to buy food or to exercise. Chicago's lakefront parks, a usual escape from my sometimes constricting Lakeview apartment, have been barricaded for eight and a half weeks. Bars and restaurants are only open for take-out and stores are shuttered. I have not stepped foot in lab, for one reason or another, in over two months. It is reported that 3,601 people in Illinois have died due to COVID-19, 83,249 in the United States, and 294,879 in the world, although all of these numbers are certainly underestimates. At least 25 million Americans have lost their jobs in the past two months, a level of unemployment not seen since the Great Depression. As I reflect on my dissertation and on my time at Northwestern, it is difficult to not put this writing into context.

This pandemic has laid bare the inequities and biases built into the American society. I will not get political here in Chapter 4 of my dissertation, but it is more clear now than ever how connected our science and our society are. Basic research must be funded. The CDC

must be supported. Healthcare must be available to everyone. We must have a strong public health system and disaster response. We must be able to preemptively attack a pandemic with the knowledge gained from any variety of biological research. As we are learning, we can not simply be reactive in the face of a scientific problem so severe. We need to be ahead of it, ready for it. Yesterday, the United States Air Force flew six F-16 Fighting Falcon jets over Chicago as a way to "honor health care workers and first responders". One wonders how many masks and ventilators each F-16 is worth, or what all of the newly unemployed hospitality workers thought of the tribute.

As science and society are connected, I hope I have conveyed throughout this dissertation that the fields of biology are connected, too. To fully understand a system, imaging or biochemistry or genetics alone are not sufficient. A fully integrated approach comprised of all these techniques best answers a question. As we continue to understand the meiotic divisions, it is important that we do not put ourselves into silos and only use the techniques we know best. We must collaborate and learn from each other to reach a holistic answer to biological questions.

My hope is that this dissertation work ultimately improves our understand of female reproduction, and that a clinician can use it to help develop how to best provide care to a woman in need. Or that a cancer researcher can use my work to understand how to inhibit kinesin-12 within cancer cells. Or perhaps that future researchers in the Wignall Lab and elsewhere can build upon this work, with the projects outlined in this chapter to answer fundamental questions about biology. But even if not, I believe this work has nevertheless pushed the sphere of knowledge to be just a little bit larger. The more biology we understand, the better we can leverage this understanding to keep all of us happy and healthy.

CHAPTER 5

Materials and Methods

5.1. Worm strains

Throughout this dissertation, 'wild-type' refers to N2 (Bristol) or EU1067 worms grown on NGM/OP50 plates, and 'control' refers to the RNAi vector control (L4440).

Strain	**Description**
N2	Bristol
EU1067	*unc-119(ed3) ruIs32[unc-119(+) pie-1promoter::GFP::H2B] III; ruIs57[pie-1promoter::GFP::tubulin + unc-119(+)]* (gift from Bruce Bowerman, University of Oregon)
VC1915	*klp-18(ok2519)IV/nT1[qIs51]* (from the CGC)
XA3504	*unc-119(ed3)III; qaEx3504[pie-1 promoter::GFP::emr-1 + unc-119(+)]* IV (from the CGC).
EU2876	*or1935[GFP::aspm-1] I; itIs37[pie-1promoter::mCherry::H2B::pie-1 3'UTR + unc-119(+)] IV* (from the CGC)
SMW9	*klp-18(tm2841)IV/nT1[qIs51]*
SMW13	SMW9 x EU1067
OD57	Bombardment strain to integrate GFP::tubulin, mCherry::histone with *pie-1* promoter. See[239] for details (gift of Jon Audhya, University of Wisconsin)
OD868	*ltSi220[pOD1249/pSW077;Pmex-5::GFP::tbb-2::operonlinker::mCHerry::his-11; cb-unc-119(+)]I.* See[251]. (Gift of Bruce Bowerman, University of Oregon)
HR1160	*or447ts(klp-18ts), dpy-20 IV*
SMW36	HR1160 x OD868 (*or447ts(klp-18ts); dpy-20 IV; ltSi220[pOD1249/pSW077;Pmex-5::GFP::tbb-2::operonlinker::mCHerry::his-11; cb-unc-119(+)]I*)

Table 5.1. **Worm strains**

5.2. Image Acquisition Statement

All microscopy (unless otherwise noted) was performed at the Biological Imaging Facility at Northwestern University, graciously supported by the Chemistry for Life Processes Institute, the NU Office for Research and the Rice Foundation.

5.3. Immunofluorescence

Chapters 2 and 3

Immunofluorescence was performed as described previously[252,253]. Oocytes were dissected into drops of M9 (To 500mL dH2O, 1.5g KH_2PO_4, 3.0g Na_2HPO_4, 2.5g NaCl, and 500μL of 1M $MgSO_4$) snap-frozen in liquid N2, freeze cracked, and fixed in -20°C MeOH for 35-40 minutes. Slides were washed with PBS, blocked with Abdil (1X PBS, 4% BSA, 0.1% Triton X-100, 0.02% Sodium Azide), then primary antibody was applied overnight. The next day slides were washed with PBST, incubated with secondary antibody, washed, incubated with Hoechst, washed, then mounted in mounting media (90% glycerol, 20mM Tris pH 8.8, 0.5% p-phenylenediamine), and sealed with nail polish. The following primary antibodies were used: Alexa Fluor 488–conjugated mouse anti–α-tubulin (1:500, DM1α; Sigma-Aldrich, St. Louis, MO), Alexa Fluor 596-conjugated goat anti-GFP (used for GFP::EMR-1, 1:250, ab6660; Abcam, Cambridge, MA), monoclonal mouse anti-GFP (used for GFP::ASPM-1, 1:200, A11120; Invitrogen, Waltham, MA), rabbit anti-KLP-18 (1:10,000) and rat anti-KLP-18 (1:200 (Chapter 2), 1:500 (Chapter 3) gifts of Olaf Bossinger, RWTH Aachen University[101]), rabbit anti–ASPM-1 (1:5000; gift of Arshad Desai, Ludwig Institute for Cancer Research; Wignall and Villeneuve, 2009), rat anti-LMN-1 (1:500; gift of Katherine Wilson, Johns Hopkins University; Gruenbaum et al., 2002), and rabbit anti–MESP-1 (1:3000). Anti–MESP-1 antibody was raised through genomic antibody technology (Strategic Diagnostics, Newark,

DE) against amino acids 60–159 and then affinity purified. Secondary antibodies used were Alexa Fluor 555–conjugated goat anti-rabbit and Alexa Fluor 647–conjugated goat anti-rat (both at 1:500; Invitrogen). Slides were imaged using a DeltaVision Core microscope with a 100X objective (NA = 1.40). All image acquisition, processing, and analysis were performed using softWoRx software (GE Biosciences). Image stacks were acquired with 0.2μm z-steps and raw images were deconvolved. All figure images are full maximum-intensity projections of the entire spindle structure unless otherwise indicated.

5.4. Live cell time-lapse imaging

Chapter 2

Two-color live imaging was performed using a spinning-disk confocal microscope with a 63x HC PL APO 1.40 NA objective lens. A spinning-disk confocal unit (CSU-X1; Yokogawa Electric Corporation, Sugar Land, TX) attached to an inverted microscope (Leica DMI6000 SD; Leica, Wetzlar, Germany) and a Spectral Applied Imaging laser merge ILE3030 and a back-thinned electron-multiplying charge-coupled device camera (Evolve 521 Delta; Photometrics, Tucson, AZ) were used for image acquisition. The microscope and attached devices were controlled using MetaMorph Image Series Environment software (Molecular Devices, Sunnyvale, CA). Twelve z-stacks at 1 μm increments were taken every 20–30 s at room temperature. Image deconvolution was done using AutoQuant X3 (Media Cybernetics, Rockville, MD). Images are shown as maximum-intensity projections of the entire data stack. Live, intact worms were mounted on 5% agarose, M9 pads in 50% live imaging solution (modified S-basal [50 mM KH2PO4, 10 mM K-citrate, 0.1 M NaCl, 0.025 mg/mL cholesterol, 3 mM MgSO4, 3 mM CaCl2, 20 mM serotonin-HCl, 0.1% tricaine, 0.01% levamisole]), and 50% 0.1 μm polystyrene Microspheres (Polysciences, Warrington, PA) and covered with a coverslip.

Chapter 3

Worms were prepared for two-color live imaging as previously described[209]. Oocytes were dissected out of worms in a drop of room temperature L-15 Blastomere buffer (final concentrations in ddH2O: 60% Leibovitz L-15, 20% heat inactivated FBS, 25mM HEPES pH 7.5, 0.5mg/mL Inulin) then a coverslip was added. Oocytes that settled onto the coverslip were filmed. Twelve z-stacks at 1 μm increments were taken every 20–30 s at room temperature. All live imaging was performed at ambient temperature (23-25°C). Images acquired using a spinning-disk confocal microscope with a 63x HC PL APO 1.40 NA objective lens. A spinning-disk confocal unit (CSU-X1; Yokogawa Electric Corporation) attached to an inverted microscope (Leica DMI6000 SD) and a Spectral Applied Imaging laser merge ILE3030 and a back-thinned electron multiplying charge-coupled device camera (Evolve 521 Delta) were used for image acquisition. The microscope and attached devices were controlled using MetaMorph Image Series Environment software (Molecular Devices).

5.5. Quantification of Spindle Morphology

Chapter 2

Spindle assembly stages were quantified by scoring (by eye) live worms mounted in anesthetic (0.2% tricaine, 0.02% levamisole in M9) with a Leica DM5500B fluorescence microscope (housed in the Wignall Lab).

Chapter 3

Intact worms were fixed in EtOH: 30-45 worms were picked into a 15°C drop of M9 (22mM KH2PO4, 22mM Na2HPO4, 85mM NaCl, 1mM MgSO4), the drop was dried with Whatman

paper, and 10μL 100% EtOH was added directly to worms. The EtOH was allowed to dry completely and another drop of 100% EtOH was added, and this was repeated for a total of 3 times. A 1:1 mixture of Vectashield:M9 was added to completely dry worms then a coverslip was added and sealed with nail polish. Slides were stored at 4°C until imaging. Slides were visualized on a DeltaVision Core microscope and spindle morphology was quantified by eye with a 40X objective or by taking a snapshot of the spindle with a 100X objective.

5.6. RNA Interference (RNAi)

Chapters 2 and 3

Individual RNAi clones picked from an RNAi feeding library[207,208] were used to inoculate Luria broth (LB) plus ampicillin (100 μg/mL) and grown overnight at 37°C. These cultures were used to seed nematode growth medium (NGM)/ampicillin (100 μg/mL)/1 mM isopropyl-β-d-thiogalactoside (IPTG) plates, and the plates were then left overnight at room temperature to induce RNA expression. Synchronized L1 worms (EU1067) were plated on induced plates and grown at 15°C for 5 d until they became gravid adults. Control plates were seeded with bacteria containing empty vector L4440 (designated as control(RNAi) throughout the article). For *tpxl-1(RNAi)* (which has multiple available clones in the library), multiple clones were tried (and yielded identical results), but clone Y39G10A_246.k was used for the experiments displayed.

5.7. Large-scale worm growth and protein extraction

Chapter 2

Large-scale worm growth was performed similarly to previous work[247]. Briefly, wild-type (N2) young adult worms were picked onto NGM plates seeded with OP50, and cultures were

allowed to starve. Between 10 and 12 of these plates were then washed into 500 mL of S-Complete (50 mM KH2PO4, 10 mM K-citrate, 0.1 M NaCl, 0.025 mg/mL cholesterol, 3 mM MgSO4, 3 mM CaCl2, 0.05 mM disodium EDTA, 0.025 mM FeSO4*7H2O, 0.01 mM MnCl2*4H2O, 0.01 mM ZnSO4*7H2O, 0.001 mM CuSO4*5H2O) seeded with OP50-1, and the culture was shaken at 16–22°C (depending on desired growth rate) until the worms were gravid adults. The culture was then bleached, and the resulting embryos were hatched in 500 mL of S-Complete shaken overnight at 20°C. OP50-1 was added to the arrested L1 larvae, and the culture was again shaken at 16–22°C until the worms were gravid adults. The culture was harvested and washed with M9 and lysis buffer (50 mM 4-(2-hydroxyethyl)-1-piperazineethanesulfonic acid [HEPES], pH 7.4, 1 mM EGTA, 1 mM MgCl2, 100 mM KCl, 10% glycerol). Worm pellets were snap frozen by dropping them into liquid nitrogen and stored at –80°C. Protein was extracted from frozen worm pellets as previously described[254]. Pellets were thawed on ice and washed in lysis buffer with protease inhibitors (EDTA-free cocktail; Roche). A 0.5 mL volume of Zirconia beads (Biospec, Bartlesville, OK) was added to resuspended worms in 750 μl of lysis buffer. The samples were vortexed six times (1 min vortexing with 20 s rest) at 4°C, and the efficiency of lysis was confirmed using a dissecting microscope. Lysate was then separated from beads, incubated on ice for 30 min, and cleared by centrifugation at 4°C (25,000 rpm for 10 min and 50,000 rpm for 20 min). Protein concentration was measured using Bradford assay (Bio-Rad), and worm lysate was kept on ice until use.

5.8. Protein domain analysis

Chapter 3

KLP-18 coiled-coil domains were identified using Paircoil2 coiled-coil prediction software[255].

Probability scores were calculated with a cutoff of 0.5. MESP-1 disordered regions predicted using PONDR[256] (http://www.pondr.com/).

5.9. Protein expression and purification

Chapter 2

GST–MESP-1 and GST were cloned into pGEX 6P-1 (GE) and expressed in BL21 *Escherichia coli* cells. Cultures were grown at 37°C to an OD of 0.6-0.8 and then induced at 28°C for 4 h with 0.1 mM IPTG. After harvesting, cells were lysed at room temperature for 15 min with B-PER Protein Extraction Reagent (ThermoFisher Scientific, Waltham, MA) including 100 μg/mL lysozyme, 20 μl DNase I (ThermoFisher), and EDTA-free protease inhibitor cocktail tablets (Roche, Indianapolis, IN). The lysate was then cleared by centrifugation at 40,000 rpm for 35 min. Lysate was applied to glutathione Sepharose resin (GE) and then washed with wash buffer (phosphate-buffered saline, pH 7.4, 250 mM NaCl, 0.1% Tween 20, 2 mM benzamidine-HCl, 1 mM dithiothreitol [DTT]). Bound protein was then eluted with elution buffer (50 mM Tris, pH 8.1, 75 mM KCl, 10 mM reduced glutathione). Protein was dialyzed into BRB80 (80 mM 1,4-piperazinediethanesulfonic acid [PIPES], pH 6.8, 1 mM ethylene glycol tetraacetic acid [EGTA], 1 mM MgCl2) overnight and stored at -80°C. For all recombinant protein purifications, purity was confirmed with SDS–PAGE and concentration determined by Bradford assay (Bio-Rad, Hercules, CA).

Chapter 3

Purification results, affinity tag, and expression system for each protein used in this work can be found in Figure 3.2. *C. elegans* cDNA was amplified from extracted mRNA from wild type worms using the iScript Select cDNA Synthesis kit (Bio-Rad). KLP-18 cDNA was amplified from whole worm cDNA with gene specific primers and Q5 DNA polymerase, then used for

cloning all KLP-18 expression constructs. N-stalk, C-stalk, and stalk pET expression constructs were assembled using restriction digest with NheI/NotI, NheI/KpnI, and NheI/KpnI respectively. Δhinge was created via site directed mutagenesis (NEB) from the stalk construct. MESP-1 cDNA was amplified from GST-MESP-1 construct (see Chapter 2 above) and inserted into MBP vector (gift of Laura Lackner and Marijn Ford) via restriction digest with NdeI/BamHI. pET His6 GFP TEV LIC cloning vector (1GFP[257]) was a gift from Scott Gradia (Addgene plasmid number 29663 ; http://n2t.net/addgene:29663 ; RRID:Addgene 29663). KLP-18 cDNA was inserted into GFP construct via Gibson Assembly. KLP-18 cDNA was inserted into the MBP construct via NdeI/BamHI to make MBP-stalk.

All proteins were purified with the same protocol and the same buffers. All expression vectors were transformed into BL21 DE3 *E. coli* cells and grown at 37°C until an O.D. of 0.6. Cells were induced with 0.1mM IPTG and grown for varying expression times and at varying temperatures, see Figure S1 for growth conditions for individual proteins. Cultures were spun at 4700rpm and resuspended in lysis buffer (80mM PIPES pH 6.8, 2mM MgCl2, 1mM EGTA, 250mM NaCl, 5-10% glycerol, 0.02% Tween, Leupeptin, Aprotinin, Pepstatin, 2mM imidazole). Cells were lysed with 1mg/mL lysozyme (incubated for 20min at 4°C) and with sonication (4 x 30sec, 2 x 20sec with rest at 60% power). Lysate was cleared by centrifugation for 45min at 11,900rpm in a Ti50.2 rotor. Ni-NTA resin was equilibrated with lysis buffer then added to cleared lysate and incubated at 4°C for 1-2 hours. Slurry was applied to a plastic column and washed with 30mL lysis buffer + 20mM imidazole. Bound protein was eluted with 5-10mL of lysis buffer + 500mM imidazole. Ni-NTA elution was either kept at 4°C overnight or applied directly to HiLoad 26/600 Superdex 200 gel filtration column run on Aktaprime FPLC system (GE Biosciences) and equilibrated with lysis buffer.

Eluted fractions from individual peaks were tested by SDS PAGE gel and fractions containing pure protein of interest were combined, concentrated, frozen by dripping into liquid N2, and stored at -80°C.

5.10. GST pull-down assay

Chapter 2

GST-tagged bait protein was incubated with worm extract for 30 min at 4°C, and then glutathione Sepharose (equilibrated with wash buffer: 50 mM HEPES, pH 7.4, 1 mM EGTA, 1 mM MgCl2, 300 mM KCl, 0.05% NP-40, 10% glycerol) was added, and the mixture was incubated at 4°C overnight. Beads were pelleted at 16,000 x g for 1 min and then resuspended in wash buffer and incubated for 10 min while being rotated. Protease inhibitors (EDTA free; Roche) and 0.5 mM DTT were added to the wash buffer. After two washes, bound protein was eluted by mixing for 10 min with 100 μl of elution buffer (50 mM Tris-HCl, pH 8.0, 75 mM KCl, 20 mM reduced glutathione) and removed from beads after centrifugation. Eluate was added to 100 μl 2x Laemmli Sample Buffer (Bio-Rad), boiled at 95°C for 10 min, and used for SDS–PAGE analysis. For Western analysis, we used the antibodies rabbit anti–KLP-18 (1:5000) and anti-GST (1:2000; gift of Jason Brickner, Northwestern University).

5.11. Microtubule co-sedimentation assay

Chapter 3

Microtubules were polymerized by incubating 100μM porcine tubulin with 1mM DTT and 1mM GTP in BRB80 (80mM PIPES pH 6.8, 2mM MgCl2, 1mM EGTA) on ice for 5min then spun at 80K rpm for 10min at 4°C. Supernatant was removed and incubated at 37°C

for 1hour. Taxol was added stepwise to the following final concentrations at 37°C: 1μM taxol then incubated for 10min, 10μM taxol then incubated for 10min, and 100μM taxol incubated for 15min. Polymerized microtubules were then diluted 1:1 in BRB80 + 50mM taxol and kept at room temperature until use.

Proteins of interest were thawed from -80°C storage and pre-cleared by spinning at 80K rpm for 10 minutes at 25°C. Soluble protein in the supernatant was removed and added to 5μM microtubules quickly to maintain protein solubility. Reactions were assembled in BRB80 + 20μM taxol with equal salt, detergent, and glycerol concentrations based on the final purification buffers (see "Protein Purification" section for details (section 5.9)) to a final volume of 25μL. Exact protein concentrations for each experiment can be found in "Figure Quantification" section of this chapter (section 5.15). Reactions were incubated at room temperature for 30min, then spun through a 100uL BRB80 + 40% glycerol + 20μM taxol cushion at 90K rpm for 15min at 25°C. 25μL from the very top of the solution was removed and added to 2X SDS Laemmli Sample Buffer to make the "supernatant" sample. The cushion was washed with BRB80 + 20μM taxol, removed, then pellet was washed with BRB80 + 20μM taxol. Pellet was resuspended with 25μL cold BRB80 + 10mM CaCl2 then added to 2X SDS Laemmli Sample Buffer to make the "pellet" sample. All spins performed in TLA120.2 rotor.

Supernatant and pellet samples were probed by Western Blot using the following antibodies and working concentrations: 1:5000 anti-6XHis-HRP (Abcam), 1:5000 mouse anti-tubulin (Invitrogen), 1:5000 anti-mouse HRP (Invitrogen). After application of BioRad Clarity ECL substrate, blots were imaged by film then scanned with a standard printer scanner. For Figure 2A non-subtilisin experiment, blot was imaged by Azure Biosystems digital imager. See "Figure Quantification" section of this chapter (section 5.15) for Western Blot quantification

details.

5.12. Microtubule bundling assay

Chapter 3

Fluorescent microtubules were polymerized by incubating 20μM porcine brain tubulin and 2μM TMR-tubulin with 1mM DTT and 1mM GTP in BRB80 (80mM PIPES pH 6.8, 2mM MgCl2, 1mM EGTA) on ice for 5min and incubated at 37°C for 2min. Taxol was added stepwise to the following final concentrations at 37°C: 0.2μM taxol then incubated for 10min, 2μM taxol then incubated for 10min, and 20μM taxol incubated for 10min. Polymerized microtubules were kept at room temperature until use.

Proteins of interest were thawed from -80°C storage and pre-cleared by spinning at 80K rpm for 10 minutes at 25°C. Protein concentrations were measured by Bradford Assay, then added to 25μL reactions with 200nM TMR-microtubules in BRB80 + 20μM taxol with equal salt, detergent, and glycerol concentrations based on the final purification buffers (see "Protein Purification" section for details). Reactions were incubated at room temperature for 30min, then fixed with 1% glutaraldehyde and incubated for an additional 3min. Reactions were then squashed onto a poly-L-lysine slide, sealed with nail polish, and imaged on a Spinning Disk Confocal microscope. For exact protein concentrations and quantification details, see "Figure Quantification" section of this chapter (section 5.15).

For experiment showing GFP-Stalk / GFP recruitment to microtubules (Figure 2C), the microtubule bundling protocol above was followed exactly, except for the addition of two proteins in the reaction. For exact protein concentrations and quantification details, see "Figure Quantification" section of this chapter (section 5.15).

5.13. MBP pulldown

Chapter 3

Proteins of interest were added to a 100uL reaction in BRB80 (80mM PIPES pH 6.8, 2mM MgCl2, 1mM EGTA) with equal salt, detergent, and glycerol concentrations based on the final purification buffers (see "Protein Purification" section for details). For exact protein concentrations and quantification details, see "Figure Quantification" section of this chapter (section 5.15). Equal volume of protein added to reactions was added to 200μL 1X Laemmli Sample Buffer for the "input" gel samples. Reactions were incubated at 4°C overnight, then equilibrated amylose resin (New England Biolabs) was added to pull out MBP tagged proteins. Amylose resin was incubated with reactions for 1 hour at 4°C, then resin was washed 4 times with 900μL BRB80. 300uL of final wash was saved for acetone precipitation to make "wash" samples. To elute bound proteins from amylose resin, 900μL BRB80 + 50mM NaCl + 10mM maltose was added to beads and incubated for 20min at 4°C. 300uL of eluate was removed for acetone precipitation to make "elution" gel samples. Wash and elution samples were concentrated via acetone precipitation as follows: 1.2mL of -20°C acetone was added to 300uL wash or elution samples, vortexed, and incubated at -20°C overnight. The next day samples were spun at 16K x g for 10min at room temperature and incubated at 50-55°C for 20min until the acetone was completely evaporated and the pellets were dry. Pellet was resuspended in 40μL 1X Laemmli Sample Buffer and boiled for 10min at 95°C to make gel samples.

5.14. Hydrodynamic analysis

Chapter 3

A purification of MBP-Stalk was split and diluted into BRB80 + 300mM NaCl (high salt)

or BRB80 + 20mM NaCl (low salt). The high salt and low salt dilutions were then applied to HiLoad 26/600 Superdex 200 column equilibrated with appropriate buffer. Identical fractions were collected for each dilution and probed by Western Blot using rabbit anti-KLP-18 at 1:5000 and anti-rabbit-HRP at 1:5000. See "Figure Quantification" section of this chapter for further details.

5.15. Western Blots

Chapter 3

For *klp-18(or447ts)* whole worm Western Blots, control (OD868) or *klp-18(or447ts)* (SMW36) plates were temperature shifted for 1 hour. 50-100 worms were picked from shifted plate to pre-warmed unseeded plate for 5min to avoid transfer of bacteria, then washed off plate with room temperature M9. Worms were pelleted by spinning at 800xg for 1min, supernatant was removed, and an equal volume of 2X SDS Laemmli Sample Buffer was added. Gel samples were boiled for 10min at 95°C, briefly vortexed, then boiled for an additional 10min at 95°C. Volume of sample corresponding to 50 worms was loaded onto gel. Worm Western Blots were imaged with an Azure Biosystems digital imager and bands were quantified in ImageJ.

Samples were run on a 8-12% SDS-PAGE acrylamide gel and transferred to a nitrocellulose membrane using a Trans-Blot Turbo Transfer System (BioRad). Membrane was blocked in 5% milk + TBST blocking solution, incubated with primary antibody in blocking solution at room temperature for 1 hour or at 4°C overnight, washed in TBST, incubated in secondary antibody at room temperature for 1 hour, washed in TBST, incubated with Clarity Western ECL substrate (BioRad) for 2 minutes, then imaged with film.

5.16. Chapter 3 Figure Quantification

Figure 3.1B: Western Blots were developed on film then scanned using a standard printer scanner. Using photoshop, the gel was cropped and converted from .pdf to .tif. The ImageJ "analyze gels" function was used to quantify band intensity in each lane. For each reaction, the total band intensity was calculated by adding the "supernatant" and "pellet" band intensities, and "shift to pellet (%)" was calculated by dividing the "pellet" band intensity by the total band intensity for the reaction. The mean +/- s.d. for n = 3 independent experiments are shown. For each experiment quantified, [tubulin] = 5μM, [N-stalk] = 1.0μM-1.26μM, [C-stalk] = 0.14μM-1μM. In the representative blots shown, [N-stalk] = 1.26μM, [C-stalk] = 0.53μM (non-subtilisin experiment) and 0.14μM (subtilisin experiment). For non-subtilisin experiment: Shift to pellet (%) +/- s.d. for N-stalk (- MT): 4.5% +/- 4.9%, N-stalk (+ MT): 3.2% +/- 3.6%, C-stalk (- MT): 1.6% +/- 2.8%, C-stalk (+ MT): 52.7% +/- 9.7%. For subtilisin experiment: Shift to pellet (%) +/- s.d. for C-stalk (- MT): 6.0 +/- 6.7, C-stalk (+ MT): 50.8% +/- 7.0%, C-stalk (+ sMT): 26.7% +/- 7.0%.

Figure 3.1D: Microtubule bundling assays were imaged on a spinning disk microscope (see below) with consistent emission intensity and exposure time across the experiment. Images were quantified in ImageJ: raw images were made into a grayscale composite then an automatic threshold was applied. Across an experiment, a threshold was applied to each image individually but with the same automatic thresholding algorithm. After the thresholding was applied, fluorescent particles were selected and the "mean size" was calculated. This measurement is the mean size of all fluorescent particles in an image and represents the degree of microtubule bundling (large bundles will have a larger mean size than individual microtubules). To normalize mean bundle area, the area from experimental images was divided by the mean area of all of the buffer-only control images, making the mean size

of unbundled microtubules equal to 1. Each plotted data point is one image's normalized bundle area. Two experiments were quantified and same result (Δhinge bundles MTs while full length stalk does not) was shown in 6 total experiments. In each reaction, [tubulin] = 200nM. Mean "Normalized bundle area (A.U.)" and n for buffer alone: 1, n = 62; 1μM stalk: 1.22, n = 67; 2μM stalk: 1.59, n = 62; 1μM Δhinge: 2.63, n = 2.63; 2μM Δhinge: 5.27, n = 62.

Figure 3.3C: The first 11 fractions after the HiLoad 26/600 Superdex 200 void volume (fractions 43-54) were collected and run on a western blot and developed film was scanned using a printer scanner. To calculate "% of total band intensity" the intensity of each band from fractions 43-49 was quantified. These intensities were then summed to calculate the total band intensity, and each individual fraction band intensity was divided by the total band intensity. Fractions 49-54 were not included in this calculation because they were the main elution peak of the protein, and we were interested in the fraction of protein shifted to a lower elution volume.

Figure 3.5A: Quantified exactly as described in Figure 3.1B. Concentrations for each experiment quantified: [tubulin] = 5μM, [MBP-MESP-1] = 1.0-5.77μM. In the representative blots shown, [MBP-MESP-1] = 1.0μM (non-subtilisin experiment) and 5.77μM (subtilisin experiment). Two non-subtilisin experiments were quantified and three subtilisin experiments were quantified. Shift to pellet (%) +/- s.d for MBP-MESP-1 (- MT): 2.9% +/- 4.1%, + MT: 56.1% +/- 3.4%. For subtilisin experiments, shift to pellet (%) +/- s.d. for MBP-MESP-1 (- MT): 0.6% +/- 0.1%, + MT: 41.6% +/- 10.9%, + sMT: 4.5% +/- 6.4%.

Figure 3.5D: Images acquired and threshold applied as described in Figure 3.1D. Across experiment, emission intensity and exposure time was held constant for each reaction. To quantify GFP localization, fluorescent particles were selected in the microtubule channel

then the mean intensity in the GFP channel was measured within the selection. Therefore, only GFP signal that was overlaid on microtubule bundles was measured. To normalize to background, an area separate from microtubules was selected and the mean intensity was measured. Normalized GFP intensity was calculated by diving mean intensity overlaid on microtubules by mean intensity of background. If this ratio is = 1, there was no enrichment over background. If ¿ 1, there is enrichment of GFP on microtubules over background. Each data point is the normalized GFP intensity for one image. Two experiments were quantified and same result (GFP-stalk is enriched on MTs in the presence of MBP-MESP-1) was shown in 5 total experiments. Concentration of all proteins in reaction were 1μM, and [tubulin] = 200nM. Mean "Normalized GFP Intensity (A.U.)" and n for each condition: MBP + GFP-stalk: 1.91, n = 42; MBP-MESP-1 + GFP: 1.03, n = 42; MBP-MESP-1 + GFP-stalk: 3.69, n = 60.

Figure 3.6A: Spindle morphology in *klp-18(or447ts)* worms fixed in EtOH (see below) was quantified by eye using 40X objective or by taking snapshots at 100X. Representative images are shown. For *klp-18(or447ts)* experiments, 4 experiments were quantified; for control 26°C, 3 experiments were quantified. Mean "percent of +1 oocytes (%)" +/- s.d. for control 26°C: 1% +/- 2%; bipolar: 26% +/- 7%; monopolar: 0% +/- 0%; collapsed: 7% +/- 4%, anaphase onward: 67% +/- 8%. Mean "percent of +1 oocytes (%)" +/- s.d. for *klp-18(or447ts)* 15°C multipolar: 4% +/- 3%; bipolar: 27% +/- 7%; monopolar: 9% +/- 4%; collapsed: 13% +/- 4%; anaphase onward: 47% +/- 6%. Mean "percent of +1 oocytes (%)" +/- s.d. for *klp-18(or447ts)* 26°C multipolar: 0 +/- 1%; bipolar: 2% +/- 2%; monopolar: 45% +/- 1%; collapsed: 22% +/- 5%; anaphase onward: 30% +/- 14%.

Figure 3.6B: Western Blot band intensities were quantified using Image J. 'KLP-18 / tubulin intensity' was calculated by dividing KLP-18 band intensity by the tubulin band intensity

in the same lane. Mean intensity +/- s.d. for n = 3 individual experiments: control 26°C: 2.06 +/- 0.78; *klp-18(or447ts)* 15°C: 2.05 +/- 0.30; *klp-18(or447ts)* 26°C: 2.69 +/- 0.85.

Figure 3.6C: KLP-18 and MESP-1 enrichment at the poles of monopolar spindles was quantified in immunofluorescence images that exhibited characteristic traits of monopolar spindles: chromosomes out in a rosette and clearly associated to microtubule bundles. Both MI and MII spindles were quantified. First, in ImageJ, the z-slice that contained the center of the pole was qualitatively chosen in the tubulin channel and a region of interest (ROI) was drawn around the pole. The ROI was then applied to the KLP-18 and MESP-1 channel at the same z-slice, and the sum of pixel intensity was measured. A background ROI of equal size was measured in the cytoplasm for both channels at the same z-slice. To calculate enrichment of KLP-18 and MESP-1 to the pole, the pole intensity was divided by the background intensity. If this ratio was greater than or equal to 1.5 (a 50% increase), KLP-18 or MESP-1 was considered enriched. This quantification is reported on the figure.

Figure 3.7A: Quantified exactly as in Figure 3.6A. For all strains and conditions, 3 experiments were quantified. In the +1 oocyte: percent of oocytes (%) for control *emb-30(RNAi)* 26°C multipolar: 2% +/- 2%; bipolar: 82% +/- 7%; monopolar: 2% +/- 2%; collapsed: 12% +/- 9%; anaphase onward: 1% +/- 2%. In the +2 oocyte: percent of oocytes (%) for control *emb-30(RNAi)* 26°C multipolar: 0% +/- 0%; bipolar: 86% +/- 8%; monopolar: 1% +/- 2%; collapsed: 9% +/- 2%; anaphase onward: 4% +/- 4%. In the +1 oocyte: Mean "percent of oocytes (%)" +/- s.d. for *klp-18(or447ts) emb-30(RNAi)* 15°C multipolar: 2% +/- 2%; bipolar 64% +/- 13%; monopolar: 22% +/- 1%; collapsed: 5% +/- 3%; anaphase onward: 7% +/- 1%. For +2 oocytes: multipolar: 0%; bipolar: 74% +/- 22%, monopolar: 8% +/- 4%; collapsed: 4% +/- 3%; anaphase onward: 4% +/- 7%. For *klp-18(or447ts) emb-30(RNAi)* 26°C +1 oocytes: multipolar: 0% +/- 0%; bipolar: 2% +/- 2%; monopolar:

93% +/- 6%; collapsed: 3% +/- 3%; anaphase onward: 2% +/- 3%. In +2 oocytes: multipolar: 0% +/- 0%; bipolar: 11% +/- 5%; monopolar: 83% +/- 12%; collapsed: 1% +/- 1%; anaphase onward: 4% +/- 7%.

Figure 3.7C: To quantify spindle length in time-lapse movies, raw data was loaded in ImageJ and the distance between poles was measured with the line tool: spindle poles were identified in the tubulin channel by a bright circular area of tubulin, and a straight line was drawn between the outer edges of pole tubulin signal to measure the spindle length. This was done for each frame of the movie. Because spindle collapse happened at slightly different times after beginning to film, the time scale was normalized such that the first frame showing rapid shortening was set as time = 0. Each trace for 14 spindles is shown on the left, and the mean spindle length (+/- s.d.) over time for the same data set is shown on the right.

Figure 3.7E: Quantified exactly as in Figure 3.6C.

References

1. Hassold, T. & Hunt, P. To err (meiotically) is human: the genesis of human aneuploidy. *Nat. Rev. Genet.* **2**, 280–291 (2001).

2. Gray, S. & Cohen, P. E. Control of meiotic crossovers: From Double-Strand break formation to designation. *Annu. Rev. Genet.* **50**, 175–210 (2016).

3. Keeney, S., Lange, J. & Mohibullah, N. Self-organization of meiotic recombination initiation: general principles and molecular pathways. *Annu. Rev. Genet.* **48**, 187–214 (2014).

4. Yu, Z., Kim, Y. & Dernburg, A. F. Meiotic recombination and the crossover assurance checkpoint in caenorhabditis elegans. *Semin. Cell Dev. Biol.* **54**, 106–116 (2016).

5. Thacker, D. & Keeney, S. Homologous recombination during meiosis. *DNA Replication, Recombination, and Repair* (2016).

6. Mihajlović, A. I. & FitzHarris, G. Segregating chromosomes in the mammalian oocyte. *Curr. Biol.* **28**, R895–R907 (2018).

7. Radford, S. J., Nguyen, A. L., Schindler, K. & McKim, K. S. The chromosomal basis of meiotic acentrosomal spindle assembly and function in oocytes. *Chromosoma* (2016).

8. Mullen, T. J., Davis-Roca, A. C. & Wignall, S. M. Spindle assembly and chromosome dynamics during oocyte meiosis. *Curr. Opin. Cell Biol.* **60**, 53–59 (2019).

9. Pintard, L. & Bowerman, B. Mitotic cell division in caenorhabditis elegans. *Genetics* **211**, 35–73 (2019).

10. Mitchison, T. & Kirschner, M. Dynamic instability of microtubule growth. *Nature* **312**, 237–242 (1984).

11. Brouhard, G. J. & Rice, L. M. Microtubule dynamics: an interplay of biochemistry and mechanics. *Nat. Rev. Mol. Cell Biol.* (2018).

12. Akhmanova, A. & Steinmetz, M. O. Microtubule minus-end regulation at a glance. *J. Cell Sci.* **132** (2019).

13. Walczak, C. E. & Heald, R. Mechanisms of mitotic spindle assembly and function. *Int. Rev. Cytol.* **265**, 111–158 (2008).

14. Severson, A. F., von Dassow, G. & Bowerman, B. Oocyte meiotic spindle assembly and function. *Curr. Top. Dev. Biol.* **116**, 65–98 (2016).

15. Ohkura, H. Meiosis: an overview of key differences from mitosis. *Cold Spring Harb. Perspect. Biol.* **7** (2015).

16. Sawin, K. E. & Mitchison, T. J. Mitotic spindle assembly by two different pathways in vitro. *J. Cell Biol.* **112**, 925–940 (1991).

17. Heald, R. *et al.* Self-organization of microtubules into bipolar spindles around artificial chromosomes in xenopus egg extracts. *Nature* **382**, 420–425 (1996).

18. Seki, T., Hayashi, N. & Nishimoto, T. RCC1 in the ran pathway. *J. Biochem.* **120**, 207–214 (1996).

19. Carazo-Salas, R. E. *et al.* Generation of GTP-bound ran by RCC1 is required for chromatin-induced mitotic spindle formation. *Nature* **400**, 178–181 (1999).

20. Gruss, O. J. *et al.* Ran induces spindle assembly by reversing the inhibitory effect of importin alpha on TPX2 activity. *Cell* **104**, 83–93 (2001).

21. Sampath, S. C. *et al.* The chromosomal passenger complex is required for chromatin-induced microtubule stabilization and spindle assembly. *Cell* **118**, 187–202 (2004).

22. Tulu, U. S., Fagerstrom, C., Ferenz, N. P. & Wadsworth, P. Molecular requirements for kinetochore-associated microtubule formation in mammalian cells. *Curr. Biol.* **16**, 536–541 (2006).

23. Maresca, T. J. *et al.* Spindle assembly in the absence of a RanGTP gradient requires localized CPC activity. *Curr. Biol.* **19**, 1210–1215 (2009).

24. Kelly, A. E. *et al.* Chromosomal enrichment and activation of the aurora B pathway are coupled to spatially regulate spindle assembly. *Dev. Cell* **12**, 31–43 (2007).

25. Tseng, B. S., Tan, L., Kapoor, T. M. & Funabiki, H. Dual detection of chromosomes and microtubules by the chromosomal passenger complex drives spindle assembly. *Dev. Cell* **18**, 903–912 (2010).

26. Theurkauf, W. E. & Hawley, R. S. Meiotic spindle assembly in drosophila females: behavior of nonexchange chromosomes and the effects of mutations in the nod kinesin-like protein. *J. Cell Biol.* **116**, 1167–1180 (1992).

27. Sköld, H. N., Komma, D. J. & Endow, S. A. Assembly pathway of the anastral drosophila oocyte meiosis I spindle. *J. Cell Sci.* **118**, 1745–1755 (2005).

28. Cesario, J. & McKim, K. S. RanGTP is required for meiotic spindle organization and the initiation of embryonic development in drosophila. *J. Cell Sci.* **124**, 3797–3810 (2011).

29. Colombié, N. *et al.* Dual roles of incenp crucial to the assembly of the acentrosomal metaphase spindle in female meiosis. *Development* **135**, 3239–3246 (2008).

30. Das, A. *et al.* Spindle assembly and chromosome segregation requires central spindle proteins in drosophila oocytes. *Genetics* **202**, 61–75 (2016).

31. Radford, S. J., Jang, J. K. & McKim, K. S. The chromosomal passenger complex is required for meiotic acentrosomal spindle assembly and chromosome biorientation. *Genetics* **192**, 417–429 (2012).

32. Goshima, G., Mayer, M., Zhang, N., Stuurman, N. & Vale, R. D. Augmin: a protein complex required for centrosome-independent microtubule generation within the spindle. *J. Cell Biol.* **181**, 421–429 (2008).

33. Goshima, G. & Kimura, A. New look inside the spindle: microtubule-dependent microtubule generation within the spindle. *Curr. Opin. Cell Biol.* **22**, 44–49 (2010).

34. Meireles, A. M., Fisher, K. H., Colombié, N., Wakefield, J. G. & Ohkura, H. Wac: a new augmin subunit required for chromosome alignment but not for acentrosomal microtubule assembly in female meiosis. *J. Cell Biol.* **184**, 777–784 (2009).

35. Colombié, N., Głuszek, A. A., Meireles, A. M. & Ohkura, H. Meiosis-specific stable binding of augmin to acentrosomal spindle poles promotes biased microtubule assembly in oocytes. *PLoS Genet.* **9**, e1003562 (2013).

36. Sánchez-Huertas, C. & Lüders, J. The augmin connection in the geometry of microtubule networks. *Curr. Biol.* **25**, R294–9 (2015).

37. Matthies, H. J., McDonald, H. B., Goldstein, L. S. & Theurkauf, W. E. Anastral meiotic spindle morphogenesis: role of the non-claret disjunctional kinesin-like protein. *J. Cell Biol.* **134**, 455–464 (1996).

38. Tavosanis, G., Llamazares, S., Goulielmos, G. & Gonzalez, C. Essential role for gamma-tubulin in the acentriolar female meiotic spindle of drosophila. *EMBO J.* **16**, 1809–1819 (1997).

39. Tovey, C. A. & Conduit, P. T. Microtubule nucleation by γ-tubulin complexes and beyond. *Essays Biochem.* EBC20180028 (2018).

40. Liu, P. *et al.* Insights into the assembly and activation of the microtubule nucleator γ-TuRC. *Nature* **578**, 467–471 (2020).

41. Endow, S. A. & Hallen, M. A. Anastral spindle assembly and γ-tubulin in drosophila oocytes. *BMC Cell Biol.* **12**, 1 (2011).

42. Romé, P. & Ohkura, H. A novel microtubule nucleation pathway for meiotic spindle assembly in oocytes. *J. Cell Biol.* (2018).

43. Hughes, S. E. *et al.* Gamma-tubulin is required for bipolar spindle assembly and for proper kinetochore microtubule attachments during prometaphase I in drosophila oocytes. *PLoS Genet.* **7**, e1002209 (2011).

44. Reschen, R. F. *et al.* Dgp71WD is required for the assembly of the acentrosomal meiosis I spindle, and is not a general targeting factor for the γ-TuRC. *Biol. Open* BIO2012596 (2012).

45. Petry, S., Pugieux, C., Nédélec, F. J. & Vale, R. D. Augmin promotes meiotic spindle formation and bipolarity in xenopus egg extracts. *Proc. Natl. Acad. Sci. U. S. A.* **108**, 14473–14478 (2011).

46. Petry, S., Groen, A. C., Ishihara, K., Mitchison, T. J. & Vale, R. D. Branching microtubule nucleation in xenopus egg extracts mediated by augmin and TPX2. *Cell* **152**, 768–777 (2013).

47. Decker, F., Oriola, D., Dalton, B. & Brugués, J. Autocatalytic microtubule nucleation determines the size and mass of xenopus laevis egg extract spindles. *Elife* **7** (2018).

48. Wolff, I. D., Tran, M. V., Mullen, T. J., Villeneuve, A. M. & Wignall, S. M. Assembly of caenorhabditis elegans acentrosomal spindles occurs without evident microtubule-organizing centers and requires microtubule sorting by KLP-18/kinesin-12 and MESP-1. *Mol. Biol. Cell* **27**, 3122–3131 (2016).

49. Edzuka, T., Yamada, L., Kanamaru, K., Sawada, H. & Goshima, G. Identification of the augmin complex in the filamentous fungus aspergillus nidulans. *PLoS One* **9**, e101471 (2014).

50. Bobinnec, Y., Fukuda, M. & Nishida, E. Identification and characterization of caenorhabditis elegans gamma-tubulin in dividing cells and differentiated tissues. *J. Cell Sci.* **113 Pt 21**, 3747–3759 (2000).

51. Strome, S. *et al.* Spindle dynamics and the role of gamma-tubulin in early caenorhabditis elegans embryos. *Mol. Biol. Cell* **12**, 1751–1764 (2001).

52. McNally, K., Audhya, A., Oegema, K. & McNally, F. J. Katanin controls mitotic and meiotic spindle length. *J. Cell Biol.* **175**, 881–891 (2006).

53. Chuang, C.-H., Schlientz, A. J., Yang, J. & Bowerman, B. Microtubule assembly and pole coalescence: early steps in caenorhabditiselegans oocyte meiosis I spindle assembly. *Biol. Open* **9** (2020).

54. Sumiyoshi, E., Fukata, Y., Namai, S. & Sugimoto, A. Caenorhabditis elegans aurora a kinase is required for the formation of spindle microtubules in female meiosis. *Mol. Biol. Cell* **26**, 4187–4196 (2015).

55. Askjaer, P., Galy, V., Hannak, E. & Mattaj, I. W. Ran GTpase cycle and importins α and β are essential for spindle formation and nuclear envelope assembly in living caenorhabditis elegans embryos. *Mol. Biol. Cell* **13**, 4355–4370 (2002).

56. Wignall, S. M. & Villeneuve, A. M. Lateral microtubule bundles promote chromosome alignment during acentrosomal oocyte meiosis. *Nat. Cell Biol.* **11**, 839–844 (2009).

57. Schumacher, J. M., Golden, A. & Donovan, P. J. AIR-2: An Aurora/Ipl1-related protein kinase associated with chromosomes and midbody microtubules is required for polar body extrusion and cytokinesis in caenorhabditis elegans embryos. *J. Cell Biol.* **143**, 1635–1646 (1998).

58. Dumont, J., Oegema, K. & Desai, A. A kinetochore-independent mechanism drives anaphase chromosome separation during acentrosomal meiosis. *Nat. Cell Biol.* **12**, 894–901 (2010).

59. Gigant, E. *et al.* Inhibition of ectopic microtubule assembly by the kinesin-13 KLP-7 prevents chromosome segregation and cytokinesis defects in oocytes. *Development* **144**, 1674–1686 (2017).

60. Chaaban, S. *et al.* The structure and dynamics of c. elegans tubulin reveals the mechanistic basis of microtubule growth. *Dev. Cell* (2018).

61. Carabatsos, M. J., Combelles, C. M., Messinger, S. M. & Albertini, D. F. Sorting and reorganization of centrosomes during oocyte maturation in the mouse. *Microsc. Res. Tech.* **49**, 435–444 (2000).

62. Ma, W. & Viveiros, M. M. Depletion of pericentrin in mouse oocytes disrupts microtubule organizing center function and meiotic spindle organization. *Mol. Reprod. Dev.* **81**, 1019–1029 (2014).

63. Baumann, C., Wang, X., Yang, L. & Viveiros, M. M. Error-prone meiotic division and subfertility in mice with oocyte-conditional knockdown of pericentrin. *J. Cell Sci.* **130**, 1251–1262 (2017).

64. Gueth-Hallonet, C. *et al.* gamma-tubulin is present in acentriolar MTOCs during early mouse development. *J. Cell Sci.* **105 (Pt 1)**, 157–166 (1993).

65. Calarco, P. G. Centrosome precursors in the acentriolar mouse oocyte. *Microsc. Res. Tech.* **49**, 428–434 (2000).

66. Palacios, M. J., Joshi, H. C., Simerly, C. & Schatten, G. Gamma-tubulin reorganization during mouse fertilization and early development. *J. Cell Sci.* **104 (Pt 2)**, 383–389 (1993).

67. George, M. A., Pickering, S. J., Braude, P. R. & Johnson, M. H. Preimplantation embryology: The distribution of α-and γ-tubulin in fresh and aged human and mouse oocytes exposed to cryoprotectant. *MHR: Basic science of reproductive medicine* **2**, 445–456 (1996).

68. Ma, W., Baumann, C. & Viveiros, M. M. NEDD1 is crucial for meiotic spindle stability and accurate chromosome segregation in mammalian oocytes. *Dev. Biol.* **339**, 439–450 (2010).

69. Clift, D. & Schuh, M. A three-step MTOC fragmentation mechanism facilitates bipolar spindle assembly in mouse oocytes. *Nat. Commun.* **6**, 7217 (2015).

70. Brunet, S. *et al.* Meiotic regulation of TPX2 protein levels governs cell cycle progression in mouse oocytes. *PLoS One* **3**, e3338 (2008).

71. So, C. *et al.* A liquid-like spindle domain promotes acentrosomal spindle assembly in mammalian oocytes. *Science* **364**, eaat9557 (2019).

72. Schuh, M. & Ellenberg, J. Self-organization of MTOCs replaces centrosome function during acentrosomal spindle assembly in live mouse oocytes. *Cell* **130**, 484–498 (2007).

73. Luksza, M., Queguigner, I., Verlhac, M.-H. & Brunet, S. Rebuilding MTOCs upon centriole loss during mouse oogenesis. *Dev. Biol.* **382**, 48–56 (2013).

74. Solc, P. *et al.* Aurora kinase a drives MTOC biogenesis but does not trigger resumption of meiosis in mouse oocytes matured in vivo. *Biol. Reprod.* **87**, 85 (2012).

75. Bury, L. *et al.* Plk4 and aurora a cooperate in the initiation of acentriolar spindle assembly in mammalian oocytes. *J. Cell Biol.* (2017).

76. Saskova, A. *et al.* Aurora kinase a controls meiosis I progression in mouse oocytes. *Cell Cycle* **7**, 2368–2376 (2008).

77. Manil-Ségalen, M. *et al.* Chromosome structural anomalies due to aberrant spindle forces exerted at gene editing sites in meiosis. *J. Cell Biol.* jcb.201806072 (2018).

78. Dumont, J. *et al.* A centriole- and RanGTP-independent spindle assembly pathway in meiosis I of vertebrate oocytes. *J. Cell Biol.* **176**, 295–305 (2007).

79. Drutovic, D., Duan, X., Li, R., Kalab, P. & Solc, P. RanGTP and importin β regulate meiosis I spindle assembly and function in mouse oocytes. *EMBO J.* e101689 (2019).

80. Woodruff, J. B. Assembly of mitotic structures through phase separation. *J. Mol. Biol.* (2018).

81. Jiang, H. *et al.* Phase transition of spindle-associated protein regulate spindle apparatus assembly. *Cell* **163**, 108–122 (2015).

82. Woodruff, J. B. *et al.* The centrosome is a selective condensate that nucleates microtubules by concentrating tubulin. *Cell* **169**, 1066–1077.e10 (2017).

83. King, M. R. & Petry, S. Phase separation of TPX2 enhances and spatially coordinates microtubule nucleation. *Nat. Commun.* **11**, 270 (2020).

84. Rale, M. J., Kadzik, R. S. & Petry, S. Phase transitioning the centrosome into a microtubule nucleator. *Biochemistry* **57**, 30–37 (2018).

85. Battaglia, D. E., Klein, N. A. & Soules, M. R. Cell cycle regulation: Changes in centrosomal domains during meiotic maturation in the human oocyte. *MHR: Basic science of reproductive medicine* **2**, 845–851 (1996).

86. Battaglia, D. E., Goodwin, P., Klein, N. A. & Soules, M. R. Fertilization and early embryology: Influence of maternal age on meiotic spindle assembly oocytes from naturally cycling women. *Hum. Reprod.* **11**, 2217–2222 (1996).

87. Holubcová, Z., Blayney, M., Elder, K. & Schuh, M. Human oocytes. error-prone chromosome-mediated spindle assembly favors chromosome segregation defects in human oocytes. *Science* **348**, 1143–1147 (2015).

88. Pickering, S. J., Johnson, M. H., Braude, P. R. & Houliston, E. Cytoskeletal organization in fresh, aged and spontaneously activated human oocytes. *Hum. Reprod.* **3**, 978–989 (1988).

89. Roeles, J. & Tsiavaliaris, G. Actin-microtubule interplay coordinates spindle assembly in human oocytes. *Nat. Commun.* **10**, 4651 (2019).

90. Verhey, K. J., Kaul, N. & Soppina, V. Kinesin assembly and movement in cells. *Annu. Rev. Biophys.* **40**, 267–288 (2011).

91. Sawin, K. E., LeGuellec, K., Philippe, M. & Mitchison, T. J. Mitotic spindle organization by a plus-end-directed microtubule motor. *Nature* **359**, 540–543 (1992).

92. Mann, B. J. & Wadsworth, P. Kinesin-5 regulation and function in mitosis. *Trends Cell Biol.* **29**, 66–79 (2019).

93. Walczak, C. E., Vernos, I., Mitchison, T. J., Karsenti, E. & Heald, R. A model for the proposed roles of different microtubule-based motor proteins in establishing spindle bipolarity. *Curr. Biol.* **8**, 903–913 (1998).

94. Yang, G., Cameron, L. A., Maddox, P. S., Salmon, E. D. & Danuser, G. Regional variation of microtubule flux reveals microtubule organization in the metaphase meiotic spindle. *J. Cell Biol.* **182**, 631–639 (2008).

95. Kapoor, T. M., Mayer, T. U., Coughlin, M. L. & Mitchison, T. J. Probing spindle assembly mechanisms with monastrol, a small molecule inhibitor of the mitotic kinesin, eg5. *J. Cell Biol.* **150**, 975–988 (2000).

96. Mailhes, J. B., Mastromatteo, C. & Fuseler, J. W. Transient exposure to the eg5 kinesin inhibitor monastrol leads to syntelic orientation of chromosomes and aneuploidy in mouse oocytes. *Mutat. Res.* **559**, 153–167 (2004).

97. Chinen, T. *et al.* NuMA assemblies organize microtubule asters to establish spindle bipolarity in acentrosomal human cells. *EMBO J.* e102378 (2019).

98. Bishop, J. D., Han, Z. & Schumacher, J. M. The caenorhabditis elegans aurora B kinase AIR-2 phosphorylates and is required for the localization of a BimC kinesin to meiotic and mitotic spindles. *Mol. Biol. Cell* **16**, 742–756 (2005).

99. Saunders, A. M., Powers, J., Strome, S. & Saxton, W. M. Kinesin-5 acts as a brake in anaphase spindle elongation. *Curr. Biol.* **17**, R453–4 (2007).

100. Laband, K. *et al.* Chromosome segregation occurs by microtubule pushing in oocytes. *Nat. Commun.* **8**, 1499 (2017).

101. Segbert, C. *et al.* KLP-18, a klp2 kinesin, is required for assembly of acentrosomal meiotic spindles in caenorhabditis elegans. *Mol. Biol. Cell* **14**, 4458–4469 (2003).

102. Connolly, A. A. *et al.* Caenorhabditis elegans oocyte meiotic spindle pole assembly requires microtubule severing and the calponin homology domain protein ASPM-1. *Mol. Biol. Cell* **25**, 1298–1311 (2014).

103. Connolly, A. A., Sugioka, K., Chuang, C.-H., Lowry, J. B. & Bowerman, B. KLP-7 acts through the ndc80 complex to limit pole number in c. elegans oocyte meiotic spindle assembly. *J. Cell Biol.* **210**, 917–932 (2015).

104. Muscat, C. C. *et al.* Kinetochore-independent chromosome segregation driven by lateral microtubule bundles. *eLife Sciences* **4**, e06462 (2015).

105. Radford, S. J., Go, A. M. M. & McKim, K. S. Cooperation between kinesin motors promotes spindle symmetry and chromosome organization in oocytes. *Genetics* **205**, 517–527 (2017).

106. Giunta, K. L., Jang, J. K., Manheim, E. A., Subramanian, G. & McKim, K. S. subito encodes a kinesin-like protein required for meiotic spindle pole formation in drosophila melanogaster. *Genetics* **160**, 1489–1501 (2002).

107. Jang, J. K., Rahman, T., Kober, V. S., Cesario, J. & McKim, K. S. Misregulation of the kinesin-like protein subito induces meiotic spindle formation in the absence of chromosomes and centrosomes. *Genetics* **177**, 267–280 (2007).

108. Jang, J. K., Rahman, T. & McKim, K. S. The kinesinlike protein subito contributes to central spindle assembly and organization of the meiotic spindle in drosophila oocytes. *Mol. Biol. Cell* **16**, 4684–4694 (2005).

109. Koffa, M. D. *et al.* HURP is part of a ran-dependent complex involved in spindle formation. *Curr. Biol.* **16**, 743–754 (2006).

110. Silljé, H. H. W., Nagel, S., Körner, R. & Nigg, E. A. HURP is a Ran-Importin β-Regulated protein that stabilizes kinetochore microtubules in the vicinity of chromosomes. *Curr. Biol.* **16**, 731–742 (2006).

111. Breuer, M. *et al.* HURP permits MTOC sorting for robust meiotic spindle bipolarity, similar to extra centrosome clustering in cancer cells. *J. Cell Biol.* **191**, 1251–1260 (2010).

112. Redemann, S. *et al.* C. elegans chromosomes connect to centrosomes by anchoring into the spindle network. *Nat. Commun.* **8**, 15288 (2017).

113. Helmke, K. J., Heald, R. & Wilbur, J. D. Interplay between spindle architecture and function. *Int. Rev. Cell Mol. Biol.* **306**, 83–125 (2013).

114. Burbank, K. S., Groen, A. C., Perlman, Z. E., Fisher, D. S. & Mitchison, T. J. A new method reveals microtubule minus ends throughout the meiotic spindle. *J. Cell Biol.* **175**, 369–375 (2006).

115. Burbank, K. S., Mitchison, T. J. & Fisher, D. S. Slide-and-cluster models for spindle assembly. *Curr. Biol.* **17**, 1373–1383 (2007).

116. Yang, G. *et al.* Architectural dynamics of the meiotic spindle revealed by single-fluorophore imaging. *Nat. Cell Biol.* **9**, 1233–1242 (2007).

117. Brugués, J., Nuzzo, V., Mazur, E. & Needleman, D. J. Nucleation and transport organize microtubules in metaphase spindles. *Cell* **149**, 554–564 (2012).

118. Liang, Z.-Y., Hallen, M. A. & Endow, S. A. Mature drosophila meiosis I spindles comprise microtubules of mixed polarity. *Curr. Biol.* **19**, 163–168 (2009).

119. Srayko, M., Kaya, A., Stamford, J. & Hyman, A. A. Identification and characterization of factors required for microtubule growth and nucleation in the early c. elegans embryo. *Dev. Cell* **9**, 223–236 (2005).

120. McNally, F. J. & Vale, R. D. Identification of katanin, an ATPase that severs and disassembles stable microtubules. *Cell* **75**, 419–429 (1993).

121. Mains, P. E., Kemphues, K. J., Sprunger, S. A., Sulston, I. A. & Wood, W. B. Mutations affecting the meiotic and mitotic divisions of the early caenorhabditis elegans embryo. *Genetics* **126**, 593–605 (1990).

122. Clark-Maguire, S. & Mains, P. E. mei-1, a gene required for meiotic spindle formation in caenorhabditis elegans, is a member of a family of ATPases. *Genetics* **136**, 533–546 (1994).

123. Srayko, M., Buster, D. W., Bazirgan, O. A., McNally, F. J. & Mains, P. E. MEI-1/MEI-2 katanin-like microtubule severing activity is required for caenorhabditis elegans meiosis. *Genes Dev.* **14**, 1072–1084 (2000).

124. Yang, H.-Y., McNally, K. & McNally, F. J. MEI-1/katanin is required for translocation of the meiosis I spindle to the oocyte cortex in c. elegans. *Dev. Biol.* **260**, 245–259 (2003).

125. Srayko, M., O'toole, E. T., Hyman, A. A. & Müller-Reichert, T. Katanin disrupts the microtubule lattice and increases polymer number in c. elegans meiosis. *Curr. Biol.* **16**, 1944–1949 (2006).

126. Joly, N., Martino, L., Gigant, E., Dumont, J. & Pintard, L. Microtubule-severing activity of the AAA+ ATPase katanin is essential for female meiotic spindle assembly. *Development* **143**, 3604–3614 (2016).

127. McNally, K. P. & McNally, F. J. The spindle assembly function of caenorhabditis elegans katanin does not require microtubule-severing activity. *Mol. Biol. Cell* **22**, 1550–1560 (2011).

128. McNally, K. *et al.* Katanin maintains meiotic metaphase chromosome alignment and spindle structure in vivo and has multiple effects on microtubules in vitro. *Mol. Biol. Cell* **25**, 1037–1049 (2014).

129. Mullen, T. J. & Wignall, S. M. Interplay between microtubule bundling and sorting factors ensures acentriolar spindle stability during c. elegans oocyte meiosis. *PLoS Genet.* **13**, e1006986 (2017).

130. Letort, G. *et al.* A computational model of the early stages of acentriolar meiotic spindle assembly. *Mol. Biol. Cell* **30**, 863–875 (2019).

131. Loughlin, R., Heald, R. & Nédélec, F. A computational model predicts xenopus meiotic spindle organization. *J. Cell Biol.* **191**, 1239–1249 (2010).

132. Heald, R., Tournebize, R., Habermann, A., Karsenti, E. & Hyman, A. Spindle assembly in xenopus egg extracts: respective roles of centrosomes and microtubule self-organization. *J. Cell Biol.* **138**, 615–628 (1997).

133. Desai, A., Murray, A., Mitchison, T. J. & Walczak, C. E. The use of xenopus egg extracts to study mitotic spindle assembly and function in vitro. *Methods Cell Biol.* **61**, 385–412 (1999).

134. Merdes, A., Ramyar, K., Vechio, J. D. & Cleveland, D. W. A complex of NuMA and cytoplasmic dynein is essential for mitotic spindle assembly. *Cell* **87**, 447–458 (1996).

135. Merdes, A., Heald, R., Samejima, K., Earnshaw, W. C. & Cleveland, D. W. Formation of spindle poles by dynein/dynactin-dependent transport of NuMA. *J. Cell Biol.* **149**, 851–862 (2000).

136. Mitchison, T. J. *et al.* Roles of polymerization dynamics, opposed motors, and a tensile element in governing the length of xenopus extract meiotic spindles. *Mol. Biol. Cell* **16**, 3064–3076 (2005).

137. Jiang, K. *et al.* Microtubule minus-end regulation at spindle poles by an ASPM-katanin complex. *Nat. Cell Biol.* (2017).

138. van der Voet, M. *et al.* NuMA-related LIN-5, ASPM-1, calmodulin and dynein promote meiotic spindle rotation independently of cortical LIN-5/GPR/Galpha. *Nat. Cell Biol.* **11**, 269–277 (2009).

139. Yang, H.-Y., Mains, P. E. & McNally, F. J. Kinesin-1 mediates translocation of the meiotic spindle to the oocyte cortex through KCA-1, a novel cargo adapter. *J. Cell Biol.* **169**, 447–457 (2005).

140. Costa, M. F. A. & Ohkura, H. The molecular architecture of the meiotic spindle is remodeled during metaphase arrest in oocytes. *J. Cell Biol.* (2019).

141. Endow, S. A. & Komma, D. J. Spindle dynamics during meiosis in drosophila oocytes. *J. Cell Biol.* (1997).

142. Cullen, C. F. & Ohkura, H. Msps protein is localized to acentrosomal poles to ensure bipolarity of drosophila meiotic spindles. *Nat. Cell Biol.* **3**, 637–642 (2001).

143. Riparbelli, M. G., Callaini, G., Glover, D. M. & Avides, M. d. C. A requirement for the abnormal spindle protein to organise microtubules of the central spindle for cytokinesis in drosophila. *J. Cell Sci.* **115**, 913–922 (2002).

144. Fitzharris, G. A shift from kinesin 5-dependent metaphase spindle function during preimplantation development in mouse. *Development* **136**, 2111–2119 (2009).

145. Bennabi, I. *et al.* Shifting meiotic to mitotic spindle assembly in oocytes disrupts chromosome alignment. *EMBO Rep.* (2018).

146. Balboula, A. Z. *et al.* Haspin kinase regulates microtubule-organizing center clustering and stability through aurora kinase C in mouse oocytes. *J. Cell Sci.* **129**, 3648–3660 (2016).

147. Wang, X., Baumann, C., De La Fuente, R. & Viveiros, M. M. CEP215 and AURKA regulate spindle pole focusing and aMTOC organization in mouse oocytes. *Reproduction* (2020).

148. Nguyen, A. L. *et al.* Genetic interactions between the aurora kinases reveal new requirements for AURKB and AURKC during oocyte meiosis. *Curr. Biol.* **28**, 3458–3468.e5 (2018).

149. Xu, X.-L. *et al.* The microtubule-associated protein ASPM regulates spindle assembly and meiotic progression in mouse oocytes. *PLoS One* **7**, e49303 (2012).

150. Kolano, A., Brunet, S., Silk, A. D., Cleveland, D. W. & Verlhac, M.-H. Error-prone mammalian female meiosis from silencing the spindle assembly checkpoint without normal interkinetochore tension. *Proc. Natl. Acad. Sci. U. S. A.* **109**, E1858–67 (2012).

151. Sedo, C. A., Schatten, H., Combelles, C. M. & Rawe, V. Y. The nuclear mitotic apparatus (NuMA) protein: localization and dynamics in human oocytes, fertilization and early embryos. *Mol. Hum. Reprod.* **17**, 392–398 (2011).

152. Duncan, F. E., Hornick, J. E. & Woodruff, T. K. Bipolar-to-monopolar spindle collapse in human eggs. *Mol. Reprod. Dev.* **79**, 587 (2012).

153. Gayek, A. S. & Ohi, R. Kinetochore-microtubule stability governs the metaphase requirement for eg5. *Mol. Biol. Cell* **25**, 2051–2060 (2014).

154. Blangy, A. *et al.* Phosphorylation by p34cdc2 regulates spindle association of human eg5, a kinesin-related motor essential for bipolar spindle formation in vivo. *Cell* **83**, 1159–1169 (1995).

155. Redemann, S. *et al.* A switch in microtubule orientation during c. elegans meiosis. *Curr. Biol.* (2018).

156. Han, X., Adames, K., Sykes, E. M. E. & Srayko, M. The KLP-7 residue S546 is a putative aurora kinase site required for microtubule regulation at the centrosome in c. elegans. *PLoS One* **10**, e0132593 (2015).

157. Miller, K. E., Session, A. M. & Heald, R. Kif2a scales meiotic spindle size in hymenochirus boettgeri. *Curr. Biol.* (2019).

158. Roberts, A. J., Kon, T., Knight, P. J., Sutoh, K. & Burgess, S. A. Functions and mechanics of dynein motor proteins. *Nat. Rev. Mol. Cell Biol.* **14**, 713–726 (2013).

159. Cianfrocco, M. A., DeSantis, M. E., Leschziner, A. E. & Reck-Peterson, S. L. Mechanism and regulation of cytoplasmic dynein. *Annu. Rev. Cell Dev. Biol.* **31**, 83–108 (2015).

160. Reck-Peterson, S. L., Redwine, W. B., Vale, R. D. & Carter, A. P. The cytoplasmic dynein transport machinery and its many cargoes. *Nat. Rev. Mol. Cell Biol.* **19**, 382–398 (2018).

161. Sweeney, H. L. & Holzbaur, E. L. F. Motor proteins. *Cold Spring Harb. Perspect. Biol.* **10** (2018).

162. She, Z.-Y. & Yang, W.-X. Molecular mechanisms of kinesin-14 motors in spindle assembly and chromosome segregation. *J. Cell Sci.* **130**, 2097–2110 (2017).

163. Lüdecke, A., Seidel, A.-M., Braun, M., Lansky, Z. & Diez, S. Diffusive tail anchorage determines velocity and force produced by kinesin-14 between crosslinked microtubules. *Nat. Commun.* **9**, 2214 (2018).

164. Beaven, R. *et al.* 14-3-3 regulation of ncd reveals a new mechanism for targeting proteins to the spindle in oocytes. *J. Cell Biol.* jcb.201704120 (2017).

165. Robin, G. *et al.* Essential kinesins: characterization of caenorhabditis elegans KLP-15. *Biochemistry* **44**, 6526–6536 (2005).

166. Vanneste, D., Takagi, M., Imamoto, N. & Vernos, I. The role of hklp2 in the stabilization and maintenance of spindle bipolarity. *Curr. Biol.* **19**, 1712–1717 (2009).

167. Tanenbaum, M. E. *et al.* Kif15 cooperates with eg5 to promote bipolar spindle assembly. *Curr. Biol.* **19**, 1703–1711 (2009).

168. Sturgill, E. G., Norris, S. R., Guo, Y. & Ohi, R. Kinesin-5 inhibitor resistance is driven by kinesin-12. *J. Cell Biol.* (2016).

169. van Heesbeen, R. G. H. P. & Medema, R. H. Kif15: A useful target for anti-cancer therapy? In Kozielski, FSB & Frank (eds.) *Kinesins and Cancer*, 77–86 (Springer Netherlands, Dordrecht, 2015).

170. Kapitein, L. C. *et al.* The bipolar mitotic kinesin eg5 moves on both microtubules that it crosslinks. *Nature* **435**, 114–118 (2005).

171. Reinemann, D. N. *et al.* Collective force regulation in anti-parallel microtubule gliding by dimeric kif15 kinesin motors. *Curr. Biol.* (2017).

172. McHugh, T., Drechsler, H., McAinsh, A. D., Carter, N. J. & Cross, R. A. Kif15 functions as an active mechanical ratchet. *Mol. Biol. Cell* **29**, 1743–1752 (2018).

173. Sturgill, E. G. & Ohi, R. Kinesin-12 differentially affects spindle assembly depending on its microtubule substrate. *Curr. Biol.* **23**, 1280–1290 (2013).

174. Kapitein, L. C. *et al.* Microtubule cross-linking triggers the directional motility of kinesin-5. *J. Cell Biol.* **182**, 421–428 (2008).

175. Shimamoto, Y., Forth, S. & Kapoor, T. M. Measuring pushing and braking forces generated by ensembles of kinesin-5 crosslinking two microtubules. *Dev. Cell* **34**, 669–681 (2015).

176. Kashina, A. S., Rogers, G. C. & Scholey, J. M. The bimc family of kinesins: essential bipolar mitotic motors driving centrosome separation. *Biochim. Biophys. Acta* **1357**, 257–271 (1997).

177. Sharp, D. J. *et al.* The bipolar kinesin, KLP61F, cross-links microtubules within interpolar microtubule bundles of drosophila embryonic mitotic spindles. *J. Cell Biol.* **144**, 125–138 (1999).

178. Gordon, D. M. & Roof, D. M. The kinesin-related protein kip1p of saccharomyces cerevisiae is bipolar. *J. Biol. Chem.* **274**, 28779–28786 (1999).

179. Hildebrandt, E. R., Gheber, L., Kingsbury, T. & Hoyt, M. A. Homotetrameric form of cin8p, a saccharomyces cerevisiae kinesin-5 motor, is essential for its in vivo function. *J. Biol. Chem.* **281**, 26004–26013 (2006).

180. Acar, S. *et al.* The bipolar assembly domain of the mitotic motor kinesin-5. *Nat. Commun.* **4**, 1343 (2013).

181. Scholey, J. E., Nithianantham, S., Scholey, J. M. & Al-Bassam, J. Structural basis for the assembly of the mitotic motor kinesin-5 into bipolar tetramers. *Elife* **3**, e02217 (2014).

182. Waitzman, J. S. *et al.* The loop 5 element structurally and kinetically coordinates dimers of the human kinesin-5, eg5. *Biophys. J.* **101**, 2760–2769 (2011).

183. Weinger, J. S., Qiu, M., Yang, G. & Kapoor, T. M. A nonmotor microtubule binding site in kinesin-5 is required for filament crosslinking and sliding. *Curr. Biol.* **21**, 154–160

(2011).

184. Bodrug, T. *et al.* The kinesin-5 tail domain directly modulates the mechanochemical cycle of the motor domain for anti-parallel microtubule sliding. *Elife* **9** (2020).

185. Skoufias, D. A. *et al.* S-trityl-L-cysteine is a reversible, tight binding inhibitor of the human kinesin eg5 that specifically blocks mitotic progression. *J. Biol. Chem.* **281**, 17559–17569 (2006).

186. Raaijmakers, J. A. *et al.* Nuclear envelope-associated dynein drives prophase centrosome separation and enables eg5-independent bipolar spindle formation. *EMBO J.* **31**, 4179–4190 (2012).

187. Saeki, E. *et al.* Involvement of c-terminal truncation mutation of kinesin-5 in resistance to kinesin-5 inhibitor. *PLoS One* **13**, e0209296 (2018).

188. Al-Obaidi, N., Mitchison, T. J., Crews, C. M. & Mayer, T. U. Identification of MAC1: A small molecule that rescues spindle bipolarity in Monastrol-Treated cells. *ACS Chem. Biol.* **11**, 1544–1551 (2016).

189. van Heesbeen, R. G. H. P. *et al.* Aurora a, MCAK, and kif18b promote eg5-independent spindle formation. *Chromosoma* (2016).

190. Gayek, A. S. & Ohi, R. CDK-1 inhibition in G2 stabilizes Kinetochore-Microtubules in the following mitosis. *PLoS One* **11**, e0157491 (2016).

191. van Heesbeen, R. G. H. P., Tanenbaum, M. E. & Medema, R. H. Balanced activity of three mitotic motors is required for bipolar spindle assembly and chromosome segregation. *Cell Rep.* **8**, 948–956 (2014).

192. Sturgill, E. G. *et al.* Kinesin-12 kif15 targets kinetochore fibers through an intrinsic two-step mechanism. *Curr. Biol.* **24**, 2307–2313 (2014).

193. Drechsler, H., McHugh, T., Singleton, M. R., Carter, N. J. & McAinsh, A. D. The kinesin-12 kif15 is a processive track-switching tetramer. *Elife* **3**, e01724 (2014).

194. Drechsler, H. & McAinsh, A. D. Kinesin-12 motors cooperate to suppress microtubule catastrophes and drive the formation of parallel microtubule bundles. *Proc. Natl. Acad. Sci. U. S. A.* **113**, E1635–44 (2016).

195. Mann, B. J., Balchand, S. K. & Wadsworth, P. Regulation of kif15 localization and motility by the c-terminus of TPX2 and microtubule dynamics. *Mol. Biol. Cell* **28**, 65–75 (2017).

196. Wittmann, T., Boleti, H., Antony, C., Karsenti, E. & Vernos, I. Localization of the kinesin-like protein xklp2 to spindle poles requires a leucine zipper, a microtubule-associated protein, and dynein. *J. Cell Biol.* **143**, 673–685 (1998).

197. Balchand, S. K., Mann, B. J., Titus, J., Ross, J. L. & Wadsworth, P. TPX2 inhibits eg5 by interactions with both motor and microtubule. *J. Biol. Chem.* **290**, 17367–17379 (2015).

198. Ma, N., Titus, J., Gable, A., Ross, J. L. & Wadsworth, P. TPX2 regulates the localization and activity of eg5 in the mammalian mitotic spindle. *J. Cell Biol.* **195**, 87–98 (2011).

199. Eckerdt, F., Eyers, P. A., Lewellyn, A. L., Prigent, C. & Maller, J. L. Spindle pole regulation by a discrete eg5-interacting domain in TPX2. *Curr. Biol.* **18**, 519–525 (2008).

200. Mann, B. J. & Wadsworth, P. Distribution of eg5 and TPX2 in mitosis: Insight from CRISPR tagged cells. *Cytoskeleton* **75**, 508–521 (2018).

201. Malaby, H. L. H., Dumas, M. E., Ohi, R. & Stumpff, J. Kinesin-binding protein ensures accurate chromosome segregation by buffering KIF18A and KIF15. *J. Cell Biol.* jcb.201806195 (2019).

202. Brouwers, N., Mallol Martinez, N. & Vernos, I. Role of kif15 and its novel mitotic partner KBP in k-fiber dynamics and chromosome alignment. *PLoS One* **12**, e0174819 (2017).

203. Oegema, K. & Hyman, A. A. Cell division. WormBook, ed. the c. elegans research community. *WormBook* (2006).

204. Nance, J. & Frøkjær-Jensen, C. The caenorhabditis elegans transgenic toolbox. *Genetics* **212**, 959–990 (2019).

205. Montgomery, M. K. RNA interference. In Gott, J. M. (ed.) *RNA Interference, Editing, and Modification: Methods and Protocols*, 3–21 (Humana Press, Totowa, NJ, 2004).

206. Gönczy, P. *et al.* Functional genomic analysis of cell division in c. elegans using RNAi of genes on chromosome III. *Nature* **408**, 331–336 (2000).

207. Fraser, A. G. *et al.* Functional genomic analysis of c. elegans chromosome I by systematic RNA interference. *Nature* **408**, 325–330 (2000).

208. Kamath, R. S. *et al.* Systematic functional analysis of the caenorhabditis elegans genome using RNAi. *Nature* **421**, 231–237 (2003).

209. Laband, K., Lacroix, B., Edwards, F., Canman, J. C. & Dumont, J. Live imaging of c. elegans oocytes and early embryos. *Methods Cell Biol.* **145**, 217–236 (2018).

210. Green, R. A. *et al.* Expression and imaging of fluorescent proteins in the c. elegans gonad and early embryo. In *Methods in Cell Biology*, vol. 85, 179–218 (Academic Press, 2008).

211. Frøkjær-Jensen, C., Davis, M. W., Ailion, M. & Jorgensen, E. M. Improved mos1-mediated transgenesis in c. elegans. *Nat. Methods* **9**, 117–118 (2012).

212. Frøkjaer-Jensen, C. *et al.* Single-copy insertion of transgenes in caenorhabditis elegans. *Nat. Genet.* **40**, 1375–1383 (2008).

213. Dickinson, D. J., Ward, J. D., Reiner, D. J. & Goldstein, B. Engineering the caenorhabditis elegans genome using cas9-triggered homologous recombination. *Nat. Methods* **10**, 1028–1034 (2013).

214. Paix, A., Folkmann, A., Rasoloson, D. & Seydoux, G. High efficiency, Homology-Directed genome editing in caenorhabditis elegans using CRISPR-Cas9 ribonucleoprotein complexes. *Genetics* **201**, 47–54 (2015).

215. Friedland, A. E. *et al.* Heritable genome editing in c. elegans via a CRISPR-Cas9 system. *Nat. Methods* **10**, 741–743 (2013).

216. Davis-Roca, A. C., Divekar, N. S., Ng, R. K. & Wignall, S. M. Dynamic SUMO remodeling drives a series of critical events during the meiotic divisions in caenorhabditis elegans. *PLoS Genet.* **14**, e1007626 (2018).

217. Davis-Roca, A. C., Muscat, C. C. & Wignall, S. M. Caenorhabditis elegans oocytes detect meiotic errors in the absence of canonical end-on kinetochore attachments. *J. Cell Biol.* (2017).

218. Dumont, J. & Desai, A. Acentrosomal spindle assembly and chromosome segregation during oocyte meiosis. *Trends Cell Biol.* **22**, 241–249 (2012).

219. McCarter, J., Bartlett, B., Dang, T. & Schedl, T. On the control of oocyte meiotic maturation and ovulation incaenorhabditis elegans. *Dev. Biol.* **205**, 111–128 (1999).

220. Pelletier, L. *et al.* The caenorhabditis elegans centrosomal protein SPD-2 is required for both pericentriolar material recruitment and centriole duplication. *Curr. Biol.* **14**, 863–873 (2004).

221. Gruss, O. J. & Vernos, I. The mechanism of spindle assembly: functions of ran and its target TPX2. *J. Cell Biol.* **166**, 949–955 (2004).

222. Neumayer, G., Belzil, C., Gruss, O. J. & Nguyen, M. D. TPX2: of spindle assembly, DNA damage response, and cancer. *Cell. Mol. Life Sci.* **71**, 3027–3047 (2014).

223. Wittmann, T., Wilm, M., Karsenti, E. & Vernos, I. TPX2, a novel xenopus MAP involved in spindle pole organization. *J. Cell Biol.* **149**, 1405–1418 (2000).

224. Heidebrecht, H.-J. *et al.* repp86: A human protein associated in the progression of mitosis. *Mol. Cancer Res.* **1**, 271–279 (2003).

225. Ozlü, N. *et al.* An essential function of the c. elegans ortholog of TPX2 is to localize activated aurora a kinase to mitotic spindles. *Dev. Cell* **9**, 237–248 (2005).

226. Karsenti, E. TPX or not TPX? *Mol. Cell* **19**, 431–432 (2005).

227. Goshima, G. Identification of a TPX2-like microtubule-associated protein in drosophila. *PLoS One* **6**, e28120 (2011).

228. Florian, S. & Mayer, T. U. Modulated microtubule dynamics enable Hklp2/Kif15 to assemble bipolar spindles. *Cell Cycle* **10**, 3533–3544 (2011).

229. Alfaro-Aco, R., Thawani, A. & Petry, S. Structural analysis of the role of TPX2 in branching microtubule nucleation. *J. Cell Biol.* (2017).

230. Serrano, L., de la Torre, J., Maccioni, R. B. & Avila, J. Involvement of the carboxyl-terminal domain of tubulin in the regulation of its assembly. *Proc. Natl. Acad. Sci. U. S. A.* **81**, 5989–5993 (1984).

231. Rodionov, V. I., Gyoeva, F. K., Kashina, A. S., Kuznetsov, S. A. & Gelfand, V. I. Microtubule-associated proteins and microtubule-based translocators have different binding sites on tubulin molecule. *J. Biol. Chem.* **265**, 5702–5707 (1990).

232. Seeger, M. A. & Rice, S. E. Microtubule-associated protein-like binding of the kinesin-1 tail to microtubules. *J. Biol. Chem.* **285**, 8155–8162 (2010).

233. Zhang, R., Roostalu, J., Surrey, T. & Nogales, E. Structural insight into TPX2-stimulated microtubule assembly. *Elife* **6** (2017).

234. Reuten, R. *et al.* Maltose-Binding protein (MBP), a Secretion-Enhancing tag for mammalian protein expression systems. *PLoS One* **11**, e0152386 (2016).

235. Wang, C., Castro, A. F., Wilkes, D. M. & Altenberg, G. A. Expression and purification of the first nucleotide-binding domain and linker region of human multidrug resistance gene product: comparison of fusions to glutathione s-transferase, thioredoxin and maltose-binding protein. *Biochem. J* **338 (Pt 1)**, 77–81 (1999).

236. Esposito, D. & Chatterjee, D. K. Enhancement of soluble protein expression through the use of fusion tags. *Curr. Opin. Biotechnol.* **17**, 353–358 (2006).

237. Furuta, T. *et al.* EMB-30: an APC4 homologue required for metaphase-to-anaphase transitions during meiosis and mitosis in caenorhabditis elegans. *Mol. Biol. Cell* **11**, 1401–1419 (2000).

238. Dumas, M. E. *et al.* Dual inhibition of kif15 by oxindole and quinazolinedione chemical probes. *Bioorg. Med. Chem. Lett.* (2018).

239. McNally, K. P., Panzica, M. T., Kim, T., Cortes, D. B. & McNally, F. J. A novel chromosome segregation mechanism during female meiosis. *Mol. Biol. Cell* (2016).

240. Xue, Y. *et al.* GPS 2.1: enhanced prediction of kinase-specific phosphorylation sites with an algorithm of motif length selection. *Protein Eng. Des. Sel.* **24**, 255–260 (2011).

241. Zhao, Q. *et al.* GPS-SUMO: a tool for the prediction of sumoylation sites and SUMO-interaction motifs. *Nucleic Acids Res.* **42**, W325–30 (2014).

242. Boxem, M. *et al.* A protein domain-based interactome network for c. elegans early embryogenesis. *Cell* **134**, 534–545 (2008).

243. Pelisch, F. *et al.* A SUMO-Dependent protein network regulates chromosome congression during oocyte meiosis. *Mol. Cell* (2016).

244. Pelisch, F., Bel Borja, L., Jaffray, E. G. & Hay, R. T. Sumoylation regulates protein dynamics during meiotic chromosome segregation in c. elegans oocytes. *J. Cell Sci.* (2019).

245. Loughlin, R., Wilbur, J. D., McNally, F. J., Nédélec, F. J. & Heald, R. Katanin contributes to interspecies spindle length scaling in xenopus. *Cell* **147**, 1397–1407 (2011).

246. Cook, D. E., Zdraljevic, S., Roberts, J. P. & Andersen, E. C. CeNDR, the caenorhabditis elegans natural diversity resource. *Nucleic Acids Res.* **45**, D650–D657 (2017).

247. Zanin, E. *et al.* Affinity purification of protein complexes in c. elegans. *Methods Cell Biol.* **106**, 289–322 (2011).

248. Zhang, L., Ward, J. D., Cheng, Z. & Dernburg, A. F. The auxin-inducible degradation (AID) system enables versatile conditional protein depletion in c. elegans. *Development* **142**, 4374–4384 (2015).

249. Farhadifar, R. *et al.* Scaling, selection, and evolutionary dynamics of the mitotic spindle. *Curr. Biol.* **25**, 732–740 (2015).

250. Andersen, E. C. *et al.* Chromosome-scale selective sweeps shape caenorhabditis elegans genomic diversity. *Nat. Genet.* **44**, 285–290 (2012).

251. Wang, S. *et al.* NOCA-1 functions with γ-tubulin and in parallel to patronin to assemble non-centrosomal microtubule arrays in c. elegans. *Elife* **4**, e08649 (2015).

252. Oegema, K., Desai, A., Rybina, S., Kirkham, M. & Hyman, A. A. Functional analysis of kinetochore assembly in caenorhabditis elegans. *J. Cell Biol.* **153**, 1209–1226 (2001).

253. Monen, J., Maddox, P. S., Hyndman, F., Oegema, K. & Desai, A. Differential role of CENP-A in the segregation of holocentric c. elegans chromosomes during meiosis and mitosis. *Nat. Cell Biol.* **7**, 1248–1255 (2005).

254. Sonneville, R., Querenet, M., Craig, A., Gartner, A. & Blow, J. J. The dynamics of replication licensing in live caenorhabditis elegans embryos. *J. Cell Biol.* **196**, 233–246 (2012).

255. McDonnell, A. V., Jiang, T., Keating, A. E. & Berger, B. Paircoil2: improved prediction of coiled coils from sequence. *Bioinformatics* **22**, 356–358 (2006).

256. Xue, B., Dunbrack, R. L., Williams, R. W., Dunker, A. K. & Uversky, V. N. PONDR-FIT: a meta-predictor of intrinsically disordered amino acids. *Biochim. Biophys. Acta* **1804**, 996–1010 (2010).

257. Pédelacq, J.-D., Cabantous, S., Tran, T., Terwilliger, T. C. & Waldo, G. S. Engineering and characterization of a superfolder green fluorescent protein. *Nat. Biotechnol.* **24**, 79–88 (2006).

258. Stiernagle, T. February 2006. maintenance of c. elegans. *The C. elegans Research Community (ed.). WormBook. doi/10. 1895/wormbook* **1** (11).

259. Simmer, F. *et al.* Genome-wide RNAi of c. elegans using the hypersensitive rrf-3 strain reveals novel gene functions. *PLoS Biol.* **1**, E12 (2003).

260. Zipperlen, P., Fraser, A. G., Kamath, R. S., Martinez-Campos, M. & Ahringer, J. Roles for 147 embryonic lethal genes on c.elegans chromosome I identified by RNA interference and video microscopy. *EMBO J.* **20**, 3984–3992 (2001).

261. Hayashi, M., Mlynarczyk-Evans, S. & Villeneuve, A. M. The synaptonemal complex shapes the crossover landscape through cooperative assembly, crossover promotion and crossover inhibition during caenorhabditis elegans meiosis. *Genetics* **186**, 45–58 (2010).

262. Praitis, V. Creation of transgenic lines using microparticle bombardment methods. *Methods Mol. Biol.* **351**, 93–107 (2006).

263. Bellanger, J.-M. *et al.* ZYG-9, TAC-1 and ZYG-8 together ensure correct microtubule function throughout the cell cycle of c. elegans embryos. *J. Cell Sci.* **120**, 2963–2973 (2007).

264. Bellanger, J. M. & Gönczy, P. TAC-1 and ZYG-9 form a complex that promotes microtubule assembly in c. elegans embryos. *Curr. Biol.* **13**, 1488–1498 (2003).

265. Srayko, M., Quintin, S., Schwager, A. & Hyman, A. A. Caenorhabditis elegans TAC-1 and ZYG-9 form a complex that is essential for long astral and spindle microtubules. *Curr. Biol.* **13**, 1506–1511 (2003).

266. Matthews, L. R., Carter, P., Thierry-Mieg, D. & Kemphues, K. ZYG-9, a caenorhabditis elegans protein required for microtubule organization and function, is a component of meiotic and mitotic spindle poles. *J. Cell Biol.* **141**, 1159–1168 (1998).

267. Milic, B., Chakraborty, A., Han, K., Bassik, M. C. & Block, S. M. KIF15 nanomechanics and kinesin inhibitors, with implications for cancer chemotherapeutics. *Proc. Natl. Acad. Sci. U. S. A.* (2018).

APPENDIX A

Methods paper: *Methods for studying cell division mechanisms in C.elegans*

This section contains figures included in my first author publication submitted to Methods in Molecular Biology entitled "Methods for studying cell division mechanisms in C. elegans". Nikita Divekar, a graduate student in our lab, also contributed to this paper. Some sections of this paper that I have written have been adapted in other chapters of this dissertation. Here, I have provided the paper in full.

A.1. Abstract

The nematode *Caenorhabditis elegans* is a widely used model organism for the study of the meiotic and mitotic divisions. These self-fertilizing worms are particularly advantageous for these studies because they rapidly reproduce (each worm lays 250 eggs in only 3-4 days) and the cell division machinery is highly conserved between worms and humans. Worms are also genetically tractable and proteins can be readily depleted using RNA interference (RNAi), allowing for the characterization of protein function *in vivo*. To assess phenotypes, spindles can be directly visualized within the worm using fluorescent protein tags or embryos can be dissected out of the worm and immunostained. A combination of these techniques allows comprehensive characterization of a protein's function in a relatively short time span. Here, we describe methods for each of these techniques: RNA interference through feeding, *in utero* live imaging, *in utero* fixed imaging, and immunofluorescence.

A.2. Introduction

Faithful chromosome segregation is critical for the development of all animals. During meiosis, chromosomes are duplicated once and then divided in two consecutive divisions: homologous chromosomes separate in meiosis I, and sister chromatids separate in meiosis II (reviewed in[8]). The resulting haploid gametes, oocytes in females or sperm in males, fuse during fertilization and create a diploid zygote. If there is an error in meiotic chromosome segregation, the resulting zygote will be aneuploid and likely inviable. In humans, the vast majority of aneuploid zygotes are a result of errors during oocyte meiosis[1]. Oocyte spindles are different from sperm and mitotic spindles because they do not contain centrosomes and therefore must assemble their spindles through different mechanisms[14]. Although possible, it is challenging to study oocyte meiosis in humans due to ethical considerations and the

scarcity of available human oocytes, which must be obtained from donors. Thus, model organism research is crucial for understanding how spindles form and how chromosomes segregate in oocytes. The self-fertilizing hermaphroditic worm *C. elegans* is a particularly powerful model organism to study these mechanisms. Each worm lays 250 eggs over its relatively brief 3-4 days of gravid adulthood, allowing for rapid characterization of a large population of oocytes. Moreover, once oocytes are fertilized, the resulting embryos serve as a powerful system for studies of the mitotic divisions[203]. Many proteins involved in both mitosis and meiosis are conserved between *C. elegans* and higher organisms, and the rapid reproductive rate allows for detailed characterization of cell division processes. In this chapter, we highlight several experimental techniques used in *C. elegans* that can be deployed for protein discovery and mechanistic dissection of cell division, and we provide detailed methods for each.

A major advantage of *C. elegans* is the variety of available genetic tools (reviewed in[204]). This organism is amenable to forward and reverse genetic approaches that can be used to dissect the molecular mechanisms of important cellular processes. The discovery of RNAi in *C. elegans* (reviewed in[205]) has been particularly impactful for the study of cell division, since this technique makes it straightforward to study genes essential for development by depleting proteins from adult worms and then looking for defects in their oocytes and embryos. Therefore, genome-wide and targeted RNAi screens have been performed to discover proteins involved in the mitotic[206–208] and meiotic division[56].

A second advantage of *C. elegans* is the ability to tag proteins of interest with fluorescent proteins, and then investigate their dynamics in the cell (reviewed in[210]). Fluorescent proteins can be integrated into the genome for germline expression in a variety of ways, including inserting transgenes through MosSCI transposon-mediated transgenesis[211,212], and by using

CRISPR-based genome editing to tag a protein of interest at its endogenous locus[213–215]; a thorough review of these and other *C. elegans* transgenic tools has been recently published[204]. Since worms are transparent, fluorescent proteins can be imaged in a live oocyte or embryo either *in utero* or *ex utero*; these methods have been widely applied to investigate protein dynamics with high temporal resolution (method recently described in[100]). However, one drawback to live imaging is that it can be time consuming and labor intensive. Moreover, since subjecting worms to high amounts of light often causes cells to arrest, the exposure times and the number of z-stacks acquired must be minimized, limiting the resolution of the resulting movies.

Given these challenges, it is often advantageous to pair time lapse imaging with other methods that enable higher resolution imaging and/or higher throughput analysis for quantification of phenotypes (Figure A.1). One alternative is to image fluorescent proteins in intact worms at high resolution by increasing exposure times and acquiring more z-stacks. For this procedure, worms can either be fixed in ethanol, which preserves the fluorescence of tagged proteins, or live worms can be anesthetized. In the latter case, since the imaging conditions halt cell cycle progression, this type of "live" imaging is analogous to fixed, in that it provides high resolution snapshots of particular stages rather than dynamic information. Regardless, an advantage of these approaches is that a large number of images can be easily acquired, making these techniques higher throughput than time lapse imaging.

Another advantage of imaging oocytes and embryos in intact worms is that the organization of the *C. elegans* gonad makes it possible to correlate chromosome and spindle morphology with different stages of meiotic progression, based on the cell's position within the germ line (Figure A.2A). The *C. elegans* gonad contains two arms, each independently

generating gametes. At the distal tip of each arm, there is a population of mitotically-dividing germline stem cells; as cells move away from this niche, they transition into meiosis and then proceed through the events of meiotic prophase I (e.g., homolog pairing and recombination) as they travel towards the proximal end of the germ line. In hermaphrodites, sperm are produced first and are packaged into the spermatheca, where they are stored; worms then switch to producing oocytes. Oocytes thus progress in a "production line" fashion towards the spermatheca, where they encounter sperm. Fertilization triggers nuclear envelope breakdown (at the"-1" position of the germline), and spindle assembly proceeds as the cell moves through and then exits the spermatheca (moving into the "+1" position). As the meiotic divisions end and the mitotic divisions begin, embryos have typically moved further down this production line (into the +2 and +3 positions). Thus, imaging intact worms has the advantage of maintaining the oocyte or embryo position in the germ line, which is useful when assessing and quantifying mutant/depletion phenotypes. For example, since spindles are usually bipolar by the time the oocyte is in the +1 position, if a large percentage of oocytes in this position have disorganized spindles in a particular mutant, it would suggest that spindle assembly is either slowed or prevented (for examples of this type of quantification, see[48,129]).

Another complementary method is fixed-cell immunofluorescence, which also allows for high resolution imaging to gain precise structural information about spindle architecture. Although this technique eliminates positional information because it requires dissecting cells out of the worm to ensure efficient antibody staining, it still has a number of advantages. Notably, immunofluorescence eliminates the need for genetically-tagging proteins, and also enables the simultaneous visualization of three or more proteins in a single cell, facilitating studies of protein localization. This technique has therefore been especially useful in assessing

the dependencies of particular proteins for proper localization. The immunofluorescence protocol we present was first developed to investigate mitotically-dividing embryos[252], and we have used it extensively to characterize spindle and chromosome architecture in oocytes (for examples see[48,56,104,129,216,217]).

Here, we describe methods for these different types of high-resolution imaging: live *in utero* imaging of fluorescent proteins within anesthetized worms, fixed *in utero* imaging of fluorescent proteins within worms fixed in ethanol, and *ex utero* immunofluorescence. We also describe a standard method for feeding RNAi. This combination of techniques allows an experimenter to deplete a protein of interest, image the resulting phenotype in intact worms, quantify the phenotype based on position in the germ line, and obtain high resolution images of spindle morphology and protein localization. These approaches coupled with time-lapse imaging (described in[100]) yield a thorough characterization of a protein's function during cell division with high temporal and structural specificity.

As an example of these techniques we show characterization of KLP-18, a kinesin motor protein essential for meiotic spindle assembly[48,56,101]. Upon fertilization of the oocyte, microtubules normally form a cage-like structure adjacent to the disassembling nuclear envelope, and these microtubules are then reorganized into a bipolar spindle, through a multipolar intermediate[48] (Figure A.2B). Instead, following RNAi depletion of *klp-18*, microtubules form a monopolar spindle immediately following cage formation. This dramatic phenotype is therefore useful to demonstrate these techniques. For these studies we use the strain OD868 that expresses mCherry::histone and GFP::tubulin[251] as an example of two-color imaging, or the EU1067 strain that expresses GFP::tubulin and GFP::histone[56] as an example of one-color imaging. In the immunofluorescence section, we stained control and *klp-18(RNAi)* oocytes for tubulin and DNA to mark the spindle, ASPM-1, which localizes to spindle poles[138], and

AIR-2 (Aurora B kinase), which is a member of a chromosome-associated ring-shaped complex[56]. An overview of *C. elegans* husbandry can be found here[258].

A.3. Materials

2.1 Feeding RNAi

1. 1M IPTG: Resuspend a 1g bottle of IPTG in 4.19mL sterile dH2O. This amount is good for 4L of media. If pouring smaller batches of plates, split up the IPTG stock appropriately and store the leftover solution at -20°C.

2. NGM/Amp/1mM IPTG plates: First, make 4L NGM by adding 12g NaCl, 10g Bacto-Peptone, and 68g Bacteriological Agar to 4L dH2O, then autoclave. Remove from autoclave and cool for 15 minutes on the bench top or put in a 50°C oven overnight. After cooling, add (in order), 4mL 1M $CaCl_2$, 4mL cholesterol, 4mL 1M $MgSO_4$, 100mL 1M KH_2PO_4, 4mL 100mg/mL ampicillin, and the 1M IPTG stock (see step 1). Pour 6cm plates by hand or with automated plate pourer (we use an Integra MediaJet). Plates are useable for one month if stored at 4°C away from light.

3. LB: Add 10g Tryptone, 5g yeast extract, and 10g NaCl per 1L dH2O and autoclave.

4. Sterile (autoclaved) toothpicks

5. 5M NaOH

6. Bleach

7. 13mL snap cap tubes

8. RNAi feeding library (described in[207,208,259,260] and available commercially)

2.2 in utero high-resolution live imaging

1. M9: To 400mL dH2O, add 1.5g KH_2PO_4, 3.0g Na_2HPO_4, and 2.5g NaCl. Bring to 500mL and autoclave. After solution cools, add 500μL of 1M $MgSO_4$.

2. Anesthetic: 0.2% tricaine, 0.02% levamisole in M9

3. 8-well imaging slide (we use Multitest slides from MP Biomedicals)

2.3 in utero imaging of fixed worms

1. M9: same as in section 2.2

2. Mounting media used for DNA staining: Dilute 1μL of a 5mg/mL Hoechst stock into 1mL M9 (make this dilution fresh every time). Add diluted Hoechst/M9 to Antifade Mounting Medium (VectaShield) in a 1:1 ratio and keep on ice until use.

3. Mounting media if DNA staining is not desired: Add M9 to Antifade Mounting Medium in a 1:1 ratio and keep on ice until use.

4. 100% Ethanol

5. Glass Coverslips (22x22 mm)

6. Nail polish for sealing slides

2.4 Immunofluorescence

1. M9: same as in section 2.2

2. Poly-L-Lysine Coated slides (commercially available)

3. Glass Coverslips (18x18 mm)

4. Methanol (Pre-chilled to -20°C)

5. Liquid Nitrogen in a dewar

6. Dissection Needle: 25G x 5/8 (0.5 mm x 16 mm)

7. Razor blades

8. Hydrophobic Marker/PAP Pen

9. PBS: In 800mL of distilled water, add 8g sodium chloride, 0.2g potassium chloride, 1.44g Sodium phosphate dibasic, and 0.24g Potassium dihydrogen phosphate. Adjust the pH to 7.4 with HCl and add distilled water until the total volume reaches 1L.

10. Antibody dilution buffer (AbDil): Add 4% BSA, 0.1% Triton X-100 and 0.02% Sodium Azide into 1X PBS (final concentrations denoted), and mix completely. Then filter the solution using a 0.22μm sterile filter and store at 4°C.

11. PBST (for washes): Add 0.1% Triton X-100 to 1X PBS (final concentration denoted) and thoroughly mix. Then filter the solution using a 0.22μm sterile filter and store at 4°C.

12. Hoechst staining buffer (if DNA staining is desired): Dilute a 5mg/mL stock of Hoechst 1:1000 in PBST.

13. Mounting Media: In a 15mL conical, add 90% glycerol (final concentration), 20mM Tris pH 8.8, and distilled water to a final volume of 2.5mL and mix well. Once the solution is mixed, add 0.5% p-phenylenediamine (which is light sensitive) to the solution. Wrap the conical in foil and place on a rocker. Periodically check the solution until the p-phenylenediamine is completely dissolved. The final solution should turn pinkish in color. Aliquot the solution and store at -80°C until use. Alternatively, Prolong Gold antifade reagent (Life Technologies) or Antifade Mounting Medium (VectaShield) can be used for mounting slides.

14. Nail polish for sealing slides

A.4. Methods

If new to *C. elegans*, refer to this excellent overview of animal husbandry for the basics on how to grow and handle the worms[258].

3.1 Feeding RNAi

For RNAi, we typically begin feeding worms at the L1 larval stage, which in most cases leads to efficient protein depletion. This protocol therefore outlines a procedure for generating a population of synchronized L1s to use for RNAi. However, for some proteins this type of long-term depletion causes defects in larval and/or germline development; should this be the case, the below protocol can be adjusted to begin feeding later stage worms. In those cases, omit the steps to prepare L1s, and simply pick worms of the desired age onto the prepared RNAi plates on Day 3.

When setting up bacterial cultures, use sterile tubes, tips, and pipets, and use sterile technique. 1 culture yields 2 RNAi plates. Bacterial cultures can be seeded from frozen glycerol stocks or directly from 96-well RNAi library plates[207,208,259,260].

Preparing RNAi Plates

Day 1:

1. Add 3mL LB + 100μg/mL ampicillin to a 13mL snap cap tube.

2. Take the RNAi library plate or glycerol stock out of the -80°C freezer. If using a glycerol stock, take a small stab with a sterile toothpick and place it into the LB/Amp and lightly re-cap the tube. Since aerating the culture is important, avoid pushing the cap all the way down and creating an air-tight seal.

3. If using a 96-well RNAi library plate, clean the foil cover of the plate with ethanol and then use a sterile toothpick to pierce the foil covering the clone that you want, removing a small stab. Place the toothpick into the LB/Amp and lightly re-cap the tube, as described in step 2. Then re-seal the plate using a new piece of foil.

4. If an empty vector control is desired, also set up a culture using a stab of bacteria containing the L4440 vector used in the RNAi library, without an insert.

5. Grow cultures overnight at 37°C. Use a rotator or shaker.

Day 2:

6. Pellet the bacteria in a tabletop centrifuge at 3500 rpm for 10 minutes (see Note 1).

7. Pour out and discard most of the media and shake the tube a few times to remove excess supernatant. Resuspend the pellet in the small amount of remaining media by pipetting up and down using a sterile tip. Split the culture between two NGM/Amp/1mM IPTG plates (usually a few drops per plate, depending on how much media there was left in the tube), and swirl the plate gently to spread the culture out. Try not to let the bacteria reach the edge of the plate.

8. Leave the plates at room temperature overnight to dry and induce dsRNA expression. Keep away from light.

Generating L1 worms for RNAi:

If you are planning to feed worms starting at L1, you should bleach adults on the same day that you pipet the overnight cultures onto the RNAi plates (Day 2), so that you have synchronized L1s to seed onto fresh plates once they are dry (on Day 3). Bleaching dissolves

adult worms and isolates embryos that then hatch as a cohort, synchronizing the worm population.

9. Wash worms off 3-4 6cm plates crowded with adults using M9 and pipet into a standard 15 mL conical tube (see Note 2). Add NaOH to a final concentration of 0.5M and bleach to 20%. Typically, we use 9mL M9, 1.5mL 5M NaOH, and 3.3mL bleach. If the M9 washes result in a volume less than 9mL, bring the volume to 9mL before adding the other components.

10. Mix well by inverting the tube or gently vortexing and leave for approximately 5 minutes. Monitor the worms under a dissecting scope carefully; as soon as the adult worms start to break open, move on to the next step. Note that if you leave the worms in the bleach solution for too long, the embryos will also be affected and will not hatch.

11. Pellet embryos for 1 minute at 800xg in a tabletop centrifuge at 4°C.

12. Gently pour off supernatant. Take care not to dislodge the embryo pellet.

13. Wash embryos 3 times using 15mL sterile M9 (add M9, mix, pellet embryos, pour off supernatant, repeat).

14. Resuspend embryos in the residual M9 left from the last wash. Drop embryos onto one or two unseeded (no food) NGM plates.

15. Allow embryos to hatch into larval L1s at 20°C overnight.

Day 3:

16. Wash hatched L1s off plates using 2-3mL sterile M9 and collect in a conical tube.

17. Use a sterile glass pipet to drop L1s onto the prepared RNAi plates. We aim for at least 50 L1s per RNAi plate. In our experience, the number of each worms in each drop varies (depending on how many L1s you recovered from the bleaching), but we typically use

around 2 drops per plate. It is best to check each drop under a dissecting scope to ensure you are not putting too many worms on each plate; you don't want your plate to starve before the worms are used in the experiment.

18. Grow worms at 15°C (see Note 3).

19. Look at worms daily to monitor growth (see Note 4).

Notes for RNAi:

1. If you wish to make a glycerol stock for use in future experiments, remove 0.5mL from the culture before spinning. Add it to 0.5mL sterile 30% glycerol (in dH2O) in a sterile screw-cap cryo tube. Store at -80°C. There will still be plenty of culture left over to set up the two RNAi plates.

2. Although RNAi can be performed in any strain background, we have found that strains can differ in their susceptibility to feeding RNAi, and therefore results can vary. For example, strains containing a particular GFP::histone transgene work particularly well for RNAi[261]; the original strain containing this transgene is AZ212[262], and this transgene is also present in EU1067[56].

3. RNAi has been successfully performed by various labs, by growing worms at different temperatures. However, for the genes that we have tested, we have achieved better depletion efficiency by growing worms at 15°C instead of at higher temperatures, so that is the growth temperature that we use and recommend.

4. In our experience, L1s added to RNAi plates on Day 3 and grown at 15°C can typically be used in experiments somewhere between Days 6 and 8 (this depends on what time you set up the plates, whether you want young or older adults, etc.). For most applications, we use worms on Day 7 (1 week after starting the protocol), when they are gravid adults with

plenty of embryos. Keep in mind that strains can grow at different rates and this timing must be optimized for every strain used.

3.2 in utero high-resolution live imaging

Set up slides immediately before imaging. The anesthetic is crucial to immobilize the worm enough to acquire a usable full-stack image. See Figure A.3A for example images and slide set-up.

1. Add a 4μL drop of M9 containing anesthetic to a well of an 8-well imaging slide (see Note 1).

2. Pick 10-15 adult worms into the drop and let sit for 3 minutes to allow anesthetic to slow worm movement.

3. Place a coverslip gently on top of the slide so that the M9 spreads to the edges of the well and immediately image.

4. Scan the slide using a low magnification objective (we use 40X) to find a worm, then switch to a high magnification 100X objective to acquire the image (see Note 2).

5. We typically acquire z-stacks with a step size of 0.2 or 0.3μm, similar to fixed imaging. Sometimes the worms will move during the acquisition of a stack; if this happens, it is usually possible to just try again.

Notes for live imaging:

1. We typically use an 8-well slide so that we can mount several populations of worms and have many worms to choose from for imaging, and we have found that the well size on an 8-well slide fits a 4μL drop nicely. However, a slide with any number of wells (6 to 12) would work if the M9 drop volume is adjusted accordingly.

2. After an extended time in the anesthetic, oocytes begin to arrest and spindle structure may change. Therefore, it is best to only acquire a small number of images of per slide, and then set up fresh wells.

3.3 in utero imaging of fixed worms

See Figure A.3B for example images and slide set-up.

1. Add 10μL of M9 onto a microscope slide and pick worms into the drop. The number of worms can vary depending on how many you need to look at for your experiment, though if you try to fix more than 30 at once, it is difficult because the worms will tend to lie on top of one another and they will be hard to visualize.

2. Once you are done picking, wick away excess liquid using Whatman paper. The goal is to remove as much liquid as you can without drying the worms completely. They will tend to clump together in the center as you do this, so try to carefully spread them out with the end of a pipet tip as you wick the liquid.

3. Add 10μL of 100% ethanol directly to the worms and let dry completely. Wait until the worms are completely dry before adding more ethanol. They should desiccate and turn black.

4. Repeat the ethanol treatment (step 3) two more times.

5. Pipet 10μL of the M9:Antifade Mounting Medium mix directly on top of the worms. For this step you can use mounting media either with or without Hoechst added (see Note 1).

6. Carefully place a 22x22mm coverslip onto the drop of mounting media and let the media spread. Try to avoid air bubbles and aspirate any excess mounting media leaking out

the sides of the coverslip. If you get air bubbles, carefully push down on the coverslip with forceps and try to push the bubbles towards the sides, away from the worms.

7. Seal coverslip with nail polish.

8. Slides can be imaged immediately or can be stored at 4°C overnight before imaging. The slides are good for about a week if stored at 4°C, though the DNA staining begins to appear less sharp in older slides.

Notes for the ethanol fix protocol:

1. The Hoechst allows you to see the DNA, and this protocol also preserves fluorescence if you are fixing GFP/mCherry-expressing worms. The GFP/mCherry is not as bright as in live worms and the fixation does not preserve the microtubules quite as well as immunofluorescence, but this protocol is usually sufficient to get a detailed view of spindle morphology, beyond the resolution of live imaging.

3.4 Fixed Immunofluorescence Staining Protocol

The immunofluorescence protocol consists of three major steps: Preparing the slides, staining, and mounting. See Figure A.3C for example images and slide set-up. All antibody concentrations and incubation times (i.e., blocking time, antibody incubation time, fixation time) must be optimized for each antibody and target protein. The examples given here are our starting point for further optimization.

1. Pick about 30 adult worms into a 5μL drop of M9.

2. Use a 25G x 5/8 (0.5 mm x 16 mm) BD Precision Glide needle to cut worms in half and release the oocytes and embryos into the drop. Aim for the middle of the worm (near the vulva) to maximize the number of oocytes and embryos that spill out. These dissections

need to be carried out rapidly in order to prevent the M9 drop from drying out. If you are a beginner and it takes a long time to dissect the worms, we recommend starting with fewer worms per slide.

3. After dissecting the worms, place a 18x18mm glass coverslip on top of the drop such that the liquid spreads out, forming a thin layer, and the embryos are slightly compressed. Applying excessive pressure when putting on the coverslip after dissections will disrupt the integrity of the embryos and oocytes, therefore only slight pressure should be used.

4. Plunge the slide into liquid nitrogen for a minimum of 4 minutes and a maximum of 10 minutes to ensure that the worm sample is frozen. Rapid change in the temperature of the slide can cause it to crack, so we use a basket or tongs to slowly lower the slide into the liquid nitrogen to minimize the chance of cracking.

5. Use tongs to remove slides one at a time from the liquid nitrogen and quickly use the edge of razor blade to snap off the coverslip from the slide (this method is known as freeze cracking). It is important to flick off the coverslip while the sample is still frozen to mechanically disrupt the cuticle of the worms and the eggshell of the embryos, so do not allow the slide to sit out at room temperature, causing the liquid to thaw, or allow the coverslip to fall off automatically.

6. After removing the coverslip, immediately plunge the slide into methanol precooled to -20°C and allow slides to incubate at -20°C for 35 minutes (see Note 1). If processing multiple slides, at this point you can retrieve another slide from the liquid nitrogen dewar and repeat step 5.

7. After the methanol step, move the slides into a slide holder containing 1X PBS at room temperature for at least 5 minutes. Slides can sit in PBS for some time, so we synchronize all of the slides in PBS before moving on to the next step.

8. Follow the first PBS wash with a second 1x PBS wash for another 5 minutes.

9. Remove slides one at a time from the PBS chamber. Dry most of the slide by wiping it with Kimwipes, but avoid the part of the slide with the embryos, as it is important that they do not dry out.

10. Place slide in a humidity chamber (see Note 2) and use a hydrophobic marker to draw a 18x18mm square around the area with the embryos. Then carefully pipet 75μL of AbDil into the square. Incubation in AbDil serves as a blocking step. At this point, if you have set up multiple slides, return to step 9 to process the next slide.

11. Allow the sample to incubate for at least 30 minutes at room temperature in the humidity chamber, ensuring that it does not dry out during the incubation (See Note 3).

12. After the blocking step, use a pipet or aspirator to carefully remove the AbDil, avoiding the embryos, and add 75μL of primary antibody diluted in AbDil. The slides can be incubated at 4°C overnight or for multiple hours at room temperature, still in the humidity chamber.

13. Aspirate off the primary antibody and wash the sample 3 times with 1X PBST. These are quick washes, where you pipet on the PBST, leave for a few seconds, carefully aspirate off the wash, and repeat.

14. After the last wash, add 1:500 of the secondary antibody diluted in AbDil (see Note 4) and allow the sample to incubate in the humidity chamber for 2 hours at room temperature.

15. Aspirate off the secondary antibody and then wash the sample 3 times with 1X PBST, as described in step 13.

16. Add 75μL of Hoechst staining buffer to the sample and allow it to incubate for 15 minutes at room temperature.

17. Aspirate off the Hoechst and wash the sample 2 times with 1X PBST, again using quick washes.

18. Pipet 5μL of mounting media onto the sample and carefully place a 18x18 mm glass coverslip on top. Ensure that the mounting media spreads evenly to the edges of the coverslip; if there are air bubbles, you can gently push down on the top of the coverslip to move them to the side.

19. Seal the coverslip in place using nail polish.

Notes for immunofluorescence:

1. Some antibodies work better with shorter or longer methanol incubations and therefore the time can be adjusted accordingly.

2. To make a humidity chamber, line a small sealable container with moist kimwipes.

3. Slides can be incubated at 4°C overnight in AbDil to reduce background staining, if needed for particular antibodies.

4. We use Alexa-Fluor conjugated secondary antibodies from Invitrogen, but antibodies from other companies could also be used.

3.5 Image Acquisition

Images can be acquired using a variety of different types of microscopes. All images in our figures were acquired on a DeltaVision Core deconvolution microscope with a 100X objective (NA = 1.4). All images in the figures (except for the timelapse imaging example) were obtained at 0.2μm z-steps and deconvolved (ratio method, 15 cycles) using SoftWoRx (Applied Precision). All images are displayed as full maximum intensity projections of data stacks encompassing the entire spindle structure.

Figure 1

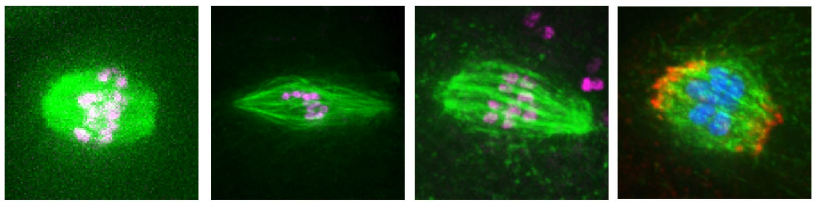

	Time lapse	*In utero* live	*In utero* fixed	IF
Time resolution	+	-	-	-
Germline position	+	+	+	-
Protein localization (3+ channels)	-	-	-	+
Requires fluorescent protein expression	+	+	+	-
High-resolution structural information	-	+	+	++
Large scale experiments	-	+	+	+

Figure A.1. **Comparison of common imaging techniques used with *C. elegans* oocytes and embryos**. The advantages and limitations of various imaging techniques are presented in the chart. A representative image of a bipolar oocyte meiotic spindle is also displayed for each technique; a strain expressing GFP::tubulin and mCherry::histone was used. Methods for *in utero* live, *in utero* fixed, and immunofluorescence are presented in this chapter. Extensive methods for timelapse imaging were recently described and can be found in[209].

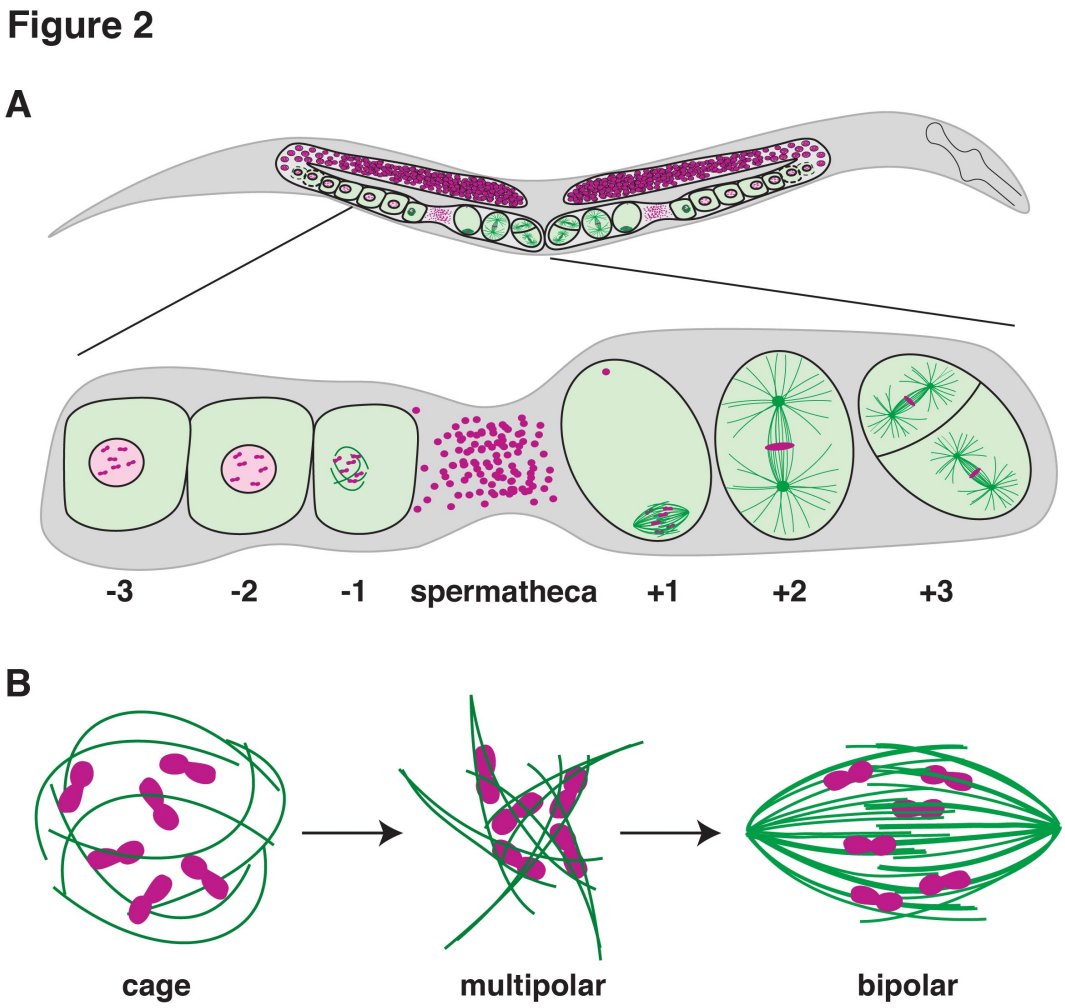

Figure A.2. **Schematics of the *C. elegans* germ line and of spindle assembly in oocytes**. Body of the worm is shown in grey, germ line is outlined, tubulin shown in green, and DNA shown in magenta. A) Germline schematic. *C. elegans* are self-fertilizing hermaphrodites that contain both oocytes and sperm. Germ cells differentiate in the distal end of the gonad and then proceed through the stages of meiotic prophase I as they move towards the spermatheca. Once oocytes are in proximity to the spermatheca (in the -1 position), they are fertilized. Upon fertilization, the oocyte moves through the spermatheca and into the +1 position and the meiotic divisions proceed. The first mitotic divisions of the embryo then occur within the worm before the egg is laid. Oocytes in the zoomed diagram are shown progressing from left to right; magenta dots in the spermatheca represent condensed sperm nuclei. B) Stages of meiotic spindle assembly in the oocyte. Upon fertilization, microtubules form a cage-like structure around the chromosomes before they are organized into a multipolar spindle with several nascent poles. Then these poles coalesce to form a bipolar spindle[48].

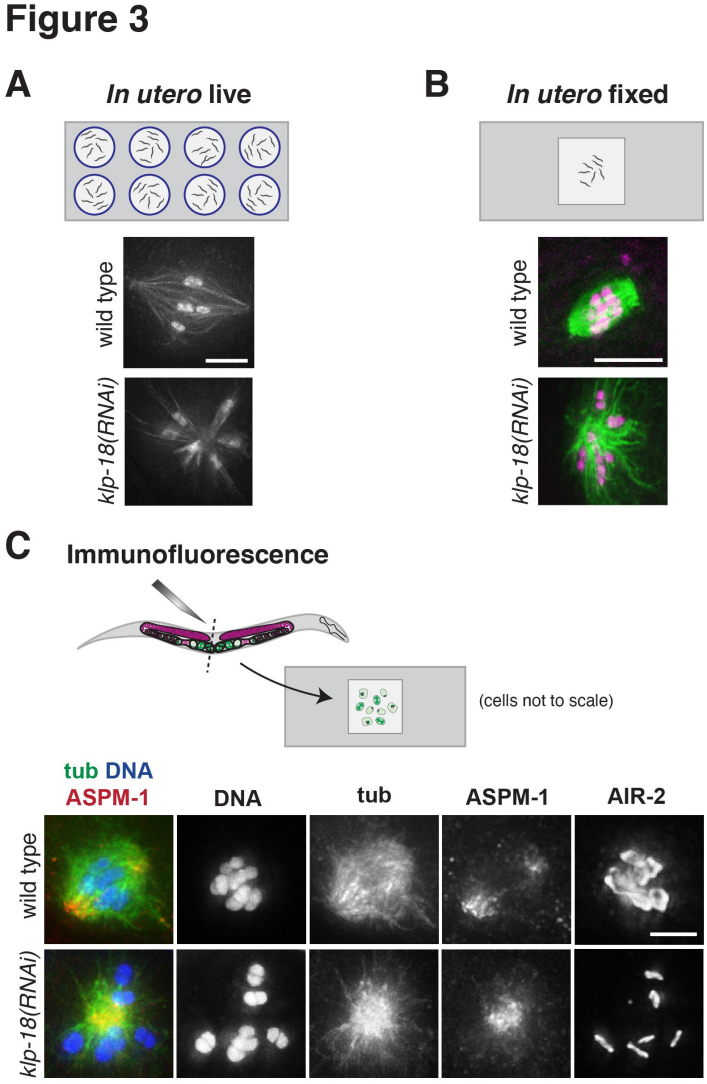

Figure A.3. **Examples of each imaging technique**. A) *in utero* live imaging allows for high resolution images of fluorescently-tagged proteins. A representative wild type (vector control) and a *klp-18(RNAi)* oocyte spindle in worms expressing GFP::histone and GFP::tubulin are shown. The slide setup is diagrammed above the images. Images adapted from[48]. B) Ethanol fixation followed by *in utero* fixed imaging allows for visualization of fluorescently-tagged proteins. A representative wild type (vector control) and a *klp-18(RNAi)* oocyte spindle in worms expressing mCherry::histone and GFP::tubulin are shown. The slide setup is diagrammed above the images. C) Immunofluorescence allows for staining of proteins of interest for which an antibody is available. A wild type (vector control) and a *klp-18(RNAi)* oocyte spindle are shown. Immunofluorescence was performed to visualize tubulin, ASPM-1 (which marks spindle poles), AIR-2 (which localizes to chromosomes) and DNA. A diagram of the experimental procedure is shown above, with an example slide featuring oocytes and embryos (that are not to scale). Scale bar = 5μm.

APPENDIX B

MESP-1 can nucleate microtubule assembly *in vitro*

In Chapter 2, I propose that MESP-1 is a functional ortholog in *C. elegans* to mammalian and *Xenopus* TPX2. TPX2 has been shown to nucleate microtubule assembly *in vitro*[83,229] and I hypothesized that MESP-1 could also perform this function. In preliminary experiments, I found that MESP-1 could indeed nucleate microtubule formation, although this finding must be tested more rigorously. In addition, a role for this activity *in vivo* is not obvious: *mesp-1(RNAi)* oocyte monopolar spindles do not have obvious microtubule nucleation defects, but this has not been tested carefully.

To test for microtubule nucleation, I incubated unpolymerized soluble fluorescent TMR-tubulin with buffer alone or with 2μM MBP-MESP-1. The reactions were squashed on a slide then imaged with a wide-field fluorescent microscope. In the buffer alone condition, I did not detect any microtubule-like structures and only saw "cloud-like" wisps of signal that were likely contaminants in the reaction (Figure B.1). In contrast, upon addition of MBP-MESP-1, I saw many microtubule-like structures that were often aggregated into large groupings (for example, see bottom right image in Figure B.1). These results suggest that MESP-1 can nucleate microtubules, similar to its functional ortholog TPX2. This must be confirmed with more rigorous and controlled experiments, for example, repeating the reaction without GTP (to test if these structures are dependent on GTP as microtubules should be) and with careful quantification of microtubule fluorescent intensity over time and MBP-MESP-1 concentration.

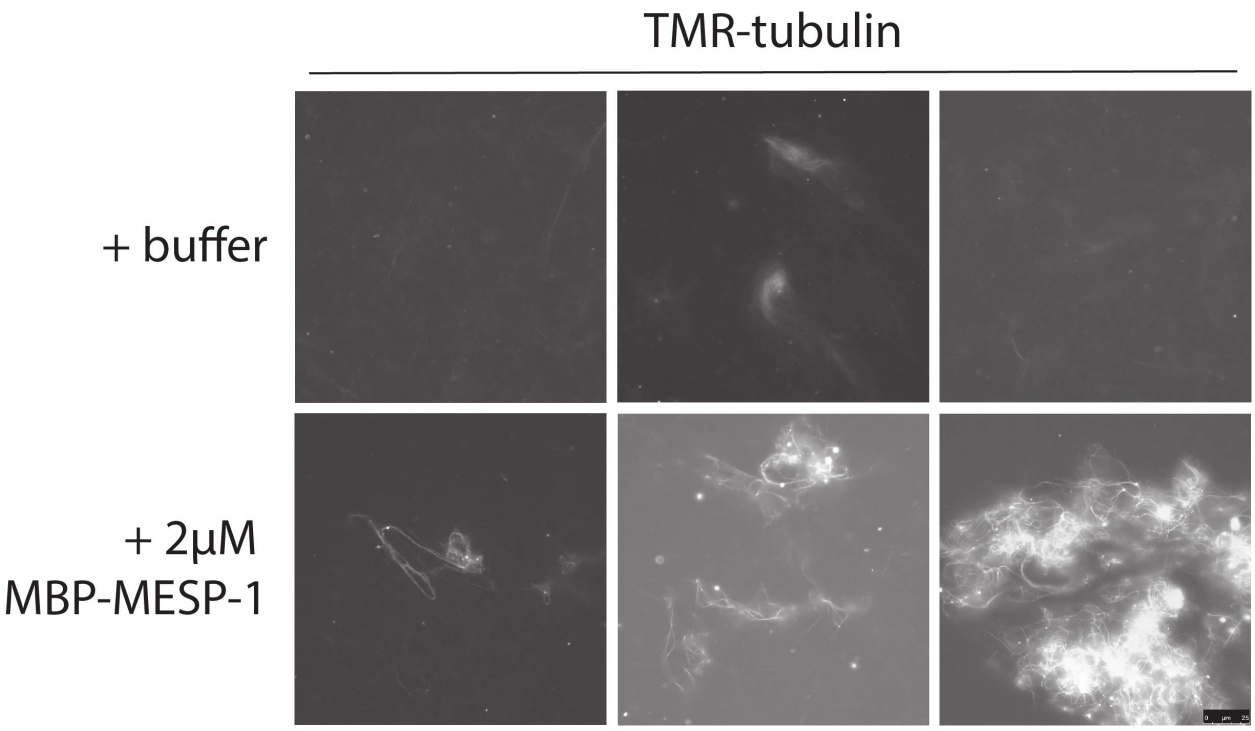

Figure B.1. **MBP-MESP-1 can nucleate microtubule assembly *in vitro***. Fluorescent TMR-tubulin was incubated with buffer alone (top) or 2μM MBP-MESP-1 then squashed on a cover slip and imaged. Microtubules were not detected in the buffer alone control, but many microtubules were seen upon addition of MBP-MESP-1 indicated that MESP-1 can nucleate microtubules in solution. Three examples of representative images for each condition are shown. Scale bar = 25μm.

APPENDIX C

KLP-18 and MESP-1 can form droplets that concentrate tubulin and associate with microtubules *in vitro*

This appendix describes a side-project I undertook to test for possible phase-separation properties of C. elegans oocyte spindle pole proteins, particularly KLP-18 and MESP-1. See 'Future Directions' in Chapter 4 for additional background.

It has been shown that centrosomes within *C. elegans* embryos are phase separated compartments that act to concentrate tubulin and other PCM components[80,82]. By concentrating tubulin dimers into a small space, phase separated compartments create a very high local concentration of tubulin that results in microtubule polymerization. This concept has recently been extended to oocytes: mouse spindles contain a liquid-like meiotic spindle domain (LISD) that contains at least 19 proteins[71]. The LISD is conserved throughout mammals including cow, sheep, and pig oocytes. Disruption of the LISD results in a decrease in spindle tubulin intensity and errors in anaphase. Because of the presence of a critical phase separated compartment in *C. elegans* embryos as well as in mammalian oocytes, I hypothesized that there is a similar structure in *C. elegans* oocytes. In Chapter 2, I propose that MESP-1 is a functional ortholog of TPX2. TPX2 has recently been shown to phase separate and this ability is essential for its microtubule nucleation activity[83]. MESP-1's apparent ability to nucleate microtubules (Figure B.1) begged further investigation in the context of phase separation. These experiments were aiming to answer a related but wider question presented in Chapter 4: what is the fundamental structure of an acentrosomal pole?

First, I used previously published methods to test if GFP-stalk or MBP-MESP-1 (see Figure 3.2) could form droplets *in vitro*[82]. These reactions contain 9% PEG used as a molecular crowding agent to mimic the crowding within the cell's cytoplasm. Using both differential interference contrast (DIC) and fluorescence microscopy, I found that MBP-MESP-1 and GFP-stalk formed spherical phase separated droplets in the presence of 9% PEG (Figure C.1A,C). To confirm that these droplets were indeed spherical, I performed cryo-TEM (transmission electron microscopy) on these reactions with the help of the NUANCE core facility. We detected spherical structures of GFP-stalk within 9% PEG (Figure C.1B), but did not see similar structures in the MBP-MESP-1 reaction (data not show) for unknown reasons. Next, to confirm that droplets formed reproducibly in these reaction conditions, I quantified number of drops and diameter of drops with a variety of proteins. I squashed the reactions on a slide then visualized GFP-stalk and used ImageJ to quantify the number of GFP spots and diameter of GFP spots over a consistent number of images for all conditions (Figure C.1D, each data point on plot represents one drop). When GFP alone was incubated with 2μM tubulin, very few droplets formed (10 drops) and they were relatively small (mean diameter 0.35μm). In contrast, when 200nM GFP-stalk was added to the reaction along with 200nM tubulin, 208 drops formed with a mean diameter of 0.94μm. Number of drops and mean drop diameter remained relatively consistent with increasing tubulin concentration (2.5μM, 0.84μm diameter) and addition of 1μM MBP or MBP-MESP-1. These results indicate that both MESP-1 and KLP-18 can form spherical droplets with molecular crowding agents *in vitro*.

Next, I aimed to test the functional activity of these drops *in vitro*. Similar droplets formed from *C. elegans* PCM components are able to specifically incorporate tubulin and

nucleate microtubules *in vitro*[82]. Therefore, I tested if KLP-18 or MESP-1 droplets could incorporate tubulin. I incubated 200nM GFP-stalk alone, with 1μM MBP, or with 1μM MBP-MESP-1 in a reaction with 9% PEG and 500nM fluorescent TMR-tubulin, then squashed the reaction on a slide and imaged it with widefield fluorescence microscopy (Figure C.2A). I saw that tubulin only concentrated within GFP-stalk droplets in the presence of MBP-MESP-1, suggesting that these droplets are biochemically active and that they selectively condense tubulin. To confirm this result, I quantified the 'Tubulin Partition Coefficient', a metric used to quantify the concentration of fluorescent proteins[82]. It is defined as the fluorescence intensity within a drop divided by the fluorescence intensity outside of the drop; if the coefficient is greater than 1, the fluorescence is concentrated above background within the drop. This quantification was performed in ImageJ. In reactions containing 200nM GFP-stalk and 500nM tubulin, when no protein (-) or 1μM MBP was added there was a very slight increase in partition coefficient (Figure C.2B). However, when increasing concentrations of MBP-MESP-1 were added (from 100nM to 1μM), the partition coefficient increased substantially to around 2, confirming that KLP-18 droplets are able to selectively recruit tubulin in the presence of MESP-1.

After discovering that these droplets could selectively incorporate tubulin, I next wanted to test if they could nucleate or associate with microtubules in solution. To test this, I incubated 200nM GFP-stalk, 1.25μM TMR-tubulin, and 1μM MBP or MBP-MESP-1 (Figure C.3A). I assembled these reactions with 1mM GTP in the solution to aid in microtubule polymerization, and let them incubate for 5-10 minutes before squashing the reaction on a slide. I did not detect any microtubules with MBP alone, however, I did see extensive microtubule networks when I added MBP-MESP-1. To confirm that these structures are in fact

microtubules, I repeated the same reaction without GTP and did not see any long microtubules, but tubulin continued to incorporate into GFP-stalk droplets. From these results, it was unclear if these droplets were actively polymerizing microtubules (as seen with PCM condensates[82]) or associating to microtubules polymerized in solution, presumably nucleated by free MBP-MESP-1 (see B.1). To directly test this, I aimed to film droplets nucleating or associating with microtubules using a spinning disk microscope. I assembled reactions with 200nM GFP-stalk, 1.25μM TMR-tubulin, 1μM MBP-MESP-1, and 1mM GTP then immediately squashed the reaction on a slide and began time-lapse imaging (Figure C.3B). As I continued filming, I saw an increasing number of microtubules associating to GFP-stalk droplets, however, I was unable to confidently detect clear microtubule nucleation from the droplets. It is clear from the movies that GFP-stalk droplets are often, if not always, associated with and anchor microtubule ends (I often saw one end of a microtubule embedded into a droplet and the other end freely moving side to side). Although more work must be done to optimize imaging conditions to fully test if droplets are nucleating microtubules or associating with microtubules formed in solution, these results clearly demonstrate that droplets can both incorporate tubulin and anchor microtubule ends.

Finally, I aimed to directly test the *in vivo* relevance of phase separated spindle components. My *in vitro* data suggests that KLP-18 and MESP-1 have the ability to form discrete structures, but is there any evidence for these structures in the oocyte? To test this, I dissected oocytes into a solution containing 20μg/mL nocodazole, a microtubule destabilizing drug, then performed immunofluorescence (see Chapter 5 or Appendix A for method). I hypothesized that if a microtubule independent structure existed, it would persist in the absence of microtubules. In contrast, if pole proteins were completely associated with microtubules, then staining would not persist when microtubules are depolymerized.

Therefore I stained nocodazole treated oocytes and embryos with antibodies staining pole protein ASPM-1 and KLP-18, which is enriched at the pole. After nocodazole treatment for 7 minutes, microtubules were depolymerized and tubulin formed a hazy cloud around chromosomes (Figure C.4). ASPM-1 colocalized with this tubulin cloud and KLP-18 interestingly relocalized to the center of bivalent chromosomes. I quantified the percent of oocytes with persistent tubulin and ASPM-1 staining with different lengths of nocodazole incubation and saw that the majority of oocytes did have persistent tubulin/ASPM-1 staining in both vector control and *mesp-1(RNAi)* conditions (I did *mesp-1(RNAi)* to test if MESP-1 had any effect on tubulin/ASPM-1 persistence- it does not seem to). These experiments show that tubulin and ASPM-1, and potentially the pole structure at large, persist in the absence of long microtubules, indicating the possibility of a microtubule-independent spindle pole structure.

Putting these results together, I propose that *C. elegans* poles may be phase separated compartments. There are two conceptual models of acentrosomal spindle poles: (1) pole proteins create a static cross-linked network of microtubule associated proteins and microtubules or (2) pole proteins create a phase separated compartment that could easily fuse together or disassemble (Figure 4.4). Spindle poles are remarkably pliable during meiosis; nascent poles of the multipolar spindle coalesce with one another to achieve bipolarity (Figure 2.1, 2.3), then poles broaden and disassemble during anaphase[104]. I stress that the results in this appendix are preliminary and must be confirmed more rigorously. However, I believe that this data points to an important characterization of the fundamental physical basis of acentrosomal spindle poles. To fully test this hypothesis, more pole proteins must be tested both *in vitro* and *in vivo*, and dynamics of the poles must be analyzed through FRAP and

other quantitative methods. See Chapter 4 for a more thorough discussion of these models and future experiments that can test these possibilities.

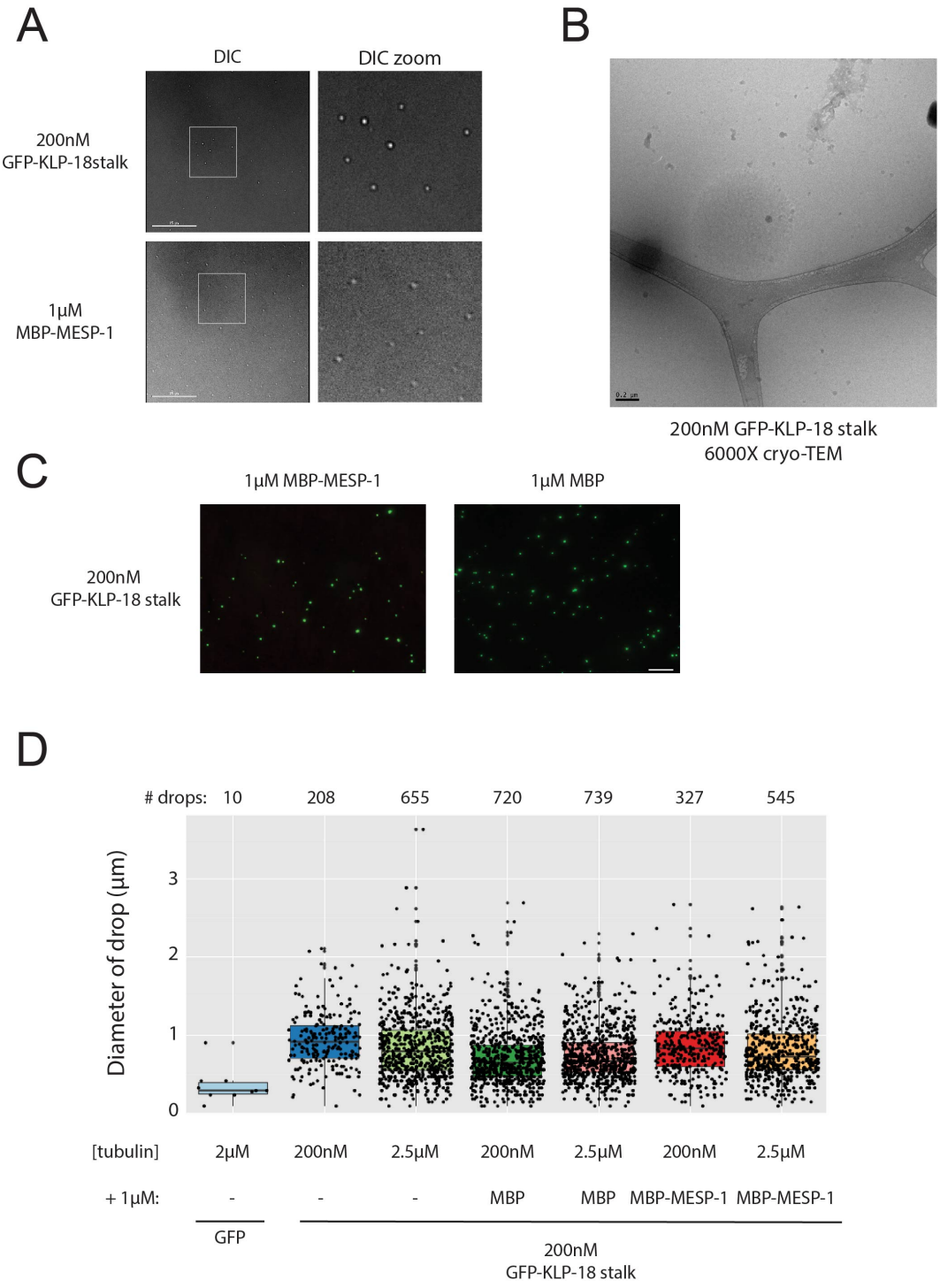
A
DIC
DIC zoom
200nM
GFP-KLP-18stalk
1µM
MBP-MESP-1
B
200nM GFP-KLP-18 stalk
6000X cryo-TEM
C
1µM MBP-MESP-1
1µM MBP
200nM
GFP-KLP-18 stalk
D
drops: 10 208 655 720 739 327 545
Diameter of drop (µm)
0
1
2
3
[tubulin] 2µM 200nM 2.5µM 200nM 2.5µM 200nM 2.5µM
+ 1µM: - - - MBP MBP MBP-MESP-1 MBP-MESP-1
GFP
200nM
GFP-KLP-18 stalk

Figure C.1

Figure C.1. **KLP-18 stalk and MESP-1 form droplets in the presence of 9% PEG *in vitro***. Varying concentrations of GFP-stalk and MBP-MESP-1 (see Figure 3.5 and 3.2) were added to reactions containing 9% PEG and visualized by DIC (A), cryo-TEM (B), and fluorescent widefield microscopy (C). In (C) and (D), GFP-stalk was added to reactions with MBP-MESP-1 or MBP alone as a control. (C) shows representative images, and (D) shows quantification of visualized drops. Scale bars: (A) 15μm, (B) 0.2μm, (C) 10μm.

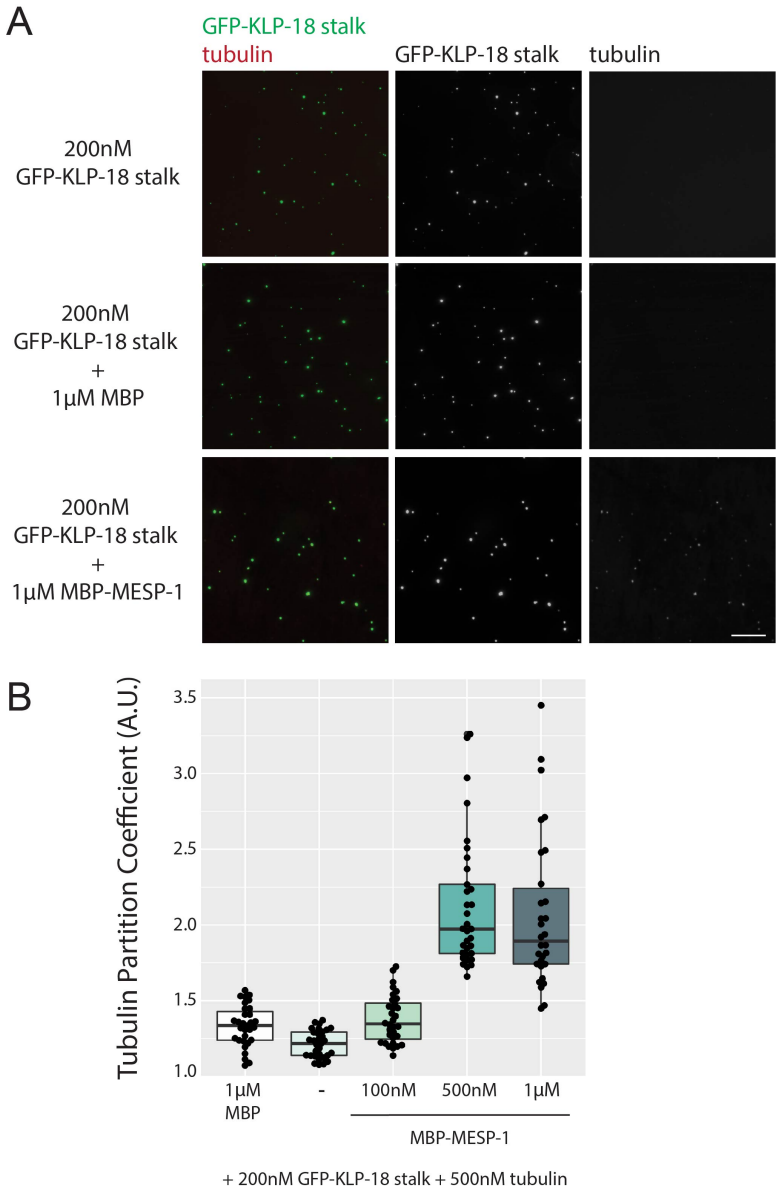

Figure C.2

Figure C.2. **MESP-1 is required for KLP-18 stalk droplets to incorporate tubulin**. (A) GFP-stalk was incubated with either MBP or MBP-MESP-1 in the presence of 9% PEG and fluorescent TMR-tubulin. Tubulin was only present in droplets in reactions containing MBP-MESP-1, indicating that MESP-1 is essential for tubulin concentration into the droplets. (B) Tubulin partition coefficient (fluorescent intensity of tubulin in drop / outside of drop) in GFP-stalk drop was quantified at different MBP and MBP-MESP-1 concentrations. Tubulin concentration into GFP-stalk droplets is dependent on concentration of MBP-MESP-1. Scale bar: 10μm.

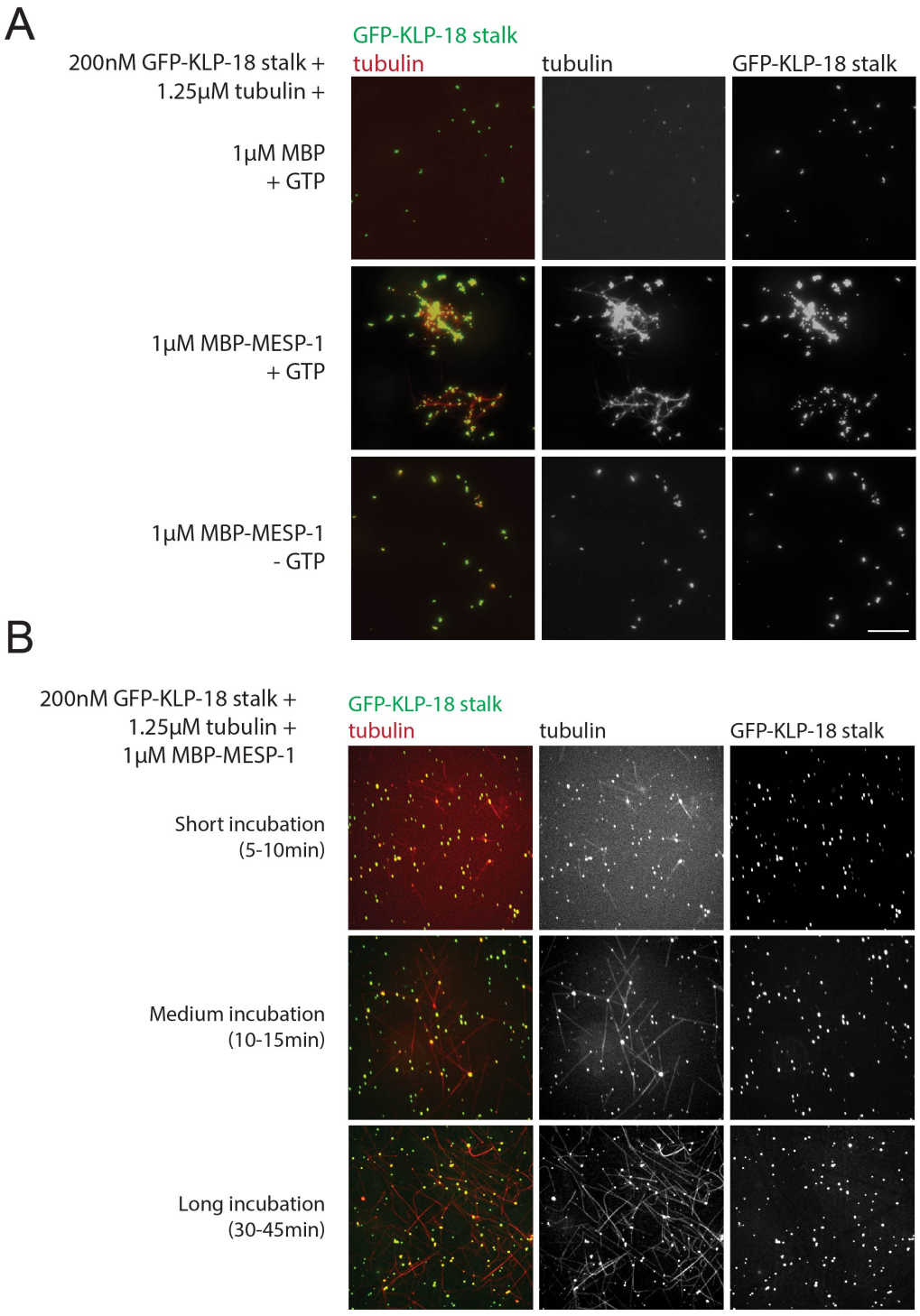
A
200nM GFP-KLP-18 stalk +
1.25μM tubulin +
1μM MBP
+ GTP
1μM MBP-MESP-1
+ GTP
1μM MBP-MESP-1
- GTP
GFP-KLP-18 stalk
tubulin
tubulin
GFP-KLP-18 stalk
B
200nM GFP-KLP-18 stalk +
1.25μM tubulin +
1μM MBP-MESP-1
Short incubation
(5-10min)
Medium incubation
(10-15min)
Long incubation
(30-45min)
GFP-KLP-18 stalk
tubulin
tubulin
GFP-KLP-18 stalk

Figure C.3

Figure C.3. **KLP-18 stalk / MESP-1 droplets nucleate or stabilize microtubules *in vitro***. (A) GFP-stalk was incubated in 9% PEG together with MBP or MBP-MESP-1 and in the presence or absence of GTP, which is essential for microtubule polymerization. GFP-stalk droplets are associated to microtubules and often form large structures. Presence of microtubules requires both MESP-1 and GTP, indicating that microtubules are either nucleated by drops directly or are nucleated in solution and then are stabilized by the droplets. I attempted to take movies of direct MT nucleation by droplets, but was unsuccessful (see B). Scale bar: 10μm. (B) Same reaction as (A) but visualized on the spinning disk confocal in an attempt to directly visualize microtubule nucleation from a droplet. Representative images are shown for three incubation lengths (reaction applied to slide, sealed with a coverslip, then incubated at room temperature). The microtubule network becomes more extensive as the reaction length increases. Droplets are often associated with microtubules either at ends or laterally along the microtubule length.

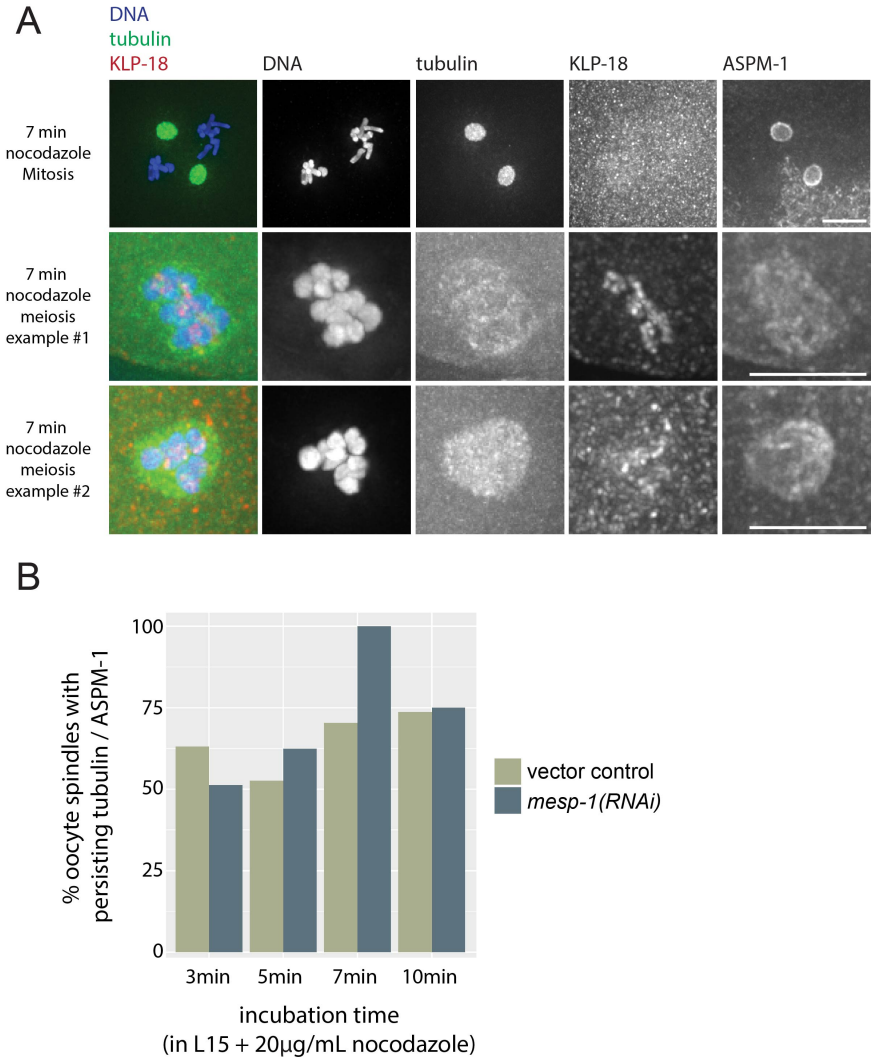

Figure C.4. **Tubulin and pole proteins persist after nocodazole treatment** (A) Mitotic embryo and oocyte spindles were treated with the microtubule destabilizing drug nocodazole for 7 minutes and representative images are shown. In mitosis, microtubules are completely disassembled and tubulin and ASPM-1 persists in phase separated centrosomes, as previously reported[82]. Oocyte spindles treated similarly with nocodazole show persisting tubulin signal around the chromosomes, in addition to persistent localization of KLP-18 to what appears to be the midbivalent ring complex at the center of the bivalent[56,58] and ASPM-1 colocalized to diffuse tubulin staining. (B) This result is consistent across different nocodazole incubation times, with the majority of oocytes in both vector control and *mesp-1(RNAi)* showing persistent tubulin and ASPM-1 localization. The diffuse tubulin staining may be an independent phase separated structure similar to mitotic centrosomes, or it may be small microtubules stabilized by chromatin. Scale bar: 5μm.

APPENDIX D

Kinesin-5 BMK-1 localization and effect on late anaphase

The role of kinesin-5 in C. elegans mitosis and meiosis remains elusive. I have made several attempts at discovering a unappreciated phenotype or role for this motor with only modest success. I have compiled these experiments here for posterity.

First, I wanted to examine BMK-1 localization during spindle assembly. BMK-1 has been shown to localize to the bipolar oocyte spindle but this imaging was low resolution, making it difficult to see discrete BMK-1 localization to different parts of the spindle (for example at the poles), and localization throughout spindle assembly was not tested[98]. I performed immunofluorescence using a previously characterized BMK-1 antibody[98] and revealed that BMK-1 is enriched on the poles of the multipolar forming spindle and on the bipolar spindle (Figure D.1A). This localization is strikingly similar to KLP-18 localization. Because I hypothesized that MESP-1 is the functional ortholog to TPX2 (see Chapter 2) and TPX2 regulates kinesin-5 in other systems[92], I wanted to test if MESP-1 regulates BMK-1 localization to the spindle. I depleted MESP-1 through RNAi then stained for both KLP-18 and MESP-1. As I have shown in Chapter 2, *mesp-1(RNAi)* results in a monopolar spindle phenotype and KLP-18 usually does not localize to monopolar spindle poles (Figure D.1B). BMK-1 follows a similar pattern: its spindle localization is decreased in *mesp-1(RNAi)*. To quantify this result using the immunofluorescence images, I measured KLP-18 and BMK-1 staining intensity at either bipolar or monopolar poles and normalized to background (Figure D.1C). For both KLP-18 and BMK-1 staining I saw a significant decrease in normalized pole

intensity on *mesp-1(RNAi)* monopoles compared to the vector control bipolar pole (each data point is a single pole). These results indicate that kinesin-5/BMK-1 co-localizes with KLP-18 during spindle assembly and requires MESP-1 to localize to the spindle.

Next, I visualized BMK-1 localization during anaphase (Figure D.2A). During early anaphase, BMK-1 and KLP-18 localize to the spindle poles. As the chromosomes segregate further (second row) BMK-1 begins to enrich on the microtubules between the separating chromosomes, while KLP-18 remains primarily enriched at the poles (but is also present between the chromosomes). This difference is more obvious during mid and late-anaphase (third and fourth row). Anaphase is the only stage in which BMK-1 does not co-localize with KLP-18 and may indicate that BMK-1 plays a more important role. To directly test for a role of BMK-1 in anaphase, I depleted BMK-1 with RNAi and found that late anaphase spindles were often splayed (Figure D.2B) compared to wild type late anaphase spindles (Figure D.2A, bottom row). This finding is generally aligned with previously published data that BMK-1 depletion leads to faster chromosome segregation than wild type[100]. BMK-1 may provide an important microtubule crosslinking force that helps to stabilize microtubules during anaphase. I stained for CPC component AIR-2 in these experiments as a readout for 'checkpoint' spindles[217]; *bmk-1(RNAi)* surprisingly does not induce the error checkpoint response in oocytes.

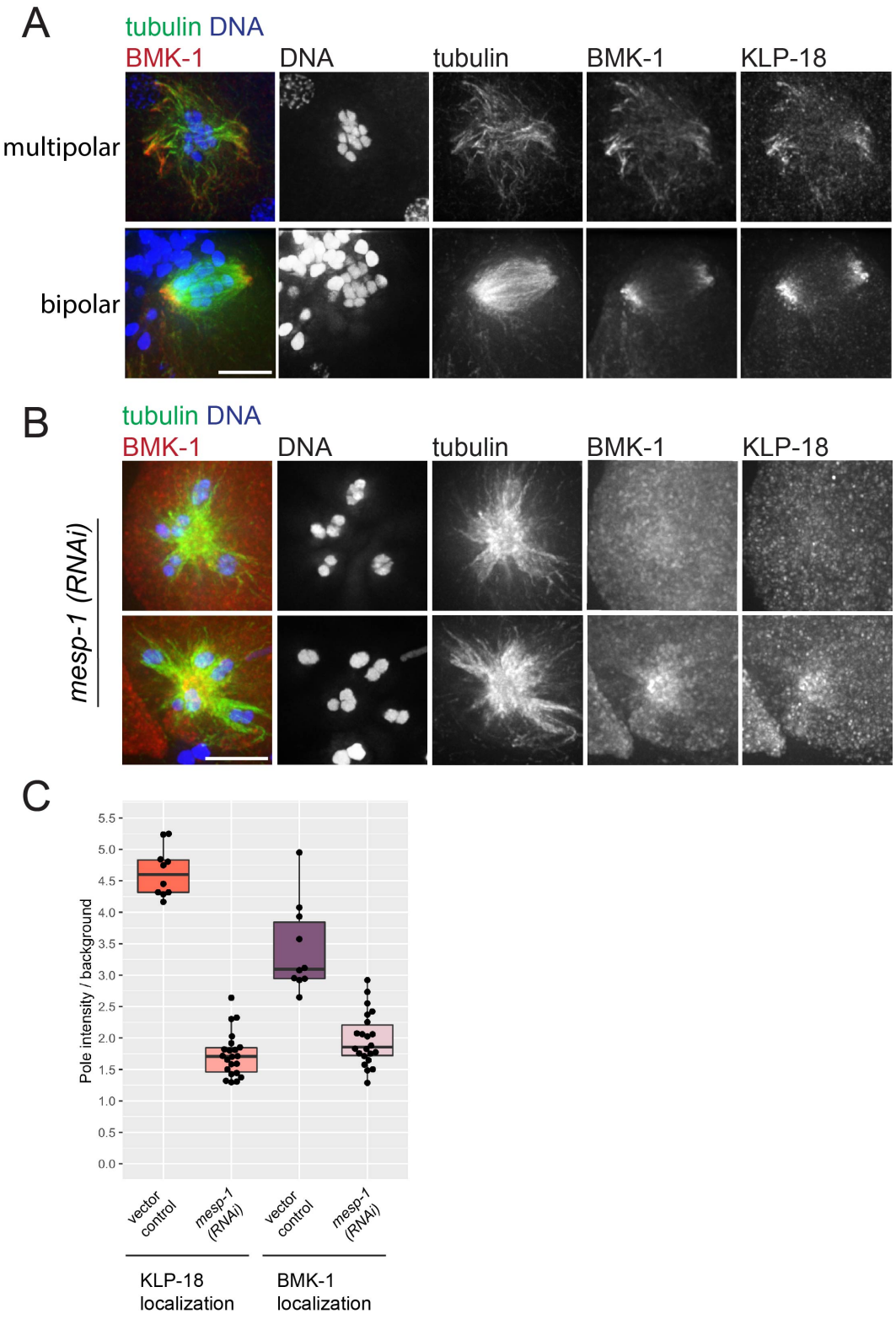
A
tubulin DNA
BMK-1
DNA
tubulin
BMK-1
KLP-18
multipolar
bipolar
B
tubulin DNA
BMK-1
DNA
tubulin
BMK-1
KLP-18
mesp-1 (RNAi)
C
Pole intensity / background
5.5
5.0
4.5
4.0
3.5
3.0
2.5
2.0
1.5
1.0
0.5
0.0
vector control
mesp-1 (RNAi)
vector control
mesp-1 (RNAi)
KLP-18 localization
BMK-1 localization

Figure D.1

Figure D.1. **BMK-1 colocalizes with KLP-18 during spindle assembly and localization is affected by MESP-1 depletion**. Oocyte spindles fixed and stained with antibodies against tubulin (green), BMK-1 (red), KLP-18 (not shown in merge) and DNA stained with Hoechst (blue). (A) BMK-1 colocalizes with KLP-18 during spindle assembly on a multipolar and bipolar spindle. (B) In *mesp-1(RNAi)* oocyte spindles, both BMK-1 and KLP-18 are often absent from the monopolar spindle (for description of phenotype, see Chapter 2). Representative images of BMK-1/KLP-18 absent from monopole (top) and persisting on monopole (bottom) are shown. (C) Quantification of KLP-18 (left) and BMK-1 (right) pole staining on vector control bipolar and *mesp-1(RNAi)* monopolar poles. Each dot is one spindle pole. The amount of pole associated KLP-18 or BMK-1 is decreased in *mesp-1(RNAi)* condition.

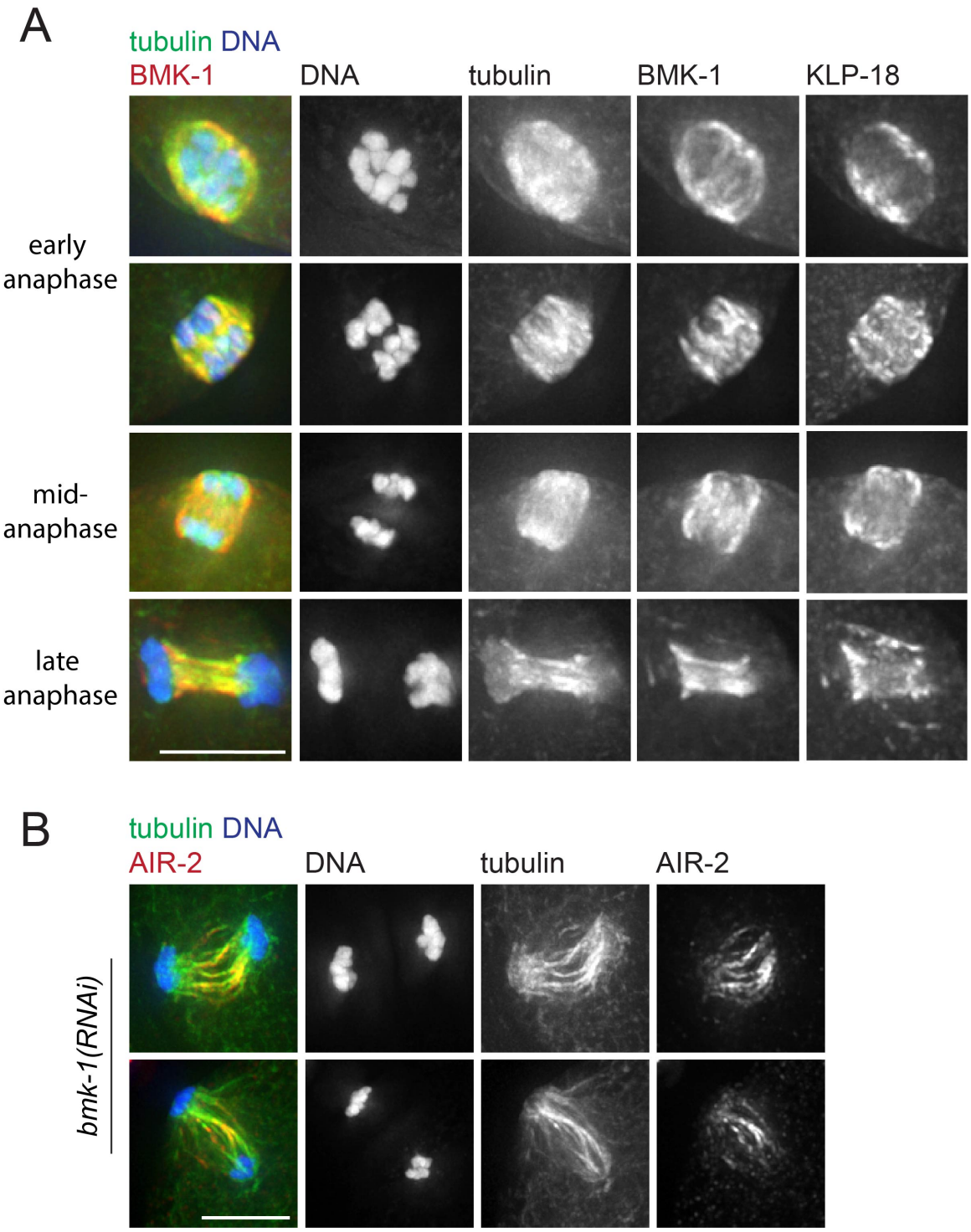
A
tubulin DNA
BMK-1
DNA
tubulin
BMK-1
KLP-18
early anaphase
mid-anaphase
late anaphase
B
tubulin DNA
AIR-2
DNA
tubulin
AIR-2
bmk-1(RNAi)

Figure D.2

Figure D.2. **BMK-1 redistributes to spindle microtubules during anaphase and depletion results in unfocused late anaphase microtubule bundles**. (A) Oocyte spindles fixed and stained with antibodies against tubulin (green), BMK-1 (red), KLP-18 (not shown in merge) and DNA stained with Hoechst (blue). BMK-1 localizes to spindle microtubules between the segregating bivalents, differing from KLP-18 that localizes to the poles of the anaphase spindle[104]. Representative images of early, mid, and late anaphase are shown. (B) Mutant *bmk-1(RNAi)* late anaphase oocyte spindles fixed and stained with antibodies against tubulin (green), AIR-2 (red), and DNA stained with Hoechst (blue). Microtubules between segregating chromosomes are much more splayed than in typical late anaphase spindles (see (A)). Scale bars: 5μm.

APPENDIX E

ZYG-9 is required for *C. elegans* oocyte spindle assembly

This figure is a part of a collaborative manuscript in preparation on which I am a co-author. The paper investigates the role of ZYG-9 during spindle assembly.

In an effort to understand the structural nature of the poles (see Appendix C), I depleted the *C. elegans* XMAP215 homolog ZYG-9. ZYG-9 had been shown to be important for oocyte spindle assembly[263–266], but its phenotype had not been visualized at high resolution. I found that depletion of ZYG-9 by RNAi resulted in small ball-like spindles that did not have apparent long microtubule bundles (Figure E.1). These ball-like spindles were not bipolar but KLP-18 and MESP-1 localized to several discrete pole-like structures. These results indicate that ZYG-9 is essential for acentrosomal spindle assembly and pole coalescence.

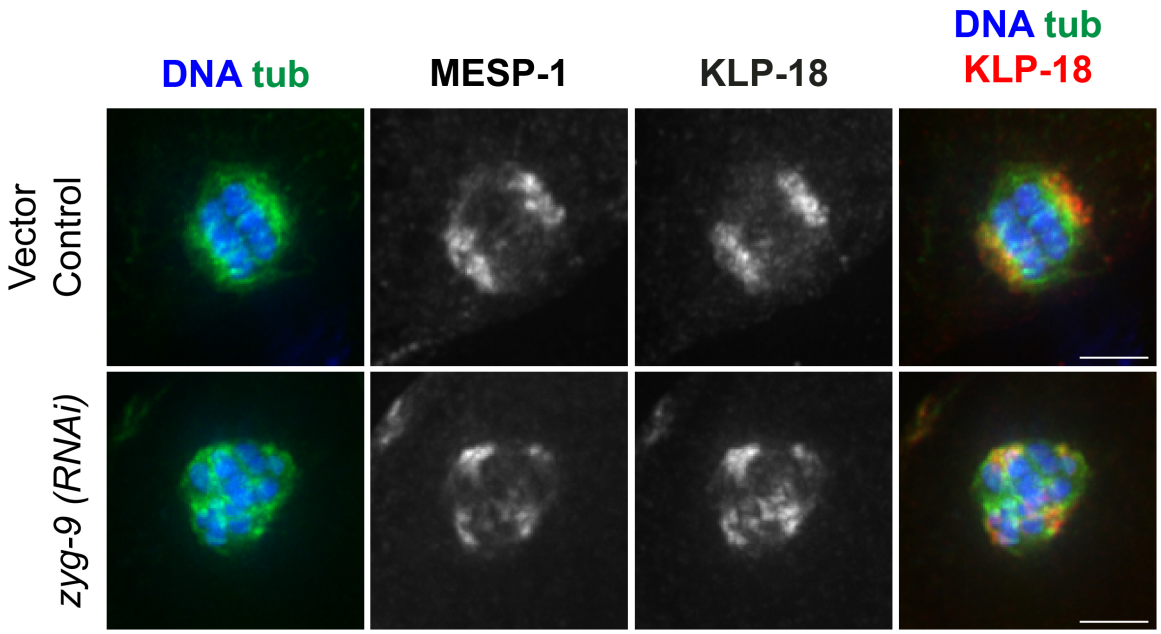

Figure E.1. **ZYG-9 is required for *C. elegans* oocyte spindle assembly**. *zyg-9(RNAi)* oocyte spindles fixed and stained with antibodies against tubulin (green), KLP-18 (red), MESP-1 (not in merge) and Hoechst to visualize DNA (blue). Spindle bipolarity was not achieved and there appeared to be defects in microtubule nucleation. KLP-18 and MESP-1, used as a pole markers in this experiment, localize to pole-like structures around a ball of tubulin. The pole structures appear to be aster-like. Scale bar: 5μm.

APPENDIX F

KLP-18 motility

Special thanks to Sarah Rice who taught me how to do these experiments, allowed me to use her lab's microscope, and aided in analyzing the results.

To put KLP-18 into biochemical context with mammalian kinesin-12 Kif15 and with kinesin-5 Kif11/Eg5 (See Introduction), I performed microtubule gliding assays with purified dimeric KLP-18 motor. In this assay, I used a purified KLP-18 dimer construct with a 6xHis tag on the protein's C-terminus (the opposite termini of the motor domains). First, a 6xHis antibody is applied to a flow chamber between a glass slide and a glass coverslip. The antibody coats the glass and binds purified motor when the motor is applied to the flow chamber. Next, fluorescent microtubules are added to the flow chamber and the reaction is imaged with time-lapse confocal microscopy. In theory, the stabilized motor dimers can bind to the microtubules and walk on them, 'gliding' them across the coverslip. This movement is visualized directly and is quantified using ImageJ. Through this quantification, I found that KLP-18 has a mean velocity of 445nm/s, higher than the reported Kif15 velocity of 350nm/s found using a similar experiment[267]. This analysis is from pooled data acquired in two separate experiments. These results are preliminary and this experiment must be performed again before publishing.

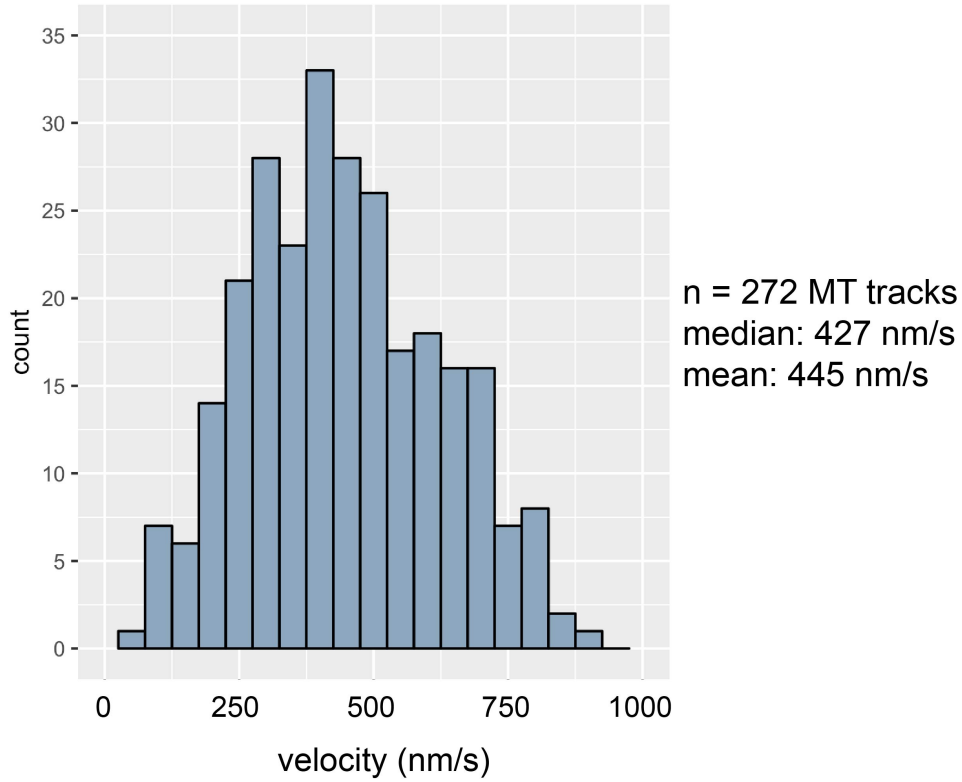

Figure F.1. **Microtubule gliding assay shows KLP-18 is a relatively fast kinesin-12 motor**. Histogram showing the distribution of microtubule track velocity over 272 microtubule tracks. The median velocity was 427nm/s and the mean velocity was 445nm/s.